AN ABSTRACT OF THE THESIS OF

Bindiya S. Abhinkar for the degree of Master of Science in Industrial Engineering presented on December 7, 2007.
Title: Modeling and Development of Fabrication Method for Embedding Membrane Based Microvalve in Bulk Microfluidic Device

Abstract approved:

_____

Brian K. Paul

PDMS membrane-based microvalves are becoming increasingly more important for the control of fluid flow within MECS applications such as microreactors used to synthesize nanoparticles and biological macromolecules. The motivation for pursuing PDMS membrane-based microvalves is for implementing a plug flow microreactor to simulate slug flow yielding a narrower residence time distribution (RTD). Barriers to the use of PDMS membrane-based microvalves within these types of MECS applications include the need to be scalable and compact, capable of operating at higher pressures in a variety of solvents. Most current bonding architectures for PDMS membrane-based microvalves are limited to one atmosphere.

This research work describes the design, analysis, fabrication, and characterization of PDMS membrane-based microvalve architecture for implementation within MECS devices for nanoparticles synthesis applications. The new fabrication approach is to make reliable bonds capable of withstanding higher pressures. The approach developed in this thesis eliminates bonding constraints within current PDMS bonding architectures (e.g. bonding of dissimilar materials and stress distribution problems) through the use of sealing bosses and enables further

miniaturization of the overall structure by entrapping the membrane between stiff polymer substrates.

A novel fabrication method has been developed for embedding PDMS membrane-based microvalves in multi-layer, arrayed microfluidic devices. This novel architecture sandwiches an elastomeric membrane between polycarbonate substrates having sealing bosses and can withstand operating pressure upto 100 psi. This meets a key requirement for MECS device architectures which require higher fluidic pressures in a chemical processing. In addition, the architecture incorporates the use of stiff polymers which can reduce the overall size of the device. Based on the fact that a polycarbonate lamina has an elastic modulus 1000 times that of a PDMS lamina (currently used in multi-layer valve architectures), plate mechanics would predict a 10 fold reduction in the thickness of those laminae to achieve the same stiffness within the stack.

Modeling and Development of Fabrication Method for Embedding Membrane Based Microvalve in Bulk Microfluidic Device

by

Bindiya S. Abhinkar

A THESIS

submitted to

Oregon State University

in partial fulfillment of
the requirements for the
degree of

Master of Science

Presented December 7, 2007
Commencement June 2008

Master of Science thesis of Bindiya S. Abhinkar
presented on December 7, 2007.

APPROVED:

_____

Major Professor, representing Industrial Engineering

_____

Head of the School of Mechanical, Industrial and Manufacturing Engineering

_____

Dean of the Graduate School

I understand that my thesis will become part of the permanent collection of Oregon State University libraries. My signature below authorizes release of my thesis to any reader upon request.

_____

Bindiya S. Abhinkar, Author

ACKNOWLEGEMENTS

The bliss and euphoria that accompanies the successful completion of my thesis would be incomplete without thanking those people who have supported, helped and guided me throughout my thesis. It is very difficult to express my gratitude in words.

I am immensely grateful to Sameer Abhinkar, my husband, for his tremendous encouragement, strength, support and co-operation for the successful completion of my thesis. It would have been incomplete without Sameer's help. I also like to express my deepest gratitude to my parents and my parents-in-law for all their moral support.

I avail this opportunity to express my gratitude and sincere thanks to my advisor Dr. Brian K. Paul, for giving me an opportunity to work under him and for his valuable advice, guidance and inspiration. This thesis would not have taken the shape and progressed without the support of Dr. Paul, who helped me resolve problems encountered during the project.

I am also grateful to Keck Foundation and Air Force Research Laboratory, for funding the project.

I express my sincere thanks to Dr. Shiwoo Lee for his support especially during the setup of LabVIEW interface and for his guidance in the statistical analysis.

I also want to thank Dr. Chih-Hung Chang and his student Hyungdae Jin for their timely help with the specification to build the microfluidic device.

I would like to express my sincere gratitude to Steve Etringer for his extra time and effort in fabricating the microfluidic devices and training me on several equipments.

I am also thankful to Keith Price for loaning the laptop to run LabVIEW programs.

I am very thankful to both Dr. Alexey Shvarev and his student Hasini Perera from the Chemistry Department who helped in writing the LabVIEW program and setting up the LabVIEW interface.

I am also thankful to Dr. Roy D. Haggerty for his time for being the Graduate Council Representative of my committee.

And finally, my deepest gratitude and many thanks to my friends and colleagues Tom Tseng, Jack Rundel, Carlos Conzalez, Corey Koch, Santosh Tiwari, Hadi Hasan, Sumantra Bose and Prashanth Chintapalli who helped me so much during my master's degree.

Without the support of all the people mentioned the completion of my thesis would have been very difficult. A big thank you to everyone!

CONTRIBUTION OF AUTHORS

Dr. Brian K. Paul assisted with the structure of the thesis. He was also involved with the design and writing all the chapters. He assisted me with the analysis and interpretation of the data. Dr. Shiwoo Lee guided me to perform statistical regression analysis in Chapter 2. He and Dr. Brian K. Paul helped me to write a conference paper for Industrial engineering research conference (IERC) 2007.

TABLE OF CONTENTS

Page

TABLE OF CONTENTS (Continued)

Page

LIST OF APPENDICES

Appendix Page

LIST OF APPENDICES (Continued)

LIST OF FIGURES

Figure Page

LIST OF FIGURES (Continued)

Figure Page

LIST OF APPENDIX FIGURES

Figure Page

LIST OF APPENDIX FIGURES (Continued)

Figure Page

LIST OF TABLES

LIST OF APPENDIX TABLES

LIST OF APPENDIX TABLES (Continued)

Table Page

Development of Fabrication Method for Embedding Membrane Based Microvalve in Bulk Microfluidic Device

1 CHAPTER.1 INTRODUCTION

This thesis describes the finite element modeling and implementation of embedding an elastomeric membrane-based microvalve within an arrayed microfluidic device. Some of the features of this design include:

- A thin elastomeric membrane-based microvalve embedded between stiff polymeric microchannel laminae allowing for a greater degree of miniaturization conducive to arraying not only across multiple microchannels on a single lamina but also across multiple laminae
- The ability to deploy using a novel method of packaging the microvalves within microchannel arrays using stiff, optically transparent, low cost materials
- Increase in flexibility in material selection because substrates are bond together conformally using mechanical pressure and sealing bosses to prevent fluid leakage
- Operating pressure such as clamping pressure can be as high as 100 psi

The document follows a manuscript thesis format and is comprised of seven main sections:

1. Chapter 1. General Introduction: This section covers a brief introduction to microfluidic devices and their application. A literature review is provided to establish the novelty of the research. The chapter ends with a problem statement.
2. Chapter 2. Microvalve Design: This chapter describes the conceptual design of the microvalve and the approach for developing a feasible detail design.
3. Chapter 3. Experimental Validation: This chapter is divided into three parts namely, experimental design, experimental setup and experimental protocol for validating the detailed design.
4. Chapter 4. Results and Discussion: This chapter covers all the results based on cut-off curves and further explains the tolerance analysis.

5. Chapter 5. Conclusion: This chapter summarizes work done in this thesis to implement elastomeric membrane-based microvalves within an arrayed microfluidic device.
6. Appendix
7. Bibliography

1.1 Introduction

Miniaturization is becoming an increasingly important topic for the advancement of energy and chemical systems. Mixing and heat transfer can be performed faster and be more tightly controlled in microchannels due to high surface area to volume ratios. Two categories of microfluidic devices which take advantage of microchannels are micro total analysis systems (μTAS) and micro energy and chemical systems (MECS). μTAS are microfluidic systems used for chemical and biological analysis. These microfluidic devices, also referred to as "lab-on-a-chip" technology, may incorporate many of the transduction concepts from ICs and microelectromechanical system (MEMS) into microchannels to perform chemical assays on nanoliters or picoliters of fluid. Over the past decade, considerable effort has been made to develop microdevices fabricated utilizing both bulk and surface micromachining techniques for μTAS (also known as BioMEMS) [2]. Micropumps and microvalves have been implemented to control fluid flows. Flow rates, measured in microliters per minute, allow for the detection of trace molecules at very low concentrations, resulting in shorter analysis times and lower reagent consumption.

MECS are microfluidic devices that rely on highly-paralleled, embedded microchannels for the bulk processing of mass and energy. Flow rates tend to be much higher than in μTAS enabled by implementations of unit operations within microchannel arrays. An example of the application of MECS technologies is the synthesis of nanoscale particles and macromolecules.

Initially, microfluidic device fabrication was accomplished mainly using silicon micromachining technology developed within the electronics industry and refined within the emerging MEMS industry. More recently, polymer materials such as polycarbonate have been used in many μTAS applications due to their excellent optical access and low cost of manufacture capable of supporting disposable applications. In μTAS, elastomeric polymers have been gaining attention for a number of reasons including low cost manufacturing [3]. Among them, polydimethylsiloxane (PDMS) is being used substantially in the fabrication of microfluidic components (pumps, microvalves and microchannels) and is one of the most suitable materials for the implementation of cheap membrane-based microvalves because of its hyperelasticity and excellent sealing property [4]. Besides its ease of use in micromolding, PDMS has additional advantages, such as it is inexpensive, transparent, and biocompatible. On the other hand, disadvantage of PDMS are the limited variety of actuation methods and it is swelled by many organic solvents and hence unsuited for use with such solvents.

Most PDMS membrane-based microvalves have been developed for μTAS applications. Two actuation methods, pneumatic and thermopneumatic have been reported [4]. In the case of pneumatic actuation, microfabricated control channels are required to channel air pressure needed to deflect a PDMS membrane into a flow microchannel. For μTAS applications, this is reasonably easy to manage since flow volumes are small requiring only two sets of laminae. However, in MECS applications, where a multilayered microchannel array is needed to process much larger flow rates, a more complicated fabrication process is required. The hyperelasticity of PDMS makes distribution of pressure throughout the multi-layered device complex causing bonding to be more difficult.

Microvalves are becoming increasingly more important for the control of fluid flow within MECS applications such as in microreactors used to synthesize

nanoparticles and biological macromolecules [29]. The motivation for pursuing membrane-based microvalves within this thesis is for implementing a plug flow microreactor to simulate slug flow yielding a narrower residence time distribution (RTD). Narrow RTDs are important within microreactors used to generate uniform nanoparticles with narrow particle size distributions [23]. Residence time is defined as the average time a fluidic molecule spends within the microreactor. Within a laminar flow (the regime in microchannels), residence time distribution is dominated by the parabolic velocity distribution (Figure 1.1 left). In single-phase laminar flow, diffusion is the only means of mixing. As a result of the parabolic fluid-velocity profile, particles near the wall spend more time in the microreactor than those in the center, resulting in broad RTDs. In two-phase flow (Figure 1.1 right), recirculation within each liquid slug brings material from the wall to the center of the microchannel. This facilitates mixing, which narrows the RTD, and results in narrower size distributions. A narrow residence time provides nearly similar reactions conditions for all particles within a flow which for growth reactions yield similar sized particles. Figure 1.1 illustrates single phase flow and segmented flow.

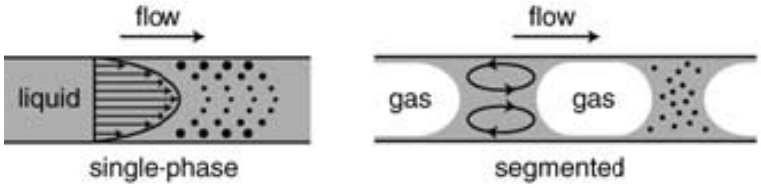

Figure 1.1. Single phase flow and segmented flow

Specific advantages of using a gas-liquid plug flow microreactor are as follows.

1. Recirculation within segments provide a mechanism of exchanging fluid elements located near the microchannel walls with those at the center which narrows the RTD and improves reactant mixing.
2. Gas–liquid flow is preferable for performing reactions at elevated temperatures, as most solvents experience increased miscibility at higher temperatures.

3. It is possible to obtain a uniform segmentation in gas–liquid flow over a very large range (over two orders of magnitude) of bubble velocities and therefore reaction timescales.

This research work describes the design, analysis, fabrication, and characterization of PDMS membrane-based microvalve architecture for implementation within MECS devices for nanoparticles synthesis applications.

1.2 Literature review

The literature review is divided into three sections: microfluidic devices with membrane-based microvalves, analytical modeling and finite element modeling.

1.2.1 Microfluidic devices with membrane-based microvalves

Today's microreactors have integrated microvalves to perform complex fluidic control, such as injecting and blocking the sample. Elastomeric (predominately PDMS) membrane-based microvalves have found extensive application. PDMS membrane-based microvalves are attractive in analytical microfluidics because of their rapid response times, capability to seal, and gentle handling. Researchers have worked on two types of pneumatically-actuated microvalves, namely, normally open and normally closed microvalves. With normally open microvalves, pressure is applied to an elastomeric membrane extending over a flow microchannel which deflects the membrane into the flow microchannel shutting off the flow. In normally closed microvalves, the membrane seats into a microvalve seat that normally blocks the flow in the microchannel but pulls away from the microvalve seat when negative pressure is applied to the membrane.

Hosokawa et al. [4] developed a three way PDMS membrane-based microvalve. The microvalve unit is normally closed by sealing the membrane against a microvalve seat and operated when negative pneumatic pressure is applied to pull it away from the microvalve seat. The fluidic chip was bonded to the membrane and pneumatic chip by treating the surfaces to oxygen plasma. The width and depth of the microchannel were 100 μm and 25 μm respectively. The depth of the control microchannel was 70 μm. Oxygen plasma bonding technique was used to bond these substrates. The microvalve pressure varied from 0 - 10.52 psi. Groover et al. [5] also developed normally closed monolithic PDMS membrane-based microvalve that was actuated when negative pneumatic pressure was applied. The membrane and the flow microchannel were anodically bonded. The pneumatic pressure varied from 1.45 – 10.8 psi. The flow microchannel had a smaller cross-section of 20 μm in width. A dead volume of greater than 10 nl had been encountered with this type of microvalve design. Pneumatic pressure was controlled by computer interface via LabVIEW.

Alternatively, Quake et al. [1] worked on developing normally open pneumatic microvalves that were actuated at pneumatic pressure around 14.5 psi. Flow microchannels were hemispherical in shape. Response times were measured at about 1 ms and the microvalves were found to maintain functionality past 4 million actuations. Hu et al. [6] developed a microcheck valve with a movable membrane flap. These valves were usually implemented as “check valves” in a micropump system. It opened under forward biased pressure and closed at reverse biased pressure. The displacement of the flap was limited to out-of-plane. When a forward flow was applied, the net pressure differential acting on the bottom of the flap separated the flap from the valve seat and allowed fluid to pass through the gap between them. On the other hand, when a reverse flow was applied, the net pressure differential exerted on the top of the flap pressed the flap against the valve seat, thus closed the orifice. These valves required additional pumping devices to create fluid flow. The check valves were fabricated using an SOI wafer. The bulk anisotropic etching process, deep reactive ion etching

(DRIE), was employed to form all structures on both sides of the SOI wafer. Other designs such as magnetic or pneumatic actuated ball or plate valves can work under high flow rate and operational pressure. However, these valve designs tend to have the disadvantage of large dead volumes. A leakage rate of 0.00001 ml/min at 87.02 psi was found. Finite element modeling using ANSYS 7 was developed to study the performance of microvalves for both dynamic and static simulations.

A PDMS membrane-based microvalve actuated by pneumatic pressure was also developed by Galas et al. [13]. Pneumatic microvalves were produced on-chip based on multi-layer soft lithography techniques. Two set of microchannels (namely flow and control channels) were produced in a cross-configuration separated by a thin film of PDMS. Applying pressure in the control channel, the PDMS film deformed so that the cross-section of the adjacent channel was changed, which resulted in an effective microvalve actuation. The layers were bonded by oxygen plasma bonding. The width and depth of the flow and control channels were 100 μm and 10 μm respectively. The flow pressure was 2.9 psi and the pneumatic actuation pressure along with the microvalve deflection was not mentioned. Wheeler et al. [14] developed a novel microfluidic device constructed from PDMS using multilayer soft lithography technology for the analysis of single cells. PDMS membrane-based microvalves were formed at the intersection between channels in distinct “control” and “fluidic” layers. As pneumatic pressure was applied to a control channel, the membrane between layers deflected and closed the fluidic channel. The pneumatic system of microvalves was digitally controlled and, therefore, was completely programmable. The width and depth of the flow microchannel were 10 μm and 5 μm respectively with a square profile. The diameter of the control channel was 20 μm having a circular cross-section.

Go et al. [7] presented a pneumatically driven in-plane PDMS membrane-based microvalve with low dead volume. In “valve-off” mode (release of membrane),

water could flow freely. As soon as the membrane bulged ("valve-on" mode), water flow was blocked. The valve took longer to release the membrane than to actuate the membrane. Pneumatic pressure of 1.45 psi was applied to actuate the microvalve and was controlled by LabVIEW.

Alternatively, Yoo et al. [8] developed a thermopneumatically-actuated PDMS membrane-based microvalve. When the air in a PDMS chamber heated up due to the applied power, it underwent volume expansion. The microfluidic system was operated when the PDMS membrane was deflected into the pump chamber and sealed the microvalve seat. On the contrary, when the ITO heater cooled down, the air contracted and restored the microvalve to its normal condition. Yang et al. [9] also developed a thermohydraulically-actuated, normally-open, silicone rubber membrane microvalve. Suspended silicon nitride membrane heaters were used for low-power thermohydraulic actuation. When the membrane was deflected and sealed the inlet on the microvalve seat, the microvalve was closed. Actuation was achieved by heating or cooling a closed cavity, which was filled with a working liquid and sealed with a glass substrate heater on one side and a deflectable membrane on the other. They reported that 14.6 psi pneumatic pressure deflected up to 1.54 mm and 5 psi pneumatic pressure deflected 520 μm.

There are a few disadvantages of using PDMS membrane-based microvalves. First, PDMS is highly gas permeable which can cause the evolution of bubbles over time. Second, PDMS is not chemically compatible with most solvents. Third, since they are based on a diaphragm, sticking of the membrane is sometimes encountered. Bien et al. [2] developed a passive microvalve made up of polycrystalline silicon. It comprised a silicon substrate with an etched aperture to form an inlet for a gas or liquid. A polycrystalline silicon movable plate was located at the centre above the inlet hole. Depending on its position; the plate either enabled or restricted the flow. The movable plate was supported by four polycrystalline silicon arms, attached to the

silicon substrate. When the pressure acted in the reverse direction, the microvalve plate was pushed against the silicon substrate, and restricted the flow. The maximum pressure applied to actuate the microvalve was 4.5 psi.

Quero et al. [10] implemented a novel pressure balance microfluidic valve. The microvalve consisted of a membrane orthogonal to the inlet and outlet orifices that prevented the fluid to pass from inlet to outlet. On the other side of the membrane, an electrode could exert a force on it and move the membrane, so that the working fluid could flow through the microvalve moving the membrane by electrostatic actuation with a pressure compensation system based on pneumatic effects. The normally closed membrane microvalve was actuated by electrostatic force. Thuillier et al. [11] developed a multilayered pneumatically actuated elastomeric membrane-based microvalve. The microvalve was made in two separate parts, a fluidic part, which was biocompatible and optically transparent material (PDMS), and a robust pneumatic interface in silicon, which were assembled together. In normal operation, with a low liquid pressure, the microvalve unit was normally closed with the membrane on the microvalve seat. If the pressure of the liquid was too high, the membrane may be needed to be pressurized to stay closed and leak-tight. An external negative pressure was necessary to deflect the membrane and open the microvalve. The upper part consisted of a PDMS membrane and the silicon cavity and the lower part consisted of a PDMS substrate with flow channels and the microvalve seat. Baechi et al. [12] also developed silicone based membrane microvalves. By heating the bottom of the cavity, the air pressure in the cavity raised. This made the membrane to bend into the channel. Thermopneumatic was actuated at 30ºC above the ambient temperature.

Based on this review of the literature, most membrane-based microvalves were fabricated using PDMS or silicon and give sketchy details regarding actuation conditions. The bonding techniques used to bond multilayer devices were either anodic bonding or oxygen plasma bonding or self bonding techniques. PDMS bonding

techniques generally can withstand a maximum pressure of 15 psi. These bonding techniques cannot be implemented in applications which require operating pressures to be greater than 15 psi. New bonding techniques are needed for withstanding pressures much greater than 15 psi. None of the papers have worked on modeling and analysis of the modulus of elasticity of the PDMS elastomeric membrane.

1.2.2 Analytical modeling

Few authors have performed modeling to study the pneumatic pressure required to actuate a membrane-based microvalve. One concern is the availability of material property data. There are two types of materials namely, linear and nonlinear material. Linear materials obey Hook's law, where stress is directly proportional to strain. In the nonlinear materials, the stress is not proportional to strain. The nonlinear materials undergo large deformation for small amount of stress. Figure 1.2 illustrates the stress-strain relation for linear and non-linear materials.

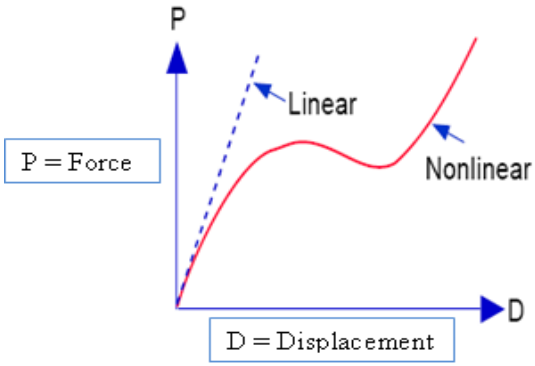

Figure 1.2. Stress-strain relationship for linear and nonlinear materials

The nonlinear materials are further divided into two types: compressible and incompressible material. Compressible materials undergo change in volume under the application of stress. Alternatively, an incompressible material is one which undergoes

no change in volume when deformed by stresses, such that the Poisson's ratio is exactly 0.5 for infinitesimal strains.

The deflection equation is very simple for linear materials. Equation (1) illustrates deflection of a plate for linear material [40].

$$\delta = \frac{\alpha q b^4}{E t^3} \qquad (1)$$

where δ is deflection, $\acute{\alpha}$ is structural factor (plate width/plate length), q is load applied per unit area, E is elastic modulus of plate, b is plate length and t is plate thickness.

Quero, et al. [10] worked on both numerical modeling and finite element analysis using ANSYS software. Khoo et al. [15] reported a novel method to characterize the mechanical properties, such as the elastic modulus, of circular microfabricated elastomeric membranes by measuring their load-displacement curve. They developed a linear elasticity equation when a load was applied on the center of a circular membrane. The equation is illustrated in Equation (2) and is strictly based on linear elasticity.

$$\frac{d^3 d_f}{d_r^3} + \frac{1}{r}\frac{d^2 d_f}{d_r^2} - \frac{1}{r^2}\frac{dd_f}{d_r} - \frac{\sigma_m}{D}\frac{dd_f}{d_r} = \frac{P_p * A_v}{2\pi D} \qquad (2)$$

where d_f is the flow microchannel depth, d_r is the function of stretch, r is the amount of stretch in the direction of load applied, σ_m is average membrane stress and A_v is area of the microvalve ($w_v * l_v$).

The term “D” is a decisive parameter which is also known as flexural rigidity and is given in Equation (3). Flexural rigidity is defined as the force couple required to bend a rigid structure to a unit curvature.

$$D = \frac{E_v t_v^{\,3}}{12(1 - v_v^{\,2})} \tag{3}$$

where t_v is microvalve thickness and v_v is Poisson’s ratio of microvalve material.

Hoel et al. [16] worked on determining the shear modulus of a PDMS sample of one square centimeter area. It is given by Equation (4), were G is the shear modulus, F the applied force during the test, δ is the stretching of the sample, S_v the surface area of the microvalve and t_v its microvalve thickness.

$$G = \frac{Ft_v}{S_v \delta} \tag{4}$$

Hout et al. [17] worked on determining a new terminology called shape factor. Elastomers are inherently viscoelastic materials and as such will display hysteresis and non-linear load-deflection characteristics which are undesirable for simple microvalve implementations. Improved mechanical characteristics are obtained through careful control of the actual shape of individual elements in a structured elastomer layer. An important index in determining the level of hysteresis and non-linearity in structured elastomer layers is called shape factor, S, which for a given array element is defined as the ratio of one loaded surface area, i.e. top surface, to the load-free surface area. For a rectangular block of length l, width w and thickness t, having bonded plates on its upper and lower surfaces and free to bulge at the sides, the shape factor has the form given in Equation (5).

$$S = \frac{l * w}{2(l * t + w * t)} = \frac{S_0}{\lambda} \quad (5)$$

The compression ratio is given by Equation (6).

$$\lambda = 1 + \frac{\Delta t_v}{t_v} \quad (6)$$

and S_0 is the unstrained shape factor. Shape factors can range from 0.2 to 0.7, but preferably towards the lower end of this scale are recommended in order to optimize elastic properties. The nominal stress–strain relation for a cube undergoing finite deformation has the general form as given in Equation (7).

$$\sigma = \frac{F}{A} = G(\lambda - \frac{1}{\lambda^2}) \quad (7)$$

where σ is the nominal stress, A is the loaded area and G is the shear modulus which is related to the linear elastic modulus E and $G = E/3$. For compression the resulting stress–strain relation has the form given in Equation (8).

$$\sigma = \frac{F}{l * w} = E_a * \frac{\Delta t}{t} = E_a(1 - \lambda) \quad (8)$$

where E_a is apparent Young's modulus.

On the other side, Tabata et al. [18] worked on determining the internal stress and elastic modulus of thin films by measuring the deflection versus pressure of the rectangular membrane materials. In order to reduce the error for the elastic modulus due to unknown Poisson's ratio, 2 mm x 8 mm rectangular membrane was adopted. They considered a rectangular membrane with sides *2a* and *2b* (a = < b). The total strain energy of the rectangular membrane was obtained by adding the strain energy of

deformation to the elastic strain energy due to internal tensile stress. The Fourier expansions of the true solution with undetermined two constants were chosen for the functional form of the displacement of a point in the membrane. Then the work input into the membrane was calculated to obtain the total potential energy of the membrane. Subsequently, the total potential energy was minimized with respect to the two constants in the displacement equations, making use of principle of virtual displacements, resulting in a relationship between the load and the deflection. The relationship is given by Equation (9).

$$P_p = \frac{C_1 \sigma_m T_v D_v}{W_c^2} + \frac{C_2 E_v T_v^2 D_v^3}{W_c^4} \tag{9}$$

where C_1 and C_2 are constants and are given by Equations (10) and (11) respectively.

$$C_1 = \frac{\pi^4 (1 + n^2)}{64} \tag{10}$$

$$C_2 = \{ \frac{\pi^6}{32} (1 - v_m^2) \} \{ \frac{(9 + 2n^2 + 9n^4)}{256} \frac{\frac{[4 + n + n^2 + 4n^3 - 3nv_m(1 + n)]^2}{2}}{[81\pi^2 (1 + n^2) + 128n + v_m(128 - 9\pi^2 (1 + n^2))]} \} \tag{11}$$

where σ_m is residual stress in the membrane, T_v is microvalve thickness, D_v is flow microchannel depth or amount of microvalve deflection, E_v is elastic modulus of membrane, v_m is Poisson's ratio of membrane, W_c is control channel width, L_c is control channel length and $n = W_c/L_c$

Yun et al. [19] worked on developing a micropump actuated by surface tension based on continuous electrowetting (CEW). They have used the surface-tension-induced motion of a mercury drop in a microchannel filled with an electrolyte as actuation energy for the micropump. Although the work reported in this paper is very different, but they introduced an interesting phenomena termed as pressure restoration and is given by Equation (12).

$$\Delta P_{vr} = 66.138\left(\frac{E_v d_f}{1 - v_m^2}\right)\left(\frac{t_v^3}{l_v^4}\right) \qquad (12)$$

where ΔP_{vr} is restoring pressure in the membrane-based microvalve, E_v is elastic modulus of the membrane, d_f is flow microchannel depth, v_m is Poisson's ratio of the membrane and t_v is microvalve thickness, l_v is microvalve channel length.

1.2.3 Finite element modeling

Finite element analysis and modeling (FEA/FEM) has been used to understand the experimental results from membrane-based microvalve investigations. Quake et al. [20] presented a design and method for the fabrication of microfluidic microvalves using multilayer soft lithography. These on-off microvalves had extremely low actuation pressures and could be used to fabricate active functions, such as pumps and mixers in integrated microfluidic chips. They characterized the performance of the microvalves by measuring both the actuation pressure and flow resistance over a wide range of design parameters, and compared them to both finite element simulations and alternative microvalve geometries. However, the authors did not quantify how well the experimental results matched with the modeling results in terms of percentage error. In order to gain insight into the experimental data, they developed a full three-dimensional, finite-deformation model of a single microvalve. The elastomer was modeled as a near incompressible Neo–Hookean material; a constitutive model which

described the behavior of rubber-like materials undergoing large deformations. They resorted to the FEM in order to represent the three dimensional geometry of the microvalves and to solve the equations governing their deformation and closure. For each microvalve geometry, the pressure was increased monotonically at 1/10 increments of the experimental actuation pressure, and the largest pressure not resulting in full closure of the microvalve was recorded as the actuation pressure. A parametric study was performed concerning the effect of membrane thickness on the actuation pressure for a 300 μm wide and 56 μm high channel. Three membrane thicknesses in the experimental range, 5, 10, and 15 μm, were considered. In this case, the actuation channel section was rectangular with widths ranging from 100 to 600 μm and 55 μm in height. They mapped the actuation pressure of the push-up microvalve structure as a function of the membrane width, length, and thickness. The results were symmetric as a function of the width with larger widths yielding smaller pressures. The authors mentioned that the predicted values closely matched the experimental data but did not mention in terms of percentage error between the predicted values and experimental data. The predictions of the model were consistent with observation, with the actuation pressure slightly under predicted for large actuation channel widths.

Pandolfi et al. [21] presented a new design of PDMS microvalves based on bistable configuration of the separation membrane. The elastomer was modeled as a near-incompressible Neo- Hookean material, a constitutive model which describes the behavior of rubber-like materials undergoing large deformations. The material behavior was characterized by two parameters: the shear modulus (μ = 0.6 MPa) and Poisson's ratio (ν = 0.45). The strain energy density W of the material was given by Equation (13).

$$W = \frac{1}{2}\lambda(\log J)^2 - \mu \log J + \frac{1}{2}\mu[trC - 3] \qquad (13)$$

where λ is the second Lame constant, J is the determinant of the deformation gradient F and $C= F^TF$ the right Cauchy-Green deformation tensor.

The elements employed in the calculations were ten-node quadratic tetrahedral with four Gauss points. The computational model was restricted to ¼ of the microvalve, with symmetry boundary conditions applied on all symmetrical planes. By way of validation, they demonstrated the fidelity of the model as regards to sensitive predictions of microvalve behavior, such as the dependence of the actuation pressure on the microvalve. A first parametric study concerned the effect of membrane thickness on the actuation pressure for a 300 μm wide and 56 μm high channel. Three membrane thicknesses of 5, 10 and 15 μm were considered. The predicted values closely match the experimental data, but the authors did not mention how closely the predicted and experimental data matched. A second parametric study concerned the effect of channel width on actuation pressure. The calculations were carried out for four actuation channel widths, 200, 300, 450 and 550 μm, and a 55 μm channel height. They reported that the predictions of the model were consistent with experimental observations, where the actuation pressure was slightly under predicted for large actuation channel width. The authors did not quantify the percentage error between the predicted model and experimental data.

1.3 Problem statement

In this thesis, a PDMS membrane-based microvalve is developed for use in MECS applications such as for a plug-flow microreactor used to synthesize nanoparticles. Barriers to the use of PDMS membrane-based microvalves within these types of MECS applications include the need to be scalable and compact, capable of operating at higher pressures in a variety of solvents.

One concern in the development of this microvalve is the need to scale the device by “numbering up”. That is, to create larger and larger flow volumes, a point is reached where the replication of microchannels is best accomplished by stacking together identical layers. This suggests that microvalves must be capable of being replicated hundreds or thousands of times within a stack of material.

Second, current multilayer structures incorporating microvalves are made from bulk PDMS. One concern is that the lack of stiffness in PDMS requires that the layers be substantially thick (> 1 mm) which reduces the compactness of the design. Therefore, it is also desired that the fabrication architecture consider integration with stiffer materials. One concern in the integration of PDMS with stiffer materials is the relatively few bonding methods that exist to integrate stiff polymers and elastomers. In addition, stress distribution through a multi-layer structure incorporating hyperelastic microvalves can be complex leading to poorly bonded joints [31].

Third, reaction conditions or backpressures within MECS devices may require pressures higher than one atmosphere (the current limit of most membrane-based microvalves). Most current bonding architectures for membrane-based microvalves are limited to one atmosphere. The new fabrication approach must consider how to make reliable bonds capable of withstanding higher pressures.

Finally, it is important that the fabrication architecture use chemically compatible materials. Polydimethylsiloxane (PDMS) can be used as the elastomeric membrane. However, as an example, of the solvents used in the synthesis of Au nanoparticles, tetrahydrofuran (THF) and pentane are not compatible with PDMS. There are a few approaches that can be implemented to make the PDMS more chemically resistant [30]. Viton or some other more chemically resistant elastomer can be spin coated onto the PDMS and cured. However, the impact of this modification to the material properties is not known. Further, Teflon lubricant can

also be sprayed onto the PDMS or the PDMS can be exposed to tetrafluoromethane (CF_4) plasma to generate Teflon-like compounds on the surface. However, these methods are generally not robust. Another approach would be to replace the elastomer with a more chemically compatible material. PDMS can be replaced by Viton, ChemRaz, Parofluor, Simriz (Simrit), Kalrez, and SIFEL. However, these elastomers are not available in the form of base oligomer and cross-linker and so it is difficult to control material properties and material form. The above elastomers are available in the form of thin sheets and have a modulus of elasticity much greater than what is needed for a functioning membrane-based microvalve. Therefore, because PDMS is easily moldable with known material properties, we will restrict this investigation to PDMS. However, it is recognized that the approach taken in this thesis is extendable to membrane-based microvalves utilizing other membrane materials.

Therefore, this thesis will seek to develop a new fabrication architecture for integrating PDMS membrane-based microvalves within multi-layer microchannel arrays. The approach developed in this thesis eliminates bonding constraints within current PDMS bonding architectures (e.g. joining of dissimilar materials and stress distribution problems) through the judicious use of sealing bosses and enables further miniaturization of the overall structure by entrapping the membrane between stiff polymer substrates. The goal is to achieve a functioning microvalve capable of operating at flow pressures significantly higher than one atmosphere. In the end, we describe a means by which to move toward a compact, multi-layer device with embedded membrane-based microvalves capable of handling higher operating pressures.

2 CHAPTER 2. MICROVALVE DESIGN

The methodology to demonstrate an acceptable microvalve architecture can be broken into two main sections: Conceptual design and detail design. The conceptual design consists of three sections: design, materials and fabrication. The detail design consists of three sections: solid model with critical dimension criteria, preliminary experiments and finite element modeling and analysis.

2.1 Conceptual design

2.1.1 Design

The basic concept of the architecture developed in this thesis consists of a conformally bond device having an elastomeric membrane sandwiched between two stiff polymers. The three layers are held together by clamping pressure. The clamping pressure distributed through the structure constrains the local operating pressure. If the operating pressure exceeds the local clamping stress, it is assumed that the fluid will begin to separate the laminae which with additional pressure will lead to leakage. At the same time, too high of a clamping pressure will deform all of the control channels and prematurely deflecting the membrane into the flow microchannel possibly causing flow blockage.

To alleviate these concerns, the top layer has a sealing boss which locally increases the sealing pressures adjacent to the microchannel without prematurely deflecting the membrane into the microchannel. Placement of the bosses on the top plate and registration of those features to the bottom plate is assumed to be critical. The top layer has an inlet for pneumatic pressure which is used to pressurize a pocket within the membrane considered the control or microvalve pocket. The bottom layer

has a flow microchannel with a round bottom profile capable of serving as a microvalve seat during actuation of the membrane adjacent to the microvalve pocket. The flow microchannel has one inlet and one outlet at the ends of the microchannel. The elastomeric membrane is sandwiched between the two polymer layers to seal the microchannel and to provide for the actuation mechanism (i.e. membrane). All three layers have through holes for clamping. Cross-sections of the model are illustrated in Figures 2.1 (a) and (b).

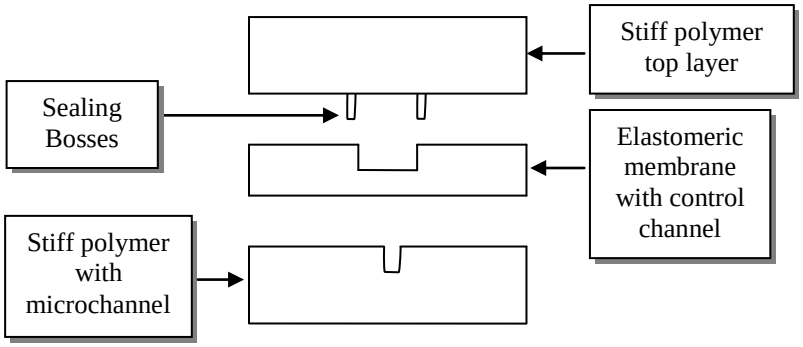

(a) Cross-section of conceptual design

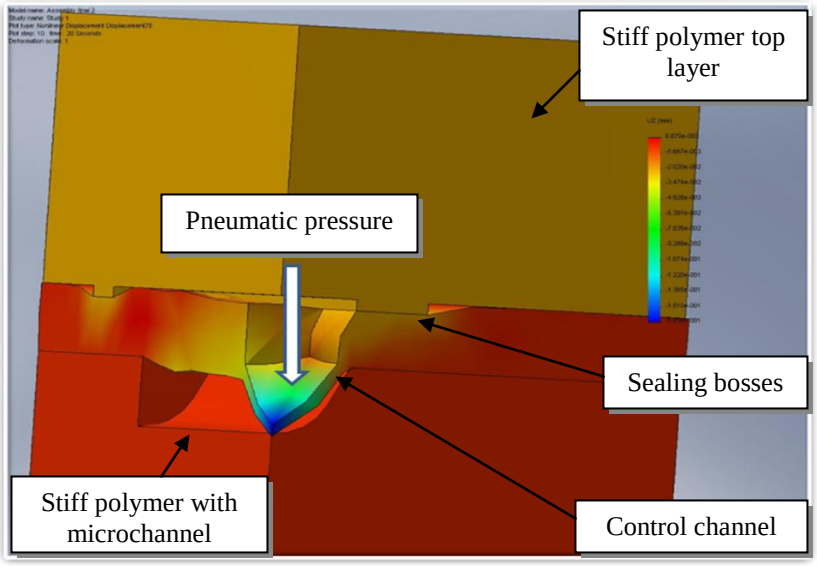

(b) Quarter model of finite element analysis

Figure 2.1. Cross-sections of device

When the stiff polymer layers are clamped, the membrane is compressed and the sealing bosses form a conformal seal over the surfaces. Another advantage of using the sealing bosses is that it reduces the requirement of flatness for all three layers. Conformal sealing generally is very difficult due to out-of-planarity conditions within the laminae. To move to higher operating pressures, requires the use of higher clamping pressures. Consequently, the thickness of the top and the bottom plates must be great enough to minimize deflection and allow for uniform distribution of pressure. Therefore, thick polymer substrates are used to build the device.

Another design trade-off regards the modulus of elasticity of the membrane. Membranes with higher modulus of elasticity can be compressed with minimal deflection into the flow microchannels and minimal distortion of microchannel dimensions. However, higher modulus requires higher pneumatic pressure to deflect the membrane into the flow microchannel for microvalve actuation. These design trade-offs need to be investigated in more detail in order to produce a feasible design.

2.1.2 Materials

Polycarbonate substrates are used for the top and bottom layers. Polycarbonates are a particular group of thermoplastic polymers. The name comes from having functional groups linked together by carbonate groups (-O-(C=O)-O-) in a long molecular chain. Polycarbonate is optically transparent, tough and easily machinable.

As discussed above, polydimethylsiloxane (PDMS) is used as the elastomeric membrane. PDMS is a synthetic elastomer with hyperelastic properties similar to that of rubber. Its structural formula is shown in Figure 2.2 [42], where n can be on the order of thousands. Molecular weights of PDMS can reach 700,000 or higher.

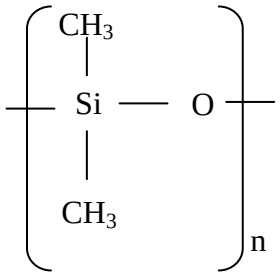

Figure 2.2. Structural formula of PDMS

The PDMS used in this micromolding process is Sylgard 184 from Dow Corning. It is supplied in two constituents: the base oligomer or monomer (that contains vinyl-terminated dimethyl siloxane and a platinum catalyst) and the cross-linker (hydride – terminated dimethyl siloxane) [31]. The addition of platinum-catalyst helps in the reaction between the vinyl functional group ($SiCH=CH_2$) of the base oligomer and the hydride functional group (SiH) of the cross-linker which results in the curing of a mixture of the two constituents. This reaction is known as hydrosilylation (hydrosilation). The normal mixing ratio of the base monomer-to-crosslinker is 10:1, which results to 227.5 psi elastic modulus. However, one can vary the mixing ratio to achieve a desired elastic modulus of the cured PDMS. Cured PDMS is stable and elastomeric from –50 °C to +200 °C.

2.1.3 Fabrication

Fabrication methods can be classified as patterning of features in the layers, alignment of the layers and clamping of the layers together to form a device.

2.1.3.1 Patterning

CNC micromilling was used to machine the sealing bosses and to make the fluidic microchannel. The milling machine used had a spindle capable of 50,000 rpm.

Firstly, the top surfaces of both top and bottom polycarbonate substrates were flattened by a fly cutter. Next, an end mill of ~3.175 mm diameter tool was used to make the sealing bosses by machining down all other surfaces to make a protruded feature. In the bottom plate, a ball-nosed end mill of 310 μm diameter was used to make the microchannel. Burrs were removed by hand. Through holes for interconnects and clamping screws were drilled. Two through holes were drilled in corners diagonal to each other for alignment. Ground pins were inserted into the holes for registration. Clamping holes in the bottom plate were tapped for 10-24 socket head bolt. The top and the bottom polycarbonate substrates are shown in Figure 2.3.

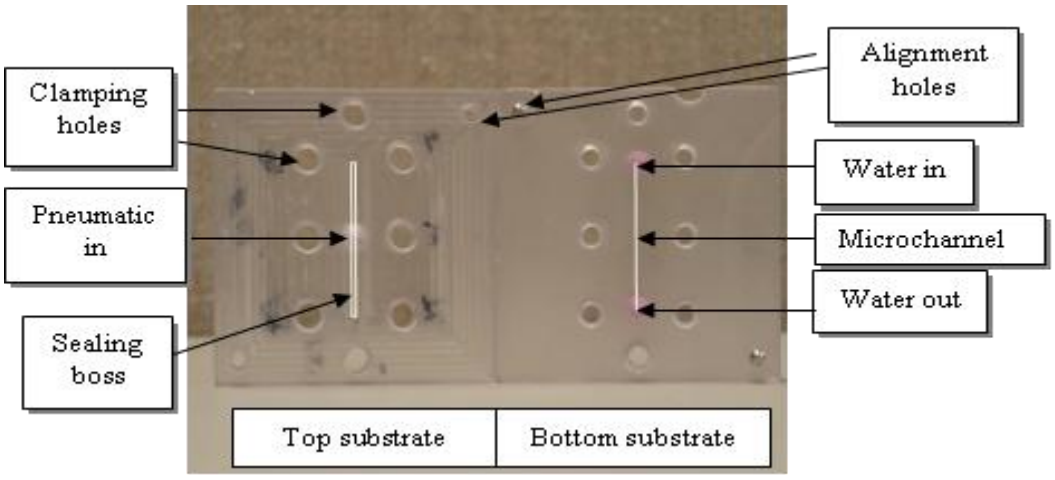

Figure 2.3. Top and bottom polycarbonate substrates

The control pocket (or channel) on the PDMS membrane was replica molded by spin casting PDMS over a patterned electroformed master. The electroformed mold is shown in Figure 2.4. The mold was formed by Nickel electroforming process by Thin Metal Parts Co., Colorado Springs, CO. The mold was produced with 24 different rectangular patterns for adjusting control channel dimensions. The Sylgard 184 PDMS elastomer was mixed at a 10:1 and 18:1 ratio of monomer or oligomer to crosslinker by mass. The PDMS layer was spun over the pattern in an effort to quickly level the monomer thickness. Control of the microvalve thickness was controlled by

the thickness of the monomer relative to the height of the electroformed features. A slow spin rate was used (~810 rpm). Afterwards, the spun on monomer was cured in mold at 100ºC for 6-8 min. The cured PDMS was then peeled slowly from the mold. Clearance holes for clamping screws were made using a needle.

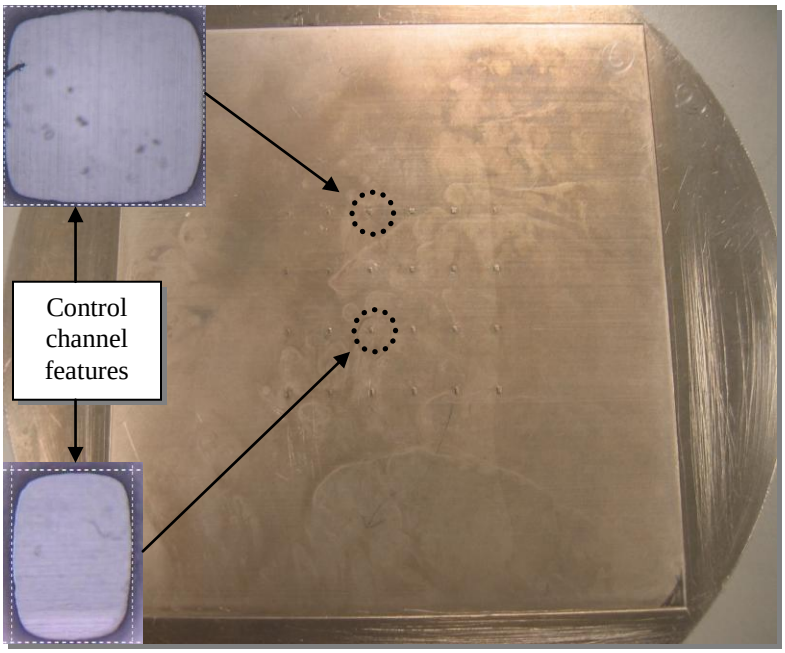

Figure 2.4. Electroformed mold with 24 control channel features

2.1.3.2 Alignment and Clamping

Alignment of the layers was accomplished by aligning the clamping holes visually on all the three substrates and inserting the alignment pins into the holes of the polycarbonate substrates. The control channel was aligned with respect to the microchannel and pneumatic inlet hole by viewing it under the optical microscope. 10-24 screws were used to clamp all the three substrates. The assembled device is shown in Figure 2.5.

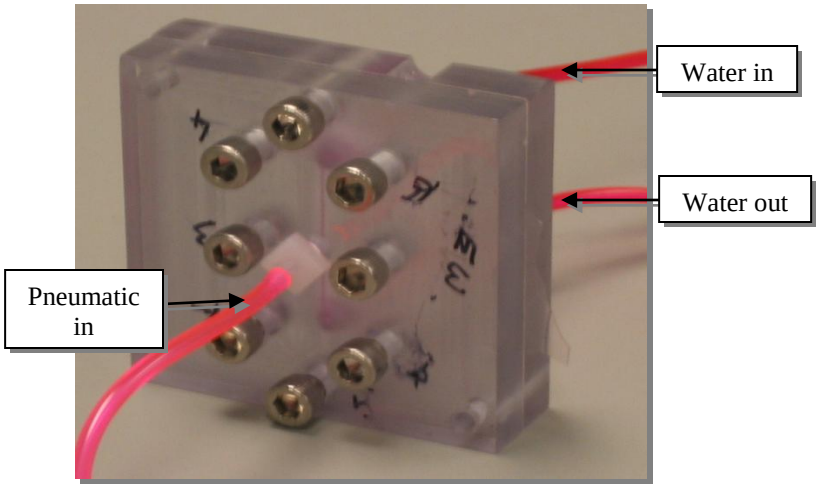

Figure 2.5. Assembled device

2.2 Detail design

The detail design consists of three main parts: a solid model with critical dimensions, preliminary experiments and finite element model and analysis.

2.2.1 Solid model

As described above, the device consists of three layers, namely, a stiff polymer top layer with sealing bosses, an elastomeric membrane with a control pocket and a stiff polymer bottom layer with a flow microchannel. Specifications of the final microvalve dimensions are shown in Section 4.1.1. Below, we discuss in more detail some of the design considerations.

The microvalve is actuated by the application of pneumatic pressure onto a microvalve membrane which deflects the membrane into a flow microchannel

blocking the flow. Through the course of this investigation, it has been found that the deflection of the membrane is a function of:

1. Clamping pressure
2. Fluid pressure inside flow microchannel
3. Pneumatic pressure
4. Width and shape of microchannel
5. Microchannel depth
6. Elastic modulus of membrane
7. Membrane thickness
8. Control channel width

2.2.1.1 Clamping pressure

Clamping pressure is the global apparent pressure applied to hold or secure the three layers tightly together to prevent movement or separation through the application of internal fluidic pressure. Clamping pressure is regulated by the amount of torque applied on the clamping screws. Local clamping pressure is controlled by the size and placement of sealing bosses. Local clamping pressure must be higher than the pressure of the liquid flowing though the microchannel and the pneumatic pressure within the control pocket (or channel). If the clamping pressure applied is high, then the sealing boss may greatly deform the elastomeric membrane resulting in the partial deflection of the membrane into the flow microchannel and causing the fluid pressure inside the microchannel to increase. If the clamping force applied is too small, then the device will leak.

2.2.1.2 Fluid pressure inside flow microchannel

The flow pressure is the pressure at some point within the liquid flowing through the microchannel. The flow pressure is dependent upon the length and width of the microchannel, flow rate of the water flowing through the microchannel and the amount of backpressure from further down the microchannel system. Under laminar

flow conditions, the fluid pressure drop [31] across the microchannel is given as shown in Equation (14).

$$\Delta P = \frac{128\mu LQ}{\pi * D^4} \qquad (14)$$

where L is the length of the microchannel (m), Q is volumetric flow rate within the flow microchannel (ml/min), μ is absolute viscosity (Poise) and D is the flow microchannel hydraulic diameter (m).

The flow pressure has to be less than the clamping pressure in order to prevent fluid leakage. The higher the flow pressure, the higher will be the pneumatic pressure required to deflect the elastomeric membrane into the microchannel to block the flow.

2.2.1.3 Pneumatic pressure

Pneumatic pressure is the air pressure applied to the control channel in the elastomeric membrane to deflect the membrane into the microchannel. The membrane acts as a proportional flow control and shut off microvalve. The higher the fluid pressure, the higher will be the pneumatic pressure required to actuate the microvalve. Pneumatic pressure is also dependent upon the shape of the microchannel. If the microchannel cross-section is rectangular, then the membrane when deflected may not completely seal the corners of the microchannel. The membrane can completely seal a microchannel with a round bottom profile.

The amount of pneumatic pressure is also dictated by the depth of the microchannel. Higher pneumatic pressure is required for microchannels with greater microchannel depths. Modulus of elasticity and thickness of the membrane at the microvalve are also other important factors that control the pneumatic pressure. From plate mechanics, we know that the stiffness of the membrane increases as the elastic

modulus of the membrane increase. This requires higher pneumatic pressure at the microvalve to deflect the membrane into the microchannel to block the flow. The width of the control channel in the elastomeric membrane is another important factor that governs the pneumatic pressure. If the width is too small, then higher pneumatic pressure is required for the air to flow through the control channel.

To summarize, the flow pressure must be less than the clamping pressure and the pneumatic pressure and pneumatic pressure must be less than the local clamping pressure.

2.2.1.4 Width and shape of microchannel

Pneumatic pressure is also dependent upon the shape of the microchannel. As mentioned, if the microchannel has a rectangular shape, then the membrane may not completely seal in the corners of the microchannel when the pneumatic pressure is applied. If the width of the microchannel is too small (i.e. less than 70 μm), then the membrane may require a higher pneumatic pressure to completely deform into the microchannel to block the flow.

2.2.1.5 Microchannel depth

The microvalve deflection is directly dependent upon depth of flow microchannel. As the depth of the microchannel increases, the pneumatic pressure required to deflect the membrane also increases.

2.2.1.6 Elastic modulus of membrane

Modulus of elasticity of the membrane is also one of the important factors that control the pneumatic pressure. As explained earlier, higher pneumatic pressure is

required for membrane with higher elastic modulus to deflect into the microchannel and block the flow. If the membrane is not very stiff, then the membrane will deform into the flow microchannel when the clamping pressure is applied distorting the microchannel. This will result in an increase in flow pressure of the liquid to flow through the microchannel.

2.2.1.7 Membrane thickness

As explained earlier, the stiffness of the membrane is proportional to the thickness of the membrane which requires a higher pneumatic pressure to block the flow. One way to reduce the stiffness of the membrane for microvalve deflection is to mold a control channel feature within the membrane in order to locally reduce the thickness of the membrane.

2.2.1.8 Control channel width

The width of the control channel in the elastomeric membrane is another important factor governing the pneumatic pressure. If the width of the control channel is significantly less than the length of the control channel, then the width of the control channel plays a significant role in defining the stiffness of the microvalve membrane. The width of the control channel should be greater than the width of the microchannel and is constrained by the width of the microchannel.

As the width of the control channel decreases, there is a corresponding increase in the microvalve deflection of the PDMS membrane. This is due to the effect of Poisson's ratio. This effect is illustrated in Figure 2.1 (b). As the control channel width increases, there is less material to compress and deform into the control channel yielding less deformation in the microvalve area.

2.2.2 Preliminary experiments

Preliminary experiments were conducted to study the feasibility of the microvalve architecture. Details of this investigation are given in Appendix A. A device was built without sealing bosses to study the characteristics of the microvalve. The experiments failed as a result of fluid leakage and membrane deflection into the flow microchannel. A second device was built with sealing bosses to better manage the distribution of pressure within the device. Leakage was eliminated and the microvalve was able to cut-off the flow of water within the microchannel when actuated. However, flow of fluid through the microchannel caused the PDMS membrane to deflect upward since there was a gap between the PDMS membrane and top lamina. The fluid also leaked outside the microchannel because there was a distance of ~1 mm from the edges of microchannel to the sealing bosses. To keep the fluid within the microchannel, it was recognized that the location and size of the sealing bosses were important.

Rather than to continue conducting empirical studies, an effort was made to use preliminary results to validate a FEM that could be used to determine a feasible space for meeting microvalve architecture requirements.

2.2.3 Finite element model

Finite element analysis and model (FEM/FEA) was performed to investigate three main microvalve requirements:

1. After applying clamping pressure but before applying flow pressure, determine a feasible set of parameter conditions which does not deflect the elastomeric membrane into the flow microchannel while conformally sealing the microchannel
2. After applying clamping pressure and introducing flow but before actuating the microvalve, determine a feasible set of parameter conditions which will maintain lamina/membrane conformality

adjacent to the microchannel (i.e. flow must stay inside the microchannel); and
3. After applying clamping pressure, flow pressure and pneumatic pressure, determine a feasible set of parameter conditions which will allow the membrane to deflect into the flow microchannel to stop the flow.

In particular, the location and size of the sealing bosses were critical in these analyses. FEM was also performed to determine the minimum clamping pressure required to precisely compress the PDMS elastomer enough to seal the flow microchannels against the operating pressure and not to overcompress it to the point that the PDMS elastomer deflected into the flow microchannels. COSMOSWorks 2007 software was used to perform FEA and Statgraphics Centurion XV software was used to perform statistical regression analysis on the results obtained from the FEM.

Development of the FEM in structural mechanics is usually based on an energy principle such as the virtual work principle or the minimum total potential energy principle. In general, there are three phases in any FEA [33]:

- Pre-processing: defines the FEM and environmental factors to be applied to it
- Analysis solver: defines a solution of FEM
- Post-processing: processes the results using visualization tools

Pre-processing

Pre-processing is the first step in using FEA [33]. Here a FEM of the structure to be analyzed is constructed. The input of a topological description of the structure's geometric features is required in most FEA packages. Once the finite element geometric model has been created, a meshing procedure is used to define and break up the model into small elements. In general, a FEM is defined by a mesh network, which is made up of the geometric arrangement of elements and nodes. Nodes represent points at which calculations are made. FEA packages use node numbers to serve as an

identification tool in viewing solutions in structures such as deflections. Elements are bounded by sets of nodes, and define localized mass and stiffness properties of the model. Elements are also defined by mesh numbers, which allow references to be made to corresponding deflections or stresses at specific model locations.

Analysis solver

The next stage of the FEA process is analysis. This stage is also known as computation of solution. The FEM conducts a series of computational procedures involving applied forces, and the properties of the elements which produce a model solution. Such a structural analysis allows the determination of effects such as deformations, strains, and stresses which are caused by applied structural loads such as force, pressure and gravity.

Post-processing

This stage is also known as visualization. These results can then be studied using visualization tools within the FEA environment to view and to fully identify implications of the analysis. Numerical and graphical tools allow the precise location of data such as stresses and deflections to be identified. Two types of modules were available to perform FEA in COSMOSWorks based on material properties.

- Linear module
- Non-linear module

Linear module

Linear analysis is based on the linearity assumption [32]. Below are few linearity assumptions:

- All the materials in the model obey Hook's law, where stress is directly proportional to strain. As the strains increase, the stress-strain relationships become nonlinear.
- The induced displacements are small enough so that the change in the stiffness caused by loading can be ignored.
- Boundary conditions do not vary during the application of loads. Loads must be constant in magnitude, direction, and distribution.

Non-linear module

A major source of nonlinearities is due to the effect of large displacements on the overall geometric configuration of structures. Structures undergoing large displacements can have significant changes in their geometry due to load-induced deformations which can cause the structure to respond nonlinearly in stiffening and/or a softening manner.

Another important source of nonlinearities stems from the nonlinear relationship between the stress and strain which has been recognized in several structural behaviors. Figure 2.6 illustrate an example of linear and non-linear stress-strain relationships. Several factors can cause the material behavior to be nonlinear. The dependency of the material stress-strain relation on the load history (as in plasticity problems), load duration (as in creep analysis), and temperature (as in thermo-plasticity) are some of these factors. For nonlinear problems, the stiffness of the structure, the applied loads, and/ or boundary conditions can be affected by the induced displacements.

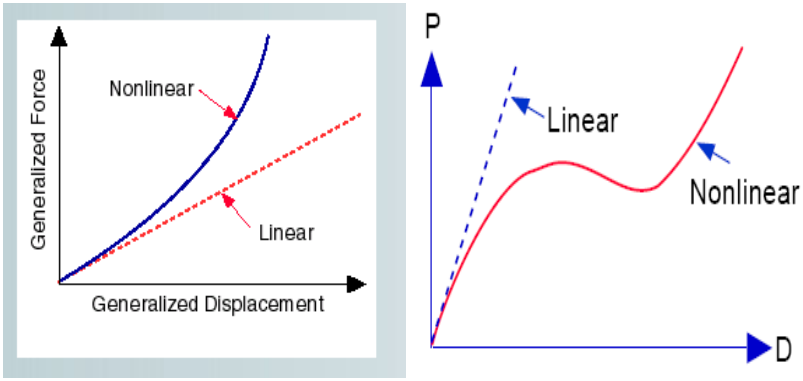

Figure 2.6. Stress-strain for linear and nonlinear material

There are several modules in COSMOSWorks that can be used to perform FEA based on the material properties.

1. Elasticity
    a) Linear elasticity
    b) Nonlinear elasticity
2. Hyperelasticity
    a) Mooney-Rivlin model
    b) Ogden model
    c) Blatz-Ko model
3. Plasticity
    a) Huber-von Mises yield criterion with isotropic or kinematic hardening rules
    b) Tresca-Saint Venant yield criterion with isotropic or kinematic hardening rules
    c) Drucker-Prager elastic-perfectly plastic model
4. Visco-elasticity
    a) Generalized Maxwell's model

The device is made of polycarbonate and PDMS elastomeric membrane. Since PDMS is hyperelastic, a hyperelastic material model was needed to model the large deformations. The elastomeric membrane was assumed to be nonlinear elastic, isotropic, and incompressible. The finite element formulation for such materials has numerical difficulties due to incompressibility. One way to deal with this inside hyperelastic models is to use a penalty method, based on the introduction of

compressibility to the strain energy density function, to assemble additional degrees of freedom into a global stiffness matrix.

The Mooney-Rivlin model was used to perform the FEA. The Mooney-Rivlin strain energy density function is given in Equations (15), (16) and (17) [32]. The material properties required for Mooney-Rivlin include Poisson's ratio and up to six Mooney-Rivlin constants. Poisson's ratio and two Mooney-Rivlin material constants for the PDMS elastomer were obtained from the literatures [1, 34, 35, and 36]. An extrapolation was made to determine the Mooney-Rivlin material constants for 10:1 and 18:1 monomer-to-crosslinker ratio PDMS membranes. The material properties for the polycarbonate are defined from the COSMOSWorks material library.

$$w_1 = A(I - 3) + B(II - 3) + X(\frac{1}{III^2} - 1) + Y(III - 1)^2 \quad (15)$$

$$w_2 = C(I - 3)(II - 3) + D(I - 3)^2 + E(II - 3)^2 + F(I - 3)^3 \quad (16)$$

$$w = w_1 + w_2 \quad (17)$$

where *I, II,* and *III* are invariants of the right Cauchy-Green deformation tensor and can be expressed in terms of principal stretch ratios; *A, B, C, D, E,* and *F* are Mooney material constants.

FEA was performed to achieve the three modeling requirements. The FEA model was developed using the Mooney-Rivlin method and validated using preliminary data. Quarter portion of the device was considered to run the analysis in order to reduce the computation time. Symmetric boundary conditions were applied on all symmetric planes. The mesh size was set to 50 μm for smaller dimensions and 1 mm for larger dimensions. Details of this modeling effort can be found in Appendix E.

2.2.3.1 Investigation of Requirement 1

An initial screening experiment was conducted to investigate the effect of the different parameters on the conformal sealing of the microchannel by the PDMS elastomeric membrane while minimizing the deflection of the microvalve or membrane into the microchannel. The least stiff membrane condition was chosen to simulate worse case conditions for deflecting the membrane into the microchannel. The width, depth and length of the microchannel were fixed based on the literatures [20, 21]. Screening experiments showed that the following parameters were less critical for Requirement 1 and that a feasible set of conditions were found to be at:

1. Monomer-to-crosslinker ratio (CR) = 18:1
2. Width of flow microchannel (W_f) = 310 μm
3. Depth of flow microchannel (D_f) = 150 μm (with round bottom)
4. Length of control channel (L_c)= 500 μm
5. Width of control channel (W_c) = 310 μm
6. Distance between boss ($Dist_b$) = 320 μm
7. Membrane thickness (T_m) = 150 μm
8. Microvalve thickness (T_v) = 30 μm

Based on the screening experiment, load conditions for this requirement were set as follows:

1. Clamping pressure (P_c) = 40 psi
2. Flow pressure (P_f) = 0 psi
3. Pneumatic pressure (P_p) = 0 psi

Based on this screening study, boss size was found to be important for meeting the first requirements of the microvalve architecture. Therefore, a parametric study of the boss width and height was performed to explore the effect of machining tolerances. The range of sealing boss sizes explored in this study was based on knowledge gained from preliminary experiments and machining constraints. The following ranges were investigated:

1. Boss width (W_b) = 150, 200, 250, 300 and 500 μm

2. Boss height (H_b) = 25 and 50 μm

Evaluation of deflection of the PDMS membrane into the flow microchannel was performed by a factional factorial design. The design consists of two factors W_b and H_b respectively and W_b had 5 levels and H_b had two levels. The amount of deflection of PDMS membrane into the flow microchannel is tabulated in Table 2.1. Statgraphics software was used to perform the regression analysis for the above results. The details of regression analysis are included in Appendix E. The equation of the fitted model is given in Equation (18). The detail FEA results are included in Appendix E.

Table 2.1. Deflection of PDMS membrane into flow microchannel

Deflection of PDMS membrane into flow microchannel (Def $_{m\_f}$) (μm)		**W_b (μm)**				
		150	***200***	***250***	***300***	***500***
H_b (μm)	***25***	31	21	19.01	17	11.38
	50	26.952	20.7	19.13	17	11.38

$$Def_{m\_f} = 48.3957 - 0.153933*W_b - 0.033296*H_b + 0.000165385*W_b^2 \quad (18)$$

Results show that an increase in the width of the boss reduces the deflection of the PDMS membrane into the flow microchannel. This is because the increase in surface area of the boss decreases the local clamping pressure adjacent to the microchannel. Results also showed that an increase in boss height reduces the deflection of PDMS membrane into flow microchannel. This is because an increase in the boss height leads to an increase in the space between the top lamina and the PDMS membrane. This space gives the PDMS membrane more room to deform upward away from the microchannel. Further, a reduced boss height distributes more of the

clamping pressure over the microchannel resulting in a deflection of PDMS membrane into flow microchannel

2.2.3.2 Investigation of Requirement 2

The second requirement was investigated by adding the flow pressure and evaluating the gap between the PDMS membrane and flow lamina. Similar to the approach to evaluating the first requirement, a screening experiment was conducted. The gap between the PDMS membrane and the flow lamina was found to be dependent upon the boss width, boss location, microvalve thickness, membrane thickness, and control channel width and length. Consequently, a parametric study was conducted by fixing the following parameters:

1. Monomer-to-crosslinker ratio (CR) = 18:1
2. Width of flow microchannel (W_f) = 310 μm
3. Depth of flow microchannel (D_f) = 150 μm (with round bottom)
4. Length of control channel (L_c)= 500 μm
5. Distance between bosses ($Dist_b$) = 320 μm
6. Boss height (H_b) = 25 μm

The load conditions for this requirement were as follows:

1. Clamping pressure (P_c) = 40 psi
2. Flow pressure (P_f) = 20 psi
3. Pneumatic pressure (P_p) = 0 psi

The study parameters were evaluated across the following ranges:

1. Boss width (W_b) = 150, 200, 250, 300 and 500 μm
2. Width of control channel (W_c) = 310 and 350 μm
3. Membrane thickness (T_m) = 150 and 200 μm
4. Microvalve thickness (T_v) = 30 and 50 μm

In order to keep the size of the analysis manageable, three parametric studies were used to evaluate the effect of these parameters on the gap between the PDMS membrane and flow lamina. Detailed results are included in Appendix E.

Parametric Study 1

Parametric study 1 evaluated the effect of two factors T_v and W_b on the second requirement with two levels for T_v and five levels for W_b. The results are tabulated in Table 2.2. Regression analysis is formed and Equation (19) describes the fitted model.

Table 2.2. Determination of gap between the PDMS membrane and flow lamina for varying W_b and T_v

Gap between membrane and flow lamina (Dist $_{f\_m}$) (μm)		**W_b (μm)**				
		150	***200***	***250***	***300***	***500***
T_v (μm)	***30***	0	.002	2.34	10.42	12.98
	50	0	0	0	3.822	13.15

$$Dist_{f\_m} = -3.65664 - 0.0877*T_v + 0.040843*W_b \quad (19)$$

From the above table it is clear that an increase in microvalve thickness results in an increase in stiffness of the microvalve, which results in decrease in the gap between the flow lamina and the microvalve at the edge of the microchannel. Alternatively, distance between flow lamina and microvalve at the edge increases with increase in boss width because not enough local clamping pressure is applied to form a conformal seal between the microvalve and the flow lamina at the edge.

Parametric Study 2

Parametric study 2 had two factors T_m and W_b with T_m at two levels and W_b at five levels. The results are tabulated in Table 2.3. Regression analysis was performed and Equation (20) describes the fitted model. From Table 2.3, it is clear that an increase in the boss width and a decrease in membrane thickness results in an increase

in the gap between the flow lamina and microvalve at the edge of the microchannel. As the membrane thickness increase, the stiffness of the membrane increases and prevents the upward deflection of membrane. Therefore, the distance between the membrane and flow lamina decrease with increase in membrane thickness.

Table 2.3. Determination of gap between the PDMS membrane and flow lamina for varying W_b and T_m

Determination of Gap between membrane and flow lamina (Dist $_{f\_m}$) (μm)		**W_b (μm)**				
		150	***200***	***250***	***300***	***500***
T_m	***150***	0	0	0	3.822	13.15
(μm)	***200***	0	0	0	1.87	10.94

$$Dist_{f\_m} = -4.49072 - 0.016648*T_m + 0.0370797*W_b \quad (20)$$

Parametric Study 3

Parametric study 3 had two factors W_c and W_b with W_c at two levels and W_b at five levels. The results are tabulated in Table 2.4. Equation (21) describes the fitted regression model. The membrane is less stiff at the microvalve. If the size of the control channel width is close to the size of microchannel width, then the membrane is less deflected in the upward direction due to its stiffness. Therefore, the microvalve will deflect in the upward direction as the width of the control channel increase, which results in an increase in gap between the flow lamina and microvalve at the edge. One can conclude that the gap between the flow lamina and the microvalve at the edge of the microchannel has a direct linear relationship with boss width and control channel width.

Table 2.4. Determination of gap between the PDMS membrane and flow lamina for varying W_b and W_c

Gap between membrane and flow lamina (Dist $_{f\_m}$) (μm)		W_b (μm)				
		150	***200***	***250***	***300***	***500***
W_c (μm)	***310***	0	0.002	2.34	10.42	12.98
	350	3.892	5.524	5.13	10.19	10.09

$$Dist_{f\_m} = -17.208 + 0.0295579*W_b + 0.04542*W_c \quad (21)$$

None of the parametric studies showed any interaction with the boss width in affecting the gap between the membrane and the bottom lamina. Consequently, it was found that microvalve thickness and membrane thickness affect the gap as expected per plate mechanics. At the levels used, the control channel dimensions seemed to give results contrary to plate mechanics. Upon investigation it was found that as the control channel widens, less material is available for interaction with the sealing boss causing less material to deform into the microchannel at greater widths. The same is true for the control channel length where less material is available to interact with the top lamina. Consistent with the first set of results, it was found that the gap between the membrane and the top plate increased with increasing boss width due to decreasing local clamping pressures. A set of feasible parametric conditions were found which satisfied requirements 1 and 2.

2.2.3.3 Investigation of Requirement 3

The third requirement was investigated by including pneumatic pressure along with clamping pressure and flow pressure in deflecting the microvalve membrane. A screening analysis was performed to determine which parameters significantly

affected microvalve deflection. The following parameters were determined based on the results of the studies associated with the first two requirements:

1. Width of flow microchannel (W_f) = 310 μm
2. Depth of flow microchannel (D_f) = 150 μm (with round bottom)
3. Boss width (W_b) = 150 μm
4. Boss height (H_b) = 25 μm
5. Width of control channel (W_c) = 310 μm
6. Distance between boss (Dist b) = 320 μm
7. Membrane thickness (T_m) = 150 μm

The following load conditions were set:

1. Clamping pressure (P_c) = 40 psi
2. Flow pressure (P_f) = 20 psi
3. Pneumatic pressure (P_p) = 25 psi

The following were found to be study parameters:

1. Monomer-to-crosslinker ratio (CR) = 18:1 and 10:1
2. Length of control channel (L_c)= 500 and 600 μm
3. Microvalve thickness (T_v) = 30 and 50 μm

As expected, microvalve deflection was found to be dependent upon the microvalve thickness, control channel dimensions and elastic modulus which in turn are dependent upon the monomer-to-crosslinker ratio. Two parametric studies were conducted to evaluate in any interactions in the effects on microvalve deflection.

Parametric Study 1

Parametric study 1 had two factors T_v and L_c with L_c at two levels and T_v at two levels. The results are tabulated in Table 2.5. Equation (22) describes the fitted model of the regression analysis. Microvalve deflection increases with a decrease in microvalve thickness. The control channel length seems to have little effect.

Table 2.5. Determination of microvalve deflection for varying T_v and L_c

Determination of microvalve deflection (Def $_v$) (μm)		L_c	
		500	***600***
T_v	***30***	165.6	161.9
	50	140.7	150.3

$$Def_v = 174.9 + 0.0295*L_c - 0.9125*T_v \quad (22)$$

Parametric Study 2

Parametric study 2 had two factors CR and L_c with CR at two levels and L_c at two levels. The results are tabulated in Table 2.6. Equation (23) describes the fitted model of the regression analysis. From the results, it is clear that the microvalve deflection increases as the elastic modulus of the membrane decreases. The control channel length seems to have had little effect. Figure 2.7 shows an exploded view of the microvalve deflection when a pneumatic pressure is applied.

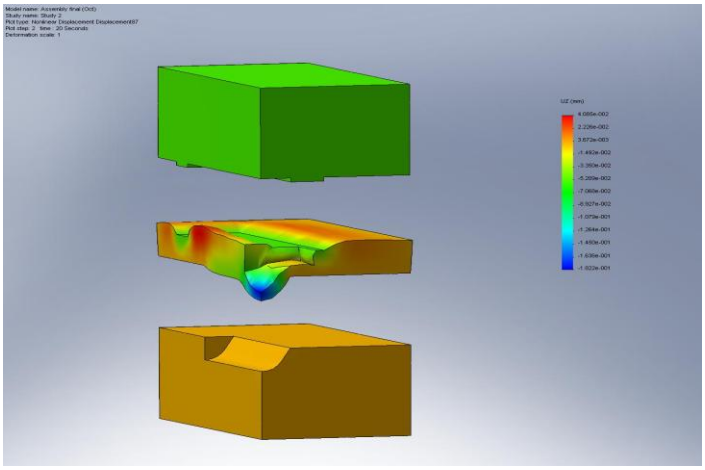

Figure 2.7. Exploded view of microvalve deflection when pneumatic pressure is applied

Table 2.6. Determination of microvalve deflection for varying CR and L_c

Determination of microvalve deflection (Def_v) (μm)		**L_c**	
		500	***600***
CR	***18:1***	165.6	161.9
	1:10	125.6	126.6

$$Def_v = 86.4625 + 4.70625*CR - 0.0135*L_c \quad (23)$$

Neither parametric study showed any interaction with the control channel length in affecting the microvalve deflection. Consequently, it was found that microvalve thickness and monomer-to-crosslinker ratio both affected the gap as expected per plate mechanics with the length of the control channel showing little effect.

2.2.3.4 Findings from finite element analyses

Based on these three sets of studies, a final set of critical dimensions were determined to permit microvalve operation as follows:

1. Width of flow microchannel = 310 μm
2. Depth of flow microchannel = 150 μm
3. Boss width = 150 μm
4. Boss height = 25 μm
5. Distance between bosses = 355 μm

To exercise the design space of this microvalve design, an experiment was designed with high and low values. To simplify execution of the experiment, it was decided that the variables would all be associated with the membrane. According to the FEA results, the microvalves should work across the following ranges:

1. Control channel width = 330 to 630 μm
2. Control channel length = 470 to 630 μm
3. Monomer-to-crosslinker ratio = 10:1 to 18:1

3 CHAPTER 3. EXPERIMENTAL VALIDATION

This chapter includes three sections: 1) experimental design; 2) experimental setup; and 3) experimental protocol.

3.1 Experimental design

The final device was fabricated based on the dimensions obtained from FEA. The width of the flow microchannel was ~330 μm, depth of microchannel was ~150 μm with a round bottom profile and length was ~30 mm. The width of the sealing boss was ~188 μm, height was ~ 26 μm and distance between the bosses was ~343 μm. In the final experiment, a design of experiment was made with a 2^2 fractional factorial design which had two factors and each factor had two levels as shown in Table 3.1 and Figure 3.1. The microvalves were characterized, based on effect of monomer-to-crosslinker ratio and width and length of the control channel. PDMS membranes with 10:1 and 18:1 monomer-to-crosslinker ratio were used to run the experiments. Two membranes with two control channel dimensions were used. One of the control channel dimension had a larger width and length and another had relatively smaller width and length. The larger control channel dimensions were width = ~618 μm and length = ~616 μm and smaller dimension were width = ~330 μm and length = ~470 μm. The average thickness of the PDMS membrane was 205 μm and accordingly the average microvalve thickness was 70 μm. The flow rate of the water flowing in the microchannel varied from 0.1 ml/min to 0.502 ml/min. Four elastomeric membranes as described in Table 3.1. were used for the experiments and the cut-off pneumatic pressure was measured for the above flow rates of water.

Table 3.1. Fractional factorial design

To Determine Cut-off Pneumatic Pressure		*Monomer-to-Crosslinker Ratio*	
		10:1 (+)	18:1 (-)
Control Channel Dimensions	Width=618 µm & Length=616 µm (+)	***(+),(+)***	***(-),(+)***
	Width=330 µm & Length=470 µm (-)	***(+),(-)***	***(-),(-)***

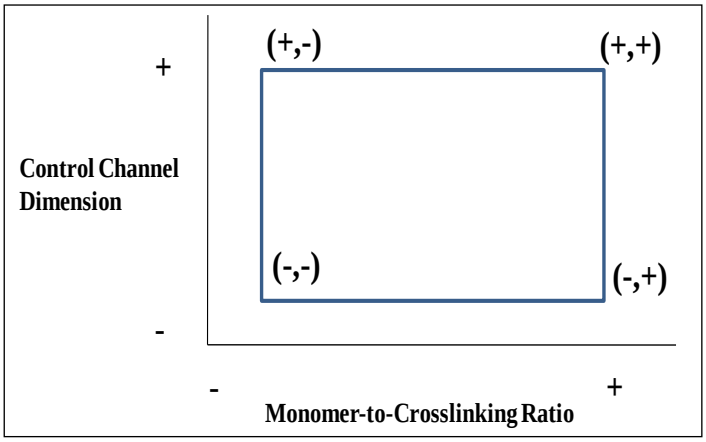

Figure 3.1. Fractional factorial design

3.2 Experimental setup

The flow and microvalve experiments were conducted using a flow test loop set up as diagramed in Figures 3.2 [31] and 3.3. Colored water was used as the fluid flowing in the microchannel and was pumped into the device by a peristaltic pump. The flow rate was controlled and read on the display panel on the pump. The fluid pressure was calculated manually based on the flow rate and the fluid pressure equation [31] is illustrated in Equation (24).

$$\Delta P = \frac{128\mu LQ}{\pi D^4} \qquad (24)$$

where ΔP is the pressure drop across the flow microchannel (psi), μ is the viscosity of the liquid (Ns/m^2), L is the length of the flow microchannel (m), Q is the flow rate of the liquid (ml/min) and D is the microchannel hydraulic diameter (m) of flow microchannel.

Pneumatic pressure was controlled with a pressure regulator (Omega, PRG101-120), precision of 0.25% and measured with pressure gauge (Omega, DPG1000B-100G). The flow rate relative to actuation pressure was noted and compared to theoretical flow rates calculated with Equation (24).

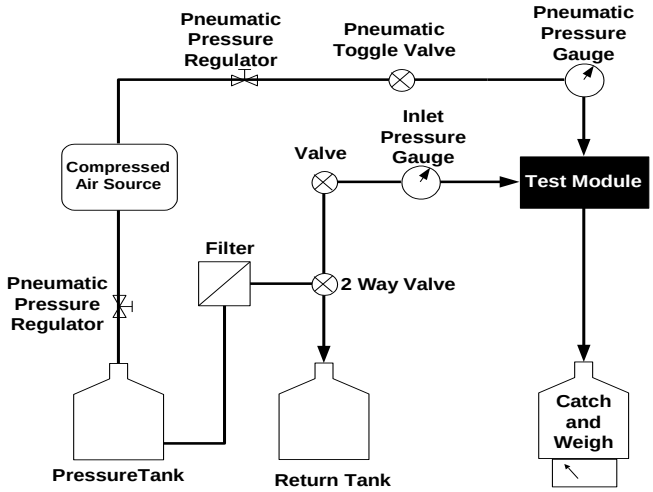

Figure 3.2. Flow loop setup

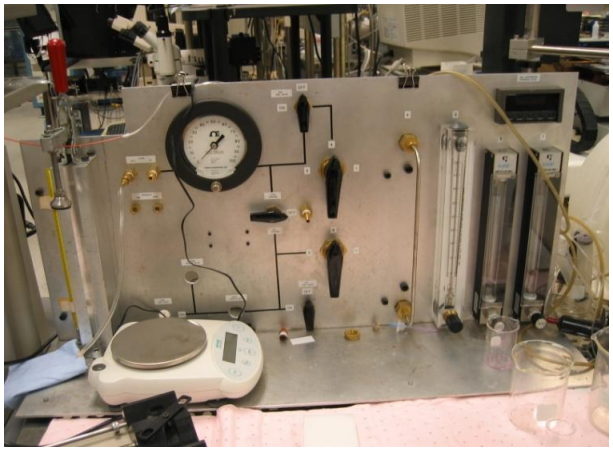

Figure 3.3. Flow loop system

The top and the bottom substrates were aligned with the help of alignment pins and all the three substrates were clamped together by clamping screws. Appropriate torque was applied on the clamping screws to achieve appropriate clamping pressure. Nanoports were used as interconnectors on the device to connect the PEEK tubings to the inlets and outlet. The tubing connected to the water inlet was mounted around the

wheel of the peristaltic pump to pump the water as soon as the wheel started to rotate. The flow rates were controlled by using the arrows on the pump to either increase or reduce the flow rate. PEEK tubing connected to the water output was placed under the microscope to visually observe when the flow of water was stopped. The pneumatic pressure was controlled by the LabVIEW interface. The experimental set up is shown in Figure 3.4.

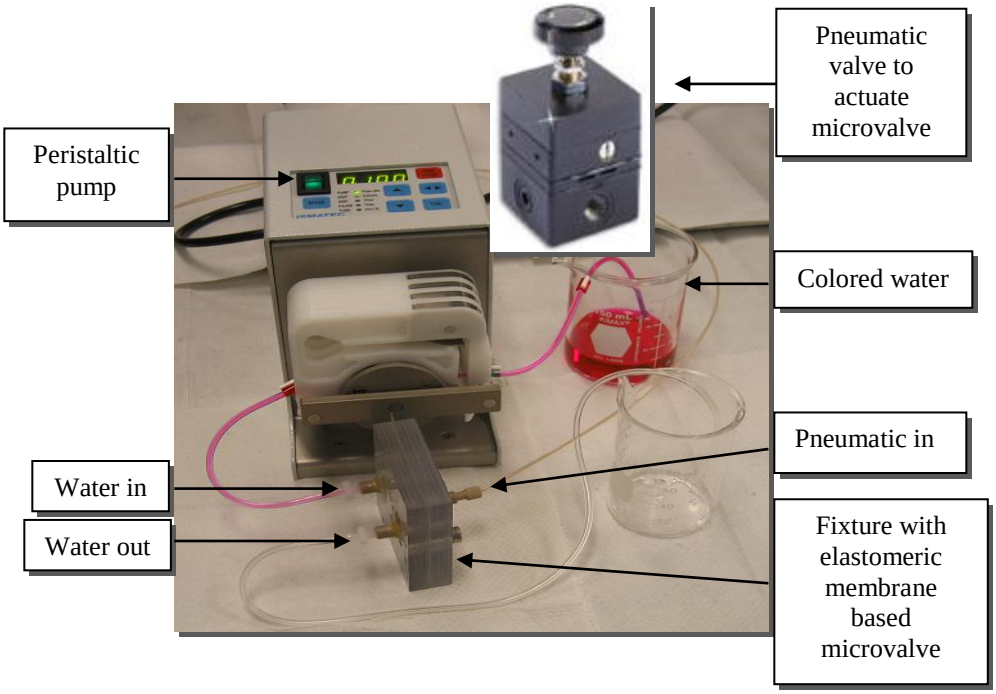

Figure 3.4. Experimental test setup

As the water was flowing, pneumatic pressure was applied to actuate the microvalve. The pneumatic pressure on the pressure regulator was increased until no fluid flow was observed visually through the output tubing under the microscope. The flow rate was then increased and appropriate pneumatic pressure was applied to actuate the microvalve and block the water flow. The flow rate and the cut-off pneumatic pressure at which the microvalve was actuated to block the flow were recorded. Experiments were repeated with PDMS membranes of 18:1 and 10:1

monomer-to-crosslinker ratio with varying length and width of the control channel. The results are shown in Chapter 4.

3.3 Experimental protocol

As explained in Chapter 2 (2.1.1), the device consist of three substrates, two polycarbonate substrates and a PDMS elastomeric membrane as shown in Figure 3.5. The polycarbonate top and bottom substrates are cleaned with isopropanol and air dried with the blower. Four PDMS membranes are casted as described in Appendix F. The PDMS membrane is carefully peeled off from the electroformed mold. One of the membranes is placed over the bottom polycarbonate substrate and the control channel on the membrane is then aligned along the microchannel on the bottom substrate and inlet pneumatic hole that is on the top polycarbonate substrate. The alignment is made under optical microscope. Clamping holes are made on the membrane using needle. The three layers are held together and clamped by clamping screws into the device.

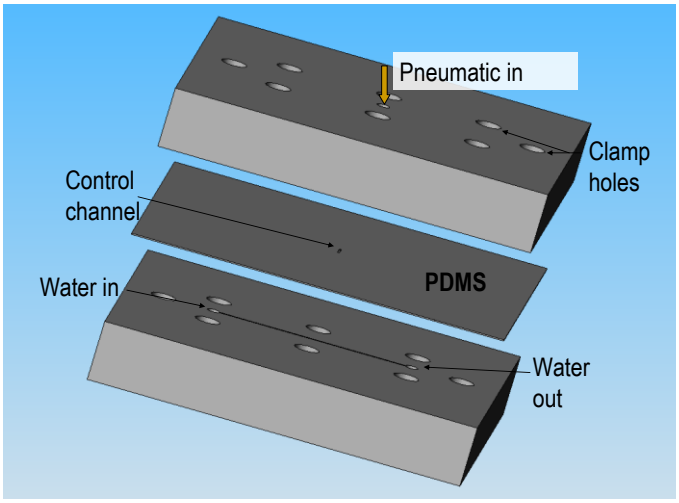

Figure 3.5. Exploded view of device

As the clamping pressure is applied to hold the substrates together, the membrane is squeezed in between the top and bottom polycarbonate substrates. Higher clamping pressure can deform the membrane into the microchannel and can distort the microchannel. If lower clamping pressure is applied, then the fluid may leak outside the microchannel when a higher fluid pressure is applied. Therefore, appropriate clamping pressure is necessary to prevent microchannel distortion and fluid leakage. The determination of appropriate clamping pressure is described in Appendix C. Torque screw driver is used to apply appropriate torque that results to 40 psi clamping pressure.

The nanoports and the PEEK tubings are connected as described in Section 3.2. Peristaltic pump and pneumatic valve is used to inject water and air respectively into the device as described in Section in 3.2. LabVIEW interface is used to control the application of pneumatic pressure to actuate the microvalve and is described in detail in Appendix D. The delay time in the LabVIEW is set to 0.3 sec, which implies that the pneumatic pressure is applied for 0.3 sec and released for 0.3 sec. The flow rate applied on the peristaltic pump is varied from 0.1 to 0.502 ml/min. 0.1 ml/min flow rate is first applied and the pneumatic pressure of 5 psi is applied. The pneumatic pressure on the main pressure valve is gradually increased until the microvalve is completely deflected into the microchannel to block the flow. The flow rate and the cut-off pneumatic pressure are recorded. The flow rate is increased and appropriate cut-off pneumatic pressure is applied. The experiments are repeated for remaining flow rates. The flow rates and the cut-off pressure are tabulated in Appendix I.

The device is then disassembled and the above procedure is followed to sandwich the remaining PDMS membranes one after the other and run the experiments. All the results are shown in Appendix I.

4 CHAPTER 4. RESULTS AND DISCUSSION

The microvalve architecture was characterized by measuring the cut-off pneumatic pressure and the flow rate by varying several parameters as described below. This chapter can be broken down into two sections: final experiments and design rules and tolerance analysis.

4.1 Final experiments

This section can be broken down into three parts,

1. Test results of microvalves
2. Comparison of pressure drop across the microchannel
3. Comparison of final experimental results with numerical results

4.1.1 Test results of microvalves

Preliminary results showed that sealing bosses could be used to seal the microchannel from the outside environment. However, these early tests also showed the need to position the bosses to keep the fluid flow within the microchannel with minimal microchannel distortion. Based on FEA results in Chapter 2, the final experiments were conducted using the following parameters:

Fixed parameters

1. Flow microchannel dimensions: Width = 330 µm, Depth = 150 µm and Length = 30 mm
2. Boss dimensions: Width = 188 µm, Height = 26 µm and Distance between bosses = 343 µm
3. Average PDMS membrane thickness = 205 µm
4. Average valve thickness = 70 µm
5. Clamping pressure = 40 psi

Variable parameters

1. Monomer-to-crosslinker ratio: 10:1 and 18:1
2. Control channel dimensions: Width = ~330 and ~618 µm and Length = ~470 and ~616 µm

Experimental parameters

1. Flow rate: 0.1 ml/min to 0.502 ml/min, accordingly pressure drop across the microchannel = ~0.14 psi to ~0.7 psi

A 2^2 fractional factorial design was used to exercise the feasible design space for the microvalve design (Table 4.1). Four PDMS elastomeric membranes were casted with two of membranes at 10:1 monomer-to-crosslinker ratio and two at 18:1 monomer-to-crosslinker ratio. The control channel dimensions and the membrane and microvalve thickness are shown in Table 4.2.

Table 4.1. Fractional factorial design

To Determine Cut-off Pneumatic Pressure		*Monomer-to-Crosslinker Ratio*	
		10:1 (+)	18:1 (-)
Control Channel Dimensions	Width=618 µm & Length=616 µm (+)	***(+),(+)***	***(-),(+)***
	Width=330 µm & Length=470 µm (-)	***(+),(-)***	***(-),(-)***

Table 4.2. Four membranes used for final experiments

CR	W_c *(μm)*	L_c *(μm)*	T_m *(μm)*	T_v *(μm)*
10:1	618	613	190	52.1
10:1	330	469	194.5	56.88
18:1	620	616	219.5	89
18:1	338	478	196	69

where, *CR* is monomer-to-crosslinker ratio, W_c is width of control channel, L_c is length of control channel, T_m is membrane thickness and T_v is microvalve thickness.

Final experiments were conducted with the four membranes as described above. The flow rate of water flowing in the microchannel was varied from 0.1 ml/min to 0.502 ml/min. The pneumatic pressure was applied to actuate the microvalve and shut-off the flow. The cut-off pneumatic pressure (the pneumatic pressure at which flow in the microchannel stopped) was recorded at each flow rate. No leakage of water outside the microchannel and the sealing bosses was observed. The cut-off pneumatic pressure and the flow rate are plotted in Figures 4.1 and 4.2 for all four membranes.

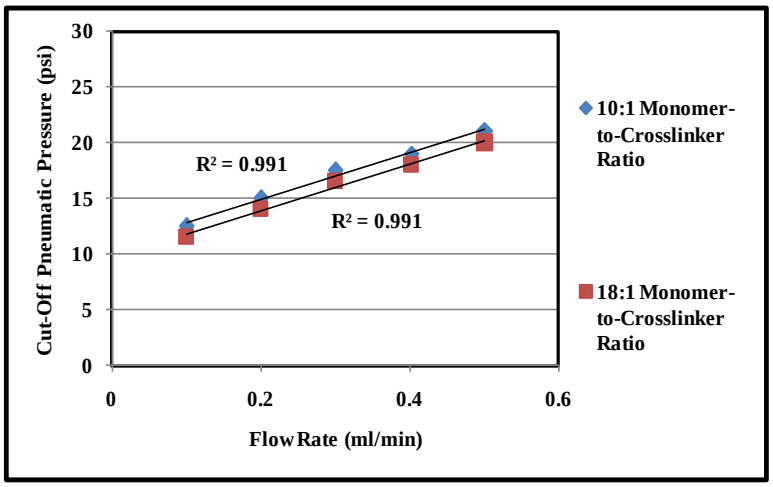

(a) Control channel width (618 μm) and length (616 μm)

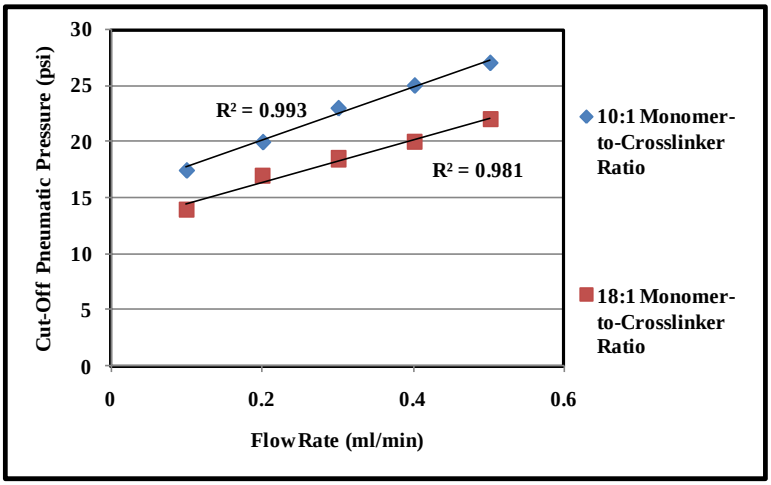

(b) Control channel width (330 µm) and length (470 µm)

Figure 4.1. Comparison of effect of flow rate on cut-off pneumatic pressure for 10:1 and 18:1 monomer-to-crosslinker ratio membranes

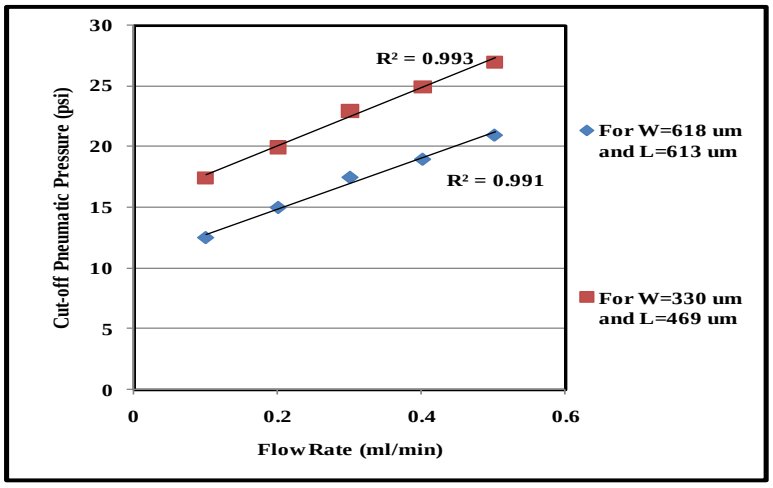

(a) 10:1 monomer-to-crosslinker ratio

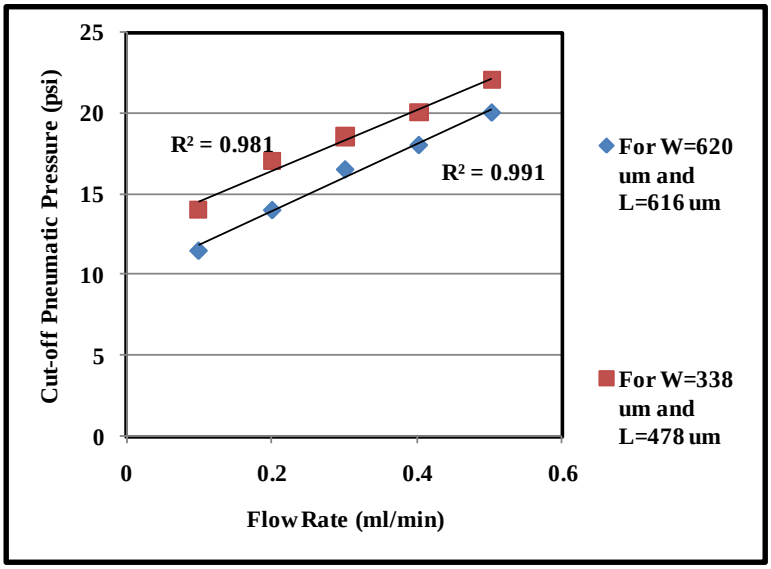

(b) 18:1 Monomer-to-crosslinker ratio

Figure 4.2. Effect of flow rate on cut-off pneumatic pressure for 10:1 and 18:1 monomer-to-crosslinker ratio for different control channel dimensions

From the graphs shown in Figures 4.1 (a) and (b), as expected, as the elastic modulus increases, the pneumatic pressure required to actuate the microvalve increases, where 10:1 monomer-to-crosslinker ratio is less elastic than the 18:1 monomer-to-crosslinker ratio. From graphs shown in Figure 4.2 (a) and (b), it is clear that the dimensions of the control channel are also important factors that determine the amount of pneumatic pressure. Again, as expected, it takes less pneumatic pressure to actuate the microvalve as the width of the control channel increases. An increase in the flow rate in the microchannel also resulted in an increase in the pneumatic pressure required to actuate the microvalve. The R-squared values for all linear regression analyses between flow rate and cut-off pneumatic pressure are close to 1.0, showing good repeatability of cut-off pneumatic pressure for a given flow rate.

4.1.2 Comparison of pressure drop across the microchannel

The pressure drop across the microchannel can be an indication of the amount of internal deformation within the microchannel. Increase in flow rate result in increase in the pressure drop across a microchannel. Therefore, the pneumatic pressure required to completely deform the membrane into the microchannel also increase. Equation (25) was used to calculate the pressure drop across the microchannel.

$$\Delta P = \frac{128\mu LQ}{\pi D^4} \qquad (25)$$

where ΔP is the pressure drop across the flow microchannel (psi), μ is the viscosity of the liquid (Ns/m^2), L is the length of the flow microchannel (m), Q is the flow rate of the liquid (ml/min) and D is the microchannel hydraulic diameter (m) of flow microchannel.

The calculated pressure drop was compared with the pressure drop measured across the microchannel using a membrane of 18:1 monomer-to-crosslinker ratio with control channel width = 627 μm and control channel length = 616 μm. A differential pressure transducer was used to measure the pressure drop across the microchannel and is explained in detail in Appendix H. The pressure drop across the microchannel was measured for flow rates from 0.1 - 0.502 ml/min. The calculated and measured pressure drops are shown in Figure 4.4. The calculated and measured pressure drops match closely with an average error of 14.29%.

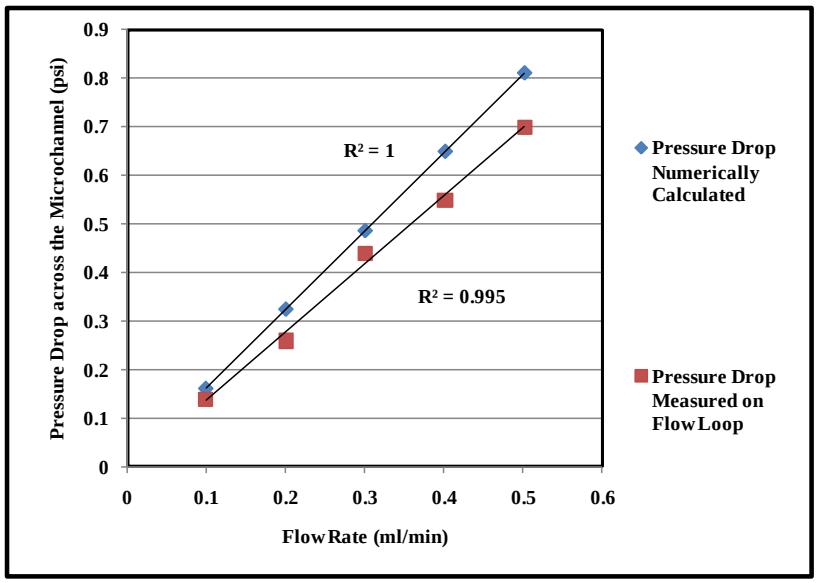

Figure 4.3. Comparison of numerically calculated and measured pressure drop of the fluid flowing in the microchannel

4.1.3 Comparison with numerical results

The final testing results were compared with results from the FEA. The three requirements of the FEA as stated in Chapter 2 (2.2.3) were:

1. After applying clamping pressure but before applying flow pressure, determine a feasible set of parameter conditions which does not deflect the elastomeric membrane into the flow microchannel while conformally sealing the microchannel
2. After applying clamping pressure and introducing flow but before actuating the microvalve, determine a feasible set of parameter conditions which will maintain lamina/membrane conformality adjacent to the microhannel (i.e. flow must stay inside the microchannel); and
3. After applying clamping pressure and flow pressure, determine a feasible set of parameter conditions which will allow the membrane to deflect into the flow microchannel to stop flow.

Requirement 1

For the first requirement, the only load applied to the model was a clamping pressure of ~40 psi. A Mooney-Rivlin hyperelastic model produced the results in Table 4.3 for each of the membranes tested. There was no gap between the top substrate and the membrane. More detailed results are shown in Appendix I.

Table 4.3. Results from requirement 1

CR	T_v *(μm)*	T_m *(μm)*	W_c *(μm)*	L_c *(μm)*	Def_{m_f} *(μm)*	D_v *(μm)*
10:1	52.1	190	618	613	23.59	-0.62
10:1	56.8	194.5	330	469	21.57	65.4
18:1	89	219.5	620	616	38.22	-.8
18:1	69	196	338	478	33	82.6

where, *CR* is monomer-to-crosslinker ratio, T_v is microvalve thickness, T_m is membrane thickness, W_c is width of control channel, L_c is length of control channel, *FR* is flow rate of water, P_p is pneumatic pressure, Def_{m_f} is max deflection of PDMS membrane along flow microchannel, D_v is microvalve deflection and Gap_{t_m} is gap between top lamina and PDMS membrane

Average deflection of the membrane into the microchannel is between 21 and 38 μm (approximately 15 to 25% deformation). Combined with the pressure drop results above, this indicates that this level of deformation is manageable.

Requirement 2

With a clamping pressure of 40 psi and fluid pressure, the second requirement was to see if there was an upward deflection of the membrane. The membrane deflection along the flow microchannel and the microvalve deflection are shown in Figures 4.4 and 4.5 respectively. The detailed results are shown in Appendix I.

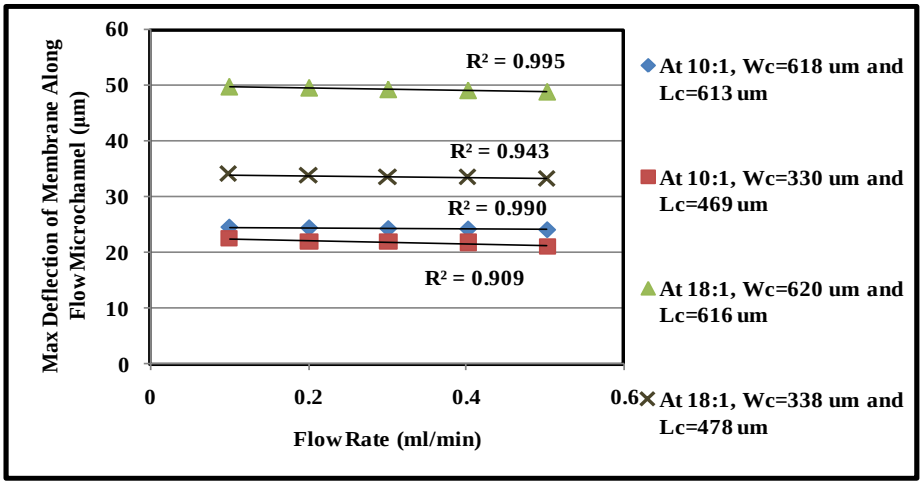

Figure 4.4. Maximum deflection of membrane along the flow microchannel for various fluid flow rates

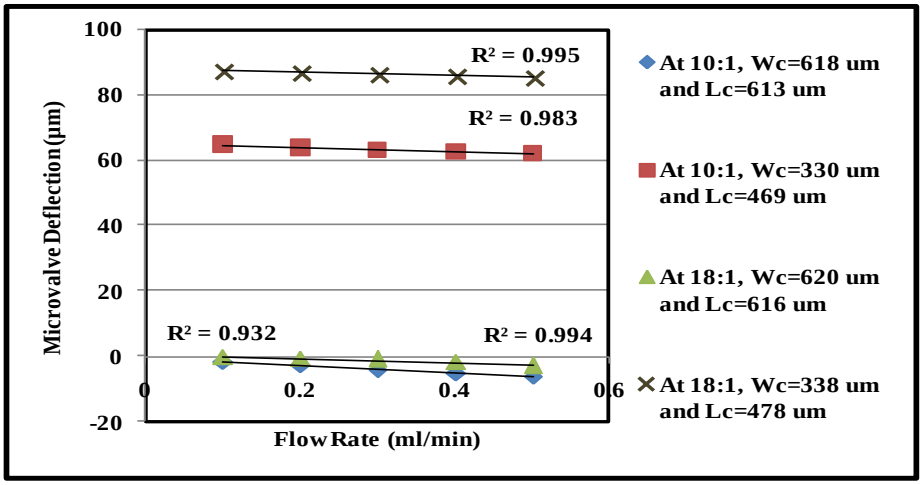

Figure 4.5. Microvalve deflection for various fluid flow rates

It is clear from the above figures that the deflection of the PDMS membrane into the flow microchannel decreases with an increase in flow rate (due to higher fluid pressure) and decrease in width and length of the control channel. There is no upward deflection of PDMS membrane when the flow pressure is applied. This suggests that the fluid is flowing within the microchannel without any leakage. Decrease in width and length of control channel results in an increase in microvalve deflection into the flow microchannel and this is due to Poisson's ratio as explained earlier.

Requirement 3

The load conditions for the third requirement are: a clamping pressure of 40 psi with fluid pressure and pneumatic pressure. Figure 4.6 shows the microvalve deflection when pneumatic pressure is applied. The microvalve deflection for flow rates ranging from 0.1 to 0.502 ml/min are plotted in the graph shown in Figure 4.7. The detailed results are shown in Appendix I.

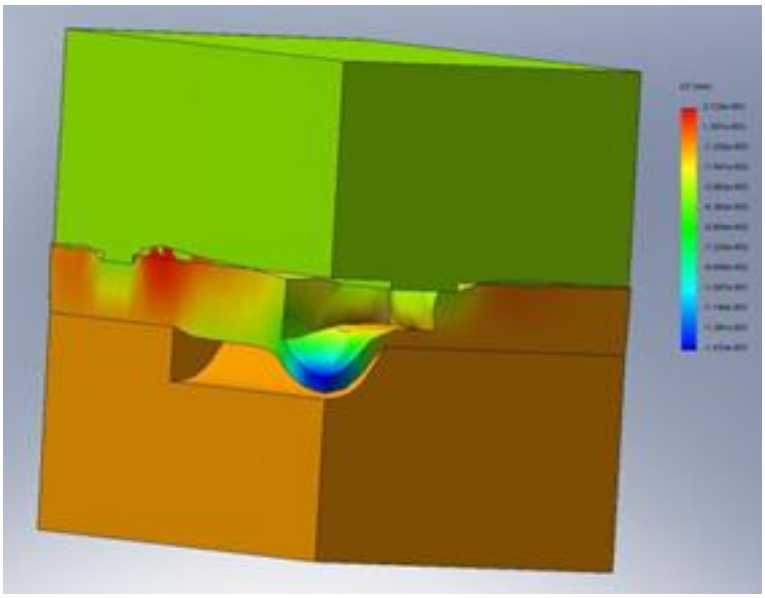

Figure 4.6. Microvalve deflection when pneumatic pressure is applied

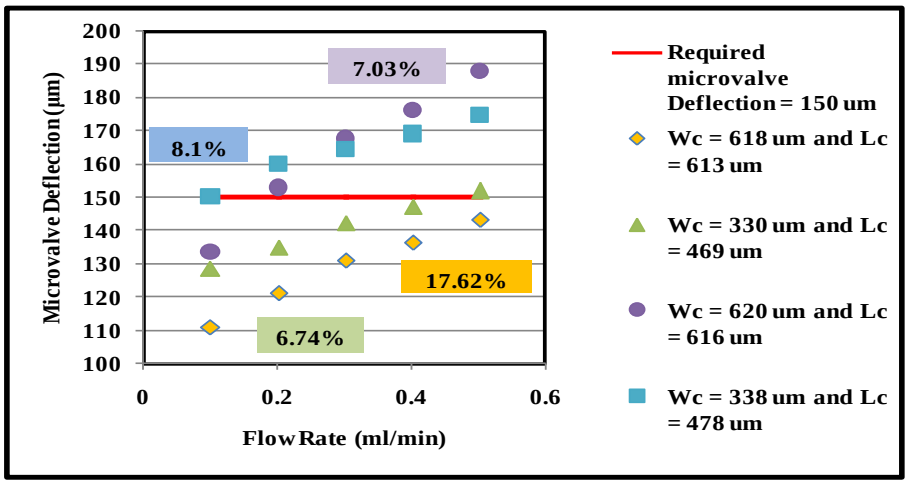

Figure 4.7. Effect of microvalve deflection on flow rates

where
Case 1: 10:1 monomer-to-crosslinker ratio, Wc = 618 µm, Lc = 613 µm
Case 2: 10:1 monomer-to-crosslinker ratio, Wc = 330 µm, Lc = 469 µm
Case 3: 18:1 monomer-to-crosslinker ratio, Wc = 620 µm, Lc = 618 µm
Case 4: 18:1 monomer-to-crosslinker ratio, Wc = 338 µm, Lc = 478 µm

In the above figure, it is assumed that the microvalve is deflected 150 µm; equivalent to the depth of the flow microchannel. The FEA results did not produce a 150 µm microvalve deflection for 10:1 monomer-to-crosslinker ratio. It appears that the model slightly overshoots the deflection for 18:1 and undershoots for 10:1 suggesting slight discrepancies in material properties. It also appears that there is a flow rate effect which may suggest that the pressure drop calculation is not accurate over the entire range of flow rates. However, the average error of 9.87 % shows excellent agreement between modeled and experimental results. This is important for future integration efforts as it suggests that the model is a good indicator of microvalve operating conditions. The error could be due to discrepancies in material properties, pressure drops or the actual microvalve deflection necessary to block the fluid flow.

4.2 Design rules and tolerance analysis

A tolerance analysis was performed to investigate the sensitivity of the device to manufacturing tolerances. Based on the findings of these studies and knowledge gained from the above design approach, a set of design rules were captured for use in integrating membrane-based microvalves into MECS devices. These design rules are captured in Appendix J. The remainder of this section discusses the results from tolerance analysis studies.

4.2.1 Misregistration of sealing bosses along the microchannel

As explained in Appendix A, the first prototype device was built without sealing bosses. Fluid leakage outside the microchannel was observed with less clamping pressure because the PDMS membrane did not form a conformal seal on the microchannel. As the clamping pressure was increased, the PDMS membrane was compressed and deformed into the flow microchannel blocking the inlet of the microchannel. This lead to the redesign of the device with sealing bosses around the microchannel to prevent fluid leakage.

A second prototype device was fabricated using sealing bosses. In this prototype, fluid leaked outside the microchannel when a higher flow pressure was applied, but remained within the sealing bosses. This validated the sealing boss concept. However, the sealing bosses were located too far away (about 1 mm) from the microchannel on each side causing flow outside the microchannel. Therefore, it was determined that the location of the sealing bosses was very important in the development of microfluidic device. When the bosses are located close to the edge of the microchannel, misregistration of the two laminae could become important. The final design suggests that the edge of the sealing bosses be located on the order of 10 μm from the edge of the microchannel.

Typical registration tolerances for past polymer bonding efforts have shown to be around 25 μm. FEA was performed to investigate what would happen if the sealing bosses were misregistered by 25 μm (lateral to the microchannel). The results show that this level of misregistration did cause some out-of-conformality between the microvalve and the microchannel lamina under typical microvalve operating conditions. However, the membrane remained conformal to the microchannel along the remainder of the membrane. Similarly, it was found that there are problems also caused by the misregistration of the sealing bosses in the Y-direction. If the sealing boss is placed too close to the inlet hole, then the PDMS membrane will deform into the hole when a higher clamping pressure is applied. However, this issue can be dealt with using judicious design.

4.2.2 Compression of the PDMS membrane

Throughout the investigation, the clamping pressure was found to be the most difficult to measure and control. Therefore, there was some interest to determine the tolerance of the device to fluctuations in clamping pressure. For the final device (40 psi clamping pressure), the typical membrane deflection was on the order of 30 μm (20% of the microchannel depth). Based on FEA, deflection was caused by buckling of the membrane due to the effects of Poisson's ratio constrained between sealing bosses. The analysis found that the final device design can withstand a maximum clamping pressure of 100 psi with a maximum deflection of the membrane around 50 μm into the microchannel (33% distortion). This is nearly a linear relationship which is consistent with plate mechanics. Pressure drop tests indicate that 15 to 20% distortion does not significantly increase pressure drop. This suggests that clamping pressure does not need to be tightly controlled in order to prevent fluid leakage and microchannel distortion.

5 CHAPTER 5. CONCLUSIONS

A novel fabrication method has been developed for embedding membrane-based microvalves in multi-layer, arrayed microfluidic devices. The novel architecture sandwiches an elastomeric membrane between polycarbonate substrates having sealing bosses to distribute clamping pressure in a manner to prevent fluid leakage and minimize microchannel distortion. This investigation has shown that while the architecture is complex having many interacting parameters, it is possible to implement functioning microvalves over a parameter space that is quite large. In this thesis, the cut-off pressure was measured for a set of microvalves across a range of flow rate and membrane conditions. Modeling results compared favorably with experimental results with an average error of 9.87%. Pressure drop studies indicate that the microchannels have little deformation.

Parametric studies indicate that the key parameters for these microvalves include sealing boss size, membrane size, control channel size and boss location. Results show that the effects of membrane size and boss location are consistent with expectations based on plate mechanics. Other results were not as straightforward. An increase in the width of the boss was found to reduce the deflection of the PDMS membrane into the flow microchannel and actually increase out-of-conformality between the membrane and flow lamina. This is because the increase in surface area of the boss decreases the local clamping pressure adjacent to the microchannel. Results also show that an increase in boss height reduces the deflection of PDMS membrane into flow microchannel. This is because an increase in the boss height leads to an increase in the space between the top lamina and the PDMS membrane. This space gives the PDMS membrane more room to deform upward away from the microchannel. Further, a reduced boss height distributes more of the clamping pressure over the microchannel resulting in a deflection of PDMS membrane into flow microchannel. Also of interest, it was found that as control channel dimensions

increase in size, less material is available for interaction with the boss and top lamina causing less material to deform into the microchannel at greater dimensions.

Even though the average clamping pressure used for final experiments was 40 psi, the device was found to withstand fluidic pressures up to 100 psi without any leakage or major microchannel distortion. This is because the sealing bosses increase the local pressure adjacent to the microchannels from 40 psi up to an average of 100 psi locally. This meets a key requirement for MECS device architectures which will typically see higher fluidic pressures as one unit operation among several in a chemical processing scheme. In addition, the architecture incorporates the use of stiff polymers which can reduce the overall form factor of the device. Based on the fact that a polycarbonate flow microchannel lamina has an elastic modulus 1000 times that of a PDMS lamina (currently used in multi-layer microvalve architectures), plate mechanics would predict a 10 fold reduction in the thickness of those laminae to achieve the same stiffness within the stack.

BIBLIOGRAPHY

1. Unger, A., Chou, H., Thorsen, T., Scherer, A., and Quake, S., 2000, "Report: Monolithic Microfabricated Valves and Pumps by Multilayer Soft Lithography," Science, 113-116.

2. Bien, D., Mitchell, S., and Gamble, H., 2003, "Fabrication and characterization of a micromachined passive valve," Journal of micromechanics and microengineering, 13(2003), 557-564.

3. Studer, V., Jameson, R., Pellereau, E., Pepin, A., and Chen, Y., 2004, "A microfluidic mammalian cell sorter based on fluorescence detection," Microelectronic engineering, 73-74, 852-857.

4. Kazuo, H., and Ryutaro, M., 2000, "A pneumatically-actuated three-way microvalve fabricated with polydimethylsiloxane using the membrane transfer technique," Journal of micromechanics and microengineering, 10(2000), 415-420.

5. Groover, W. H., Skelley, A. M., Liu, C. N., Lagally, E. T. and Mathies, R. A., 2003, " Monolithic membrane valves and diaphragm pumps for practical large scale integration into glass microfluidic devices," Sensors and actuators, 315-323.

6. Hu, M., Du, H., Ling, S., Fu, Y., Chen, Q., Chow, L. and Li, B., 2004, "A silicon-on-insulator based micro check valve," Journal of micromechanics and microengineering, 14 (2004) 382–387.

7. Go, J. S., and Shoji, S., 2004, "A disposable, dead volume-free and leak-free in-plane PDMS microvalve," Sensors and actuators, A 114 (2004) 438–444.

8. Yoo, J.C., Moon, M. C., Choi, Y. J., Kang, C/ J. and Kim Y. S., 2006, "A high performance microfluidic system integrated with the micropump and microvalve on the same substrate," Microelectronic engineering, 83 (2006) 1684–1687.

9. Yang, X., Grosjean, C. and Tai, Y., 1999, "Design, fabrication, and testing of micromachined silicone rubber membrane valves," Journal of microelectromechanical systems, Vol. 8, No. 4, 393-402.

10. Quero, J. M., Luque, A. and Franquelo, L.G., 2002, "A novel pressure balanced microfluidic valve," IEEE International symposium on circuits and systems, 2(2002), 588-591.

11. Thuillier, G. and Malek, C. K., 2005, "Development of a low cost hybrid Si/PDMS multi-layered pneumatic microvalve,",Microsystem Technologies (2005) 12, 180–185.

12. Baechi, D., Buser, R. and Dual, J., 2002, "A high density microchannel network with integrated valves and photodiodes," Sensors and actuators, A 95 (2002), 77-83.

13. Galas, J. C., Studer, V., and Chen, Y., 2005, "Characterization of pneumatically activated microvalves by measuring electrical conductance," Microelectronic engineering, 78–79 (2005), 112–117.

14. Wheeler, A. R., Throndset, W. R., Whelan, R. J., Leach, A. M., Zare, R. N., Liao, Y. H., Farrell, K., Manger, I. D. and Daridon, A., 2003, "Microfluidic Device for Single-Cell Analysis," Analytical chemistry, (75) 2003, 3581-3586.

15. Khoo, H., Liu, K., and Tseng, F., 2005, "Characterization of the mechanical properties of microscale elastomeric membranes," Measurement science and technology, 16(2005), 653-658.

16. Hoel, A., and Jullien, M., "Modelisation of a hyperelastic polymer membrane deformation".

17. Hout, J., Scheurer, J., and Casey, V., 2003, "Elastomer microspring arrays for biomedical sensors fabricated using micromachined silicon molds," Journal of micromechanics and microengineering, 13(2003), 885-891.

18. Tabata, O., Kawahata, K., Sugiyama, S., and Igarashi, I., "Mechanical property measurements of thin films using load-deflection of composite rectangular membrane".

19. Yun, K., Bu, J., Kim, C., and Yoon, E., 2002, "A Surface-Tension Driven Micropump for Low-Voltage and Low-Power Operations," Journal of microeletromechanical system, 11(5), 454-461.

20. Studer, V., Hang, G., Pandolfi, A., Ortiz, M., Anderson, W. F. and Quake, S. R., 2004, "Scaling properties of a low-actuation pressure microfluidic valve," Journal of applied physics, Vol. 95, No. 1, 393-398.

21. Pandolfi, A. and Ortiz, M., 2006, "Modeling New Design of Fluidic Microvalves," IEEE 7th International conference on thermal, mechanical and multiphysics

simulation and experiments in Micro-electronics and micro-systems, EuroSimE 2006, 1-4.

22. Gunther, A., Jhunjhunwala, M., Thalmann, M., Schmidt, M. A. and Jensen, K. F., 2005, "Micromixing of miscible liquids in segmented gas-liquid flow," American chemical society, Langmuir, (21)2005, 1547-1555.

23. Yen, B., Gunther, A., Schmidt, M. A., Jensen, K. F., and Bawendi, M. G., 2005, "A microfabricated gas–liquid segmented flow reactor for high-temperature synthesis: the case of cdse quantum dots," Microreactor fluidics, Angewandte Chemie. Int. Ed., (44)2005, 5447 –5451.

24. Vacassy, R., Lemaitre, J. and Hofmann, H., 2000, "Calcium Carbonate Precipitation Using New Segmented Flow Tubular Reactor," AIChE Journal, Vol. 46, No. 6, 1241-1253.

25. Kohler, J. M., Henkel, T., Grodrian, A., Kirner, T, Roth, M., Martin, K., and Metze, J., 2004, "Digital reaction technology by micro segmented flow-components, concepts and applications," Chemical Engineering Journal, 101 (2004), 201–216.

26. User manual of Flexiforce sensors (http://www.tekscan.com/pdfs/FlexiforceUserManual.pdf).

27. Website: http://www.itinscale.com/imada_dsd4_torque_screwdriver.htm.

28. LabVIEW user manual and http://en.wikipedia.org/wiki/Labview.

29. Abhinkar, B.S., Shiwoo, L. and Paul, B.K., 2007, "A Conformal Membrane Microvalve for the Plug-Flow Reaction of Nanomaterials," Proceedings of the 2007 Industrial engineering research conference.

30. Website: http://etd.caltech.edu/etd/available/etd-12052005-234258/unrestricted/03_Chapter_3.pdf.

31. Blackwell, E. P. and Paul, B. K., 2005, "Novel architecture for entrapment of elastomeric membranes in microfluidic systems," M.S. Thesis.

32. COSMOSWorks 2007 user manual.

33. Website: http://en.wikipedia.org/wiki/Finite_element_analysis.

34. Jackson, W.C., Tran, Hy D., O'Brien, M. J., Rabinovich, E. and Lopez, G. P., 2001, "Rapid prototyping of active microfluidic components based on magnetically modified elastomeric materials," Journal of vacuum science and technology B, 19(2), 596-599.

35. Park, C. S., Characterizing the Material Properties of Polymer-Based Microelectrode Arrays for Retinal Prosthesis," Thesis.

36. Website: http://www.midwest-ansys-ug.com/051805_presentations/ANSYS%20Users%20Group_Hyperelastic%20Materials.pdf.

37. Thomas, J. S. and Paul, B. K., 2002, "Thermally-enhanced edge registration for aligning metallic microlaminated devices," Society of Manufacturing Engineers. MS, n MS02-182, 1-8.

38. Website: www.omega.com.

39. Website: www.coleparmer.com.

40. Book: Roarks formula for stress and strain (sixth edition).

41. Website: www.wikipedia.org.

42. T-seng, T. and Paul, B. K., 2003, "The impact of fabrication methods on the mass flux characteristics of contactor membranes in absorption/desorption cycle micro-scale heat pumps," M.S. Thesis.

APPENDICES

APPENDIX A. DESIGN DEVELOPMENT

A design rationale was developed to characterize the membrane-based microvalves. Figure A.1 illustrate the design rationale. The design rationale consists of three models:

- Model 1: Development of fixture
- Model 2: Development of device with sealing bosses
- Model 3: Development of device with improved dimensions

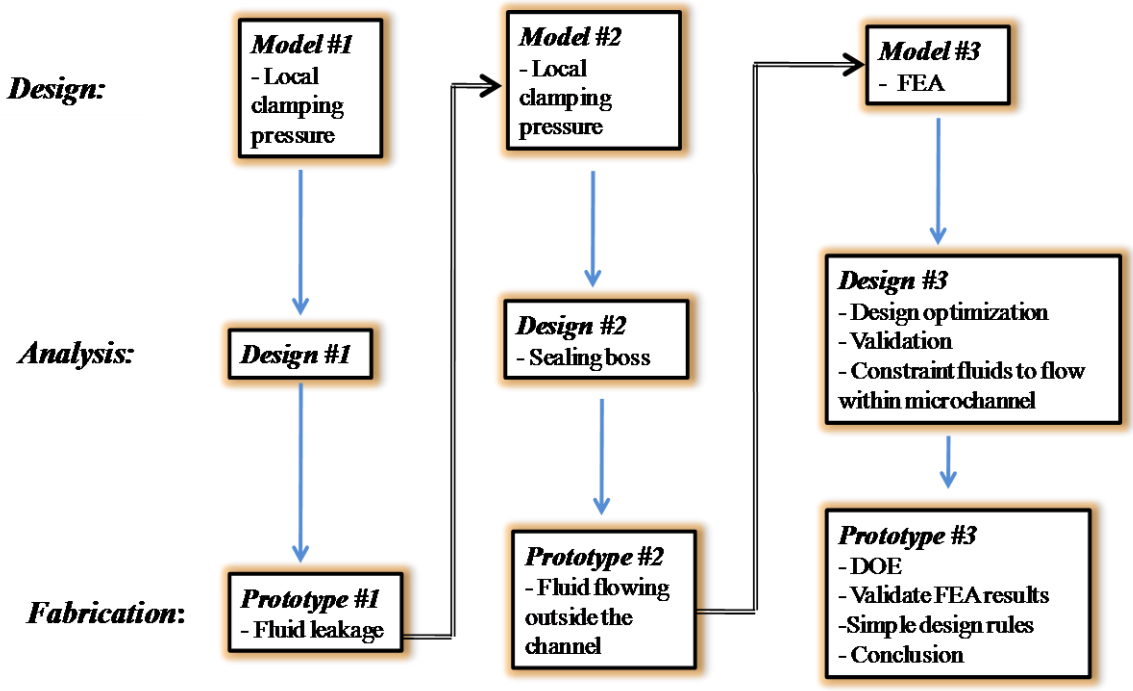

Figure A.1. Design Rationale

Model 1

In model 1, a fixture was developed without sealing bosses to characterize elastomeric membrane-based microvalves. The fixture consisted of three polycarbonate plates: top, middle and bottom. The top plate had nine inlets for pneumatic pressure. The middle polycarbonate plate had three flow microchannels with different depths. The bottom plate consisted of inputs and outputs for fluid flow in the microchannel. A PDMS elastomeric membrane with three control channels of different widths was sandwiched between the top and the middle polycarbonate substrates. All the substrates had clamping holes and were held together by clamping screws. The fixture is illustrated in Figures A.2 and A.3.

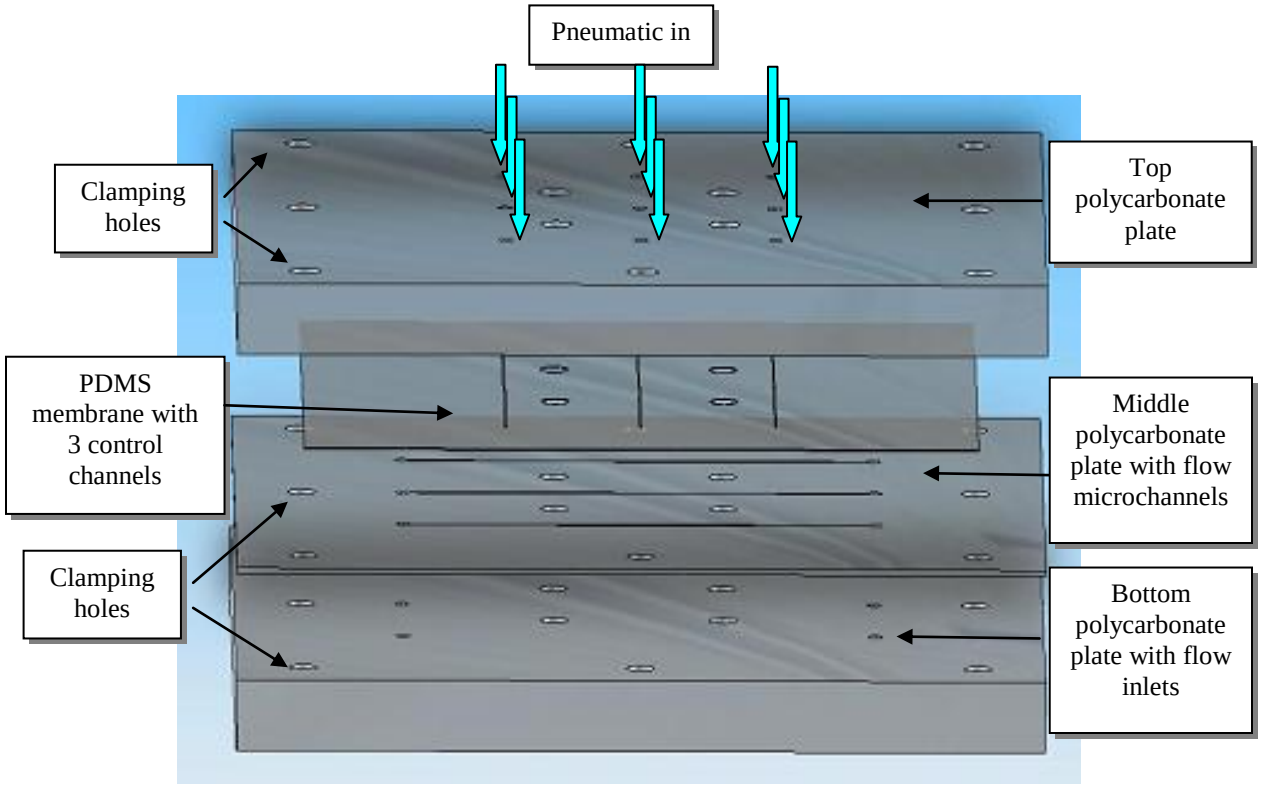

Figure A.2. Exploded view of fixture

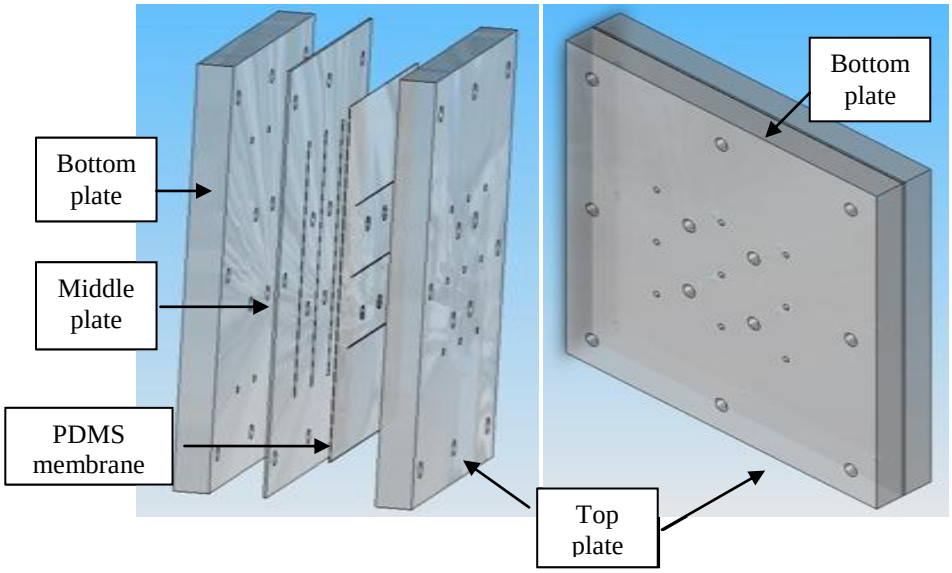

Figure A.3. Exploded and assembled view

The polycarbonate plates were fabricated by micromilling machine. The control channel on the PDMS elastomeric membrane was fabricated by replica micromolding process, by spin casting PDMS over a patterned Aluminum (Al) mold. The Al mold was also fabricated by micromilling machine. The width of the three flow microchannels was 125 μm and depths were 100, 125 and 150 μm respectively. The widths of the control channels were 200, 250 and 300 μm and height of the control channel on the mold was 170 μm. Nanoports were used as interconnectors along with PEEK tubings. Peristaltic pump was used to inject the water into the flow microchannel and pneumatic valve was used to inject the air to actuate the microvalves. 10-24 screws were used to clamp all the substrates together and clamping pressure was applied. Clamping pressure was not tightly controlled. Fluid leakage outside the microchannel was observed with less clamping pressure because the PDMS membrane did not form a conformal seal on the microchannel since the surface of polycarbonate plates were not flat. As the clamping pressure was increased, the PDMS membrane was compressed and deformed into the flow microchannel blocking the inlet of the microchannel. This lead to the development of model 2.

Model 2

The device developed in model 2 consisted of two polycarbonate substrates. The top polycarbonate substrate had sealing bosses to prevent fluid leakage and one inlet for pneumatic pressure. The bottom substrate had one microchannel and one input and one output for fluid flow. PDMS membrane was placed in between the two polycarbonate substrates. The top and bottom polycarbonate substrates were fabricated as explained in Section 2.1.3. The width of the flow microchannel was ~120 μm, depth of microchannel was ~110 μm with a round bottom profile and length was ~30 mm. The width of the sealing boss was ~ 477 μm, height was ~73 μm and distance between the bosses was ~ 2.6 mm. The PDMS membrane was built with a control channel and was fabricated by spin casting process on an Al mold as explained in Appendix F. Width of the control channel was 391 μm and length of the control channel was ~5.5 mm. Clamping pressure was applied with the help of clamping screws. The clamping pressure was not tightly controlled. Parameters such as flow microchannel dimensions and control channel dimensions were kept constant during the course of the preliminary experiments. As colored water was flowing through microchannel, the flow rate was increased and appropriate pneumatic pressure was applied to actuate the microvalve. The flow rate and the cut-off pneumatic pressure at which the microvalve was actuated to block the flow were recorded. Figure A.4 illustrate the device of model 2.

The microvalves were characterized, based on effect of membrane thickness and the effect of monomer-to-crosslinker ratio. Two types of PDMS membranes were tested with and without a control channel. In addition, two monomer-to-crosslinker ratios; 10:1 and 18:1, which determine elastic modulus of the membrane, were used to characterize the microvalves. The cut-off pneumatic pressure was measured for different flow rates, microvalve thicknesses and membrane moduli. According to per plate mechanics, the amount of pneumatic pressure was related to the elastic modulus

and thickness of the control channel membrane. Stiffer membrane required a higher pneumatic pressure to actuate the microvalve. On the other hand, if the membrane was too compliant, then the membrane distorted the microchannel as the clamping pressure was applied.

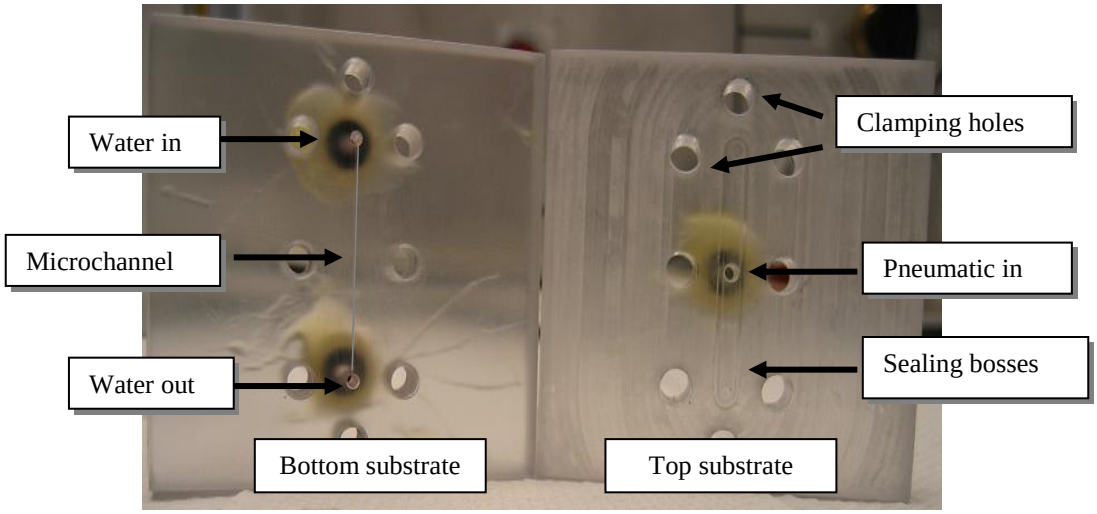

Figure A.4. Device developed in model 2

If the clamping pressure applied was too large, then the elastomeric membrane deflected into the microchannel distorting the microchannel dimensions. This required a higher flow pressure for the water to make it through the microchannel which resulted in higher pneumatic pressure required to actuate the microvalve. If the clamping pressure applied was too small, then fluid leakage was observed. As the flow pressure increased, the PDMS membrane deflected in the upward direction since there was a gap between the top lamina and PDMS membrane and there was a distance of ~1 mm from the edge of the microchannel and sealing boss. This resulted in the leakage of water outside the microchannel, but remained within the sealing bosses. To prevent the fluid leakage the location of sealing bosses and boss sizes were very important.

APPENDIX B. CALIBRATION

It is very important to calibrate the instruments prior to conducting the experiments. Along with the calibration, repeatability and resolution are also very important. Calibration is defined as setting or correcting of a measuring device or base level, usually by adjusting it to match or conform to a dependably known and unvarying measure [41]. Repeatability is the variation in measurements taken by a single person or instrument on the same item and under the same conditions [41]. A measurement may be said to be repeatable when this variation is smaller than some agreed limit. Resolution is the ability of the measurement system to detect and indicate small changes in the characteristic of the measurement result [41]. Optical microscope, surface profiler and pneumatic pressure gauge were calibrated as described below.

Microscope

Leica optical microscope was used to measure the width of microchannels, width and length of control channels, width of sealing bosses, distance between bosses, control channel features on Ni electroformed mold, Al mold and membrane and microvalve thickness of the PDMS membrane. The optical microscope is a type of microscope which uses visible light and a system of lenses to magnify images of small samples [41]. The microscope was calibrated by a KR-812 glass calibration scale purchased from Leica microsystems, which had divisions of 0.02 mm, 0.1 mm, and 1 mm. The glass scale was placed under the microscope under each lens. The grids, which is used to measure the distance between two points, were adjusted to align with the divisions. Then, the readings on the distance between the grids were changed to match the readings on the divisions. The scale was measured several times to check the repeatability and resolution of the microscope. Each of the dimensions was measured five times at various locations and the average was taken. The thickness of

the polymer substrate was measured by vernier caliper at five different locations and the average was taken. The control channel dimensions are shown in Figures B.1 and B.2. The microvalve thickness was measured by making a slit across the control channel and measured it under the microscope.

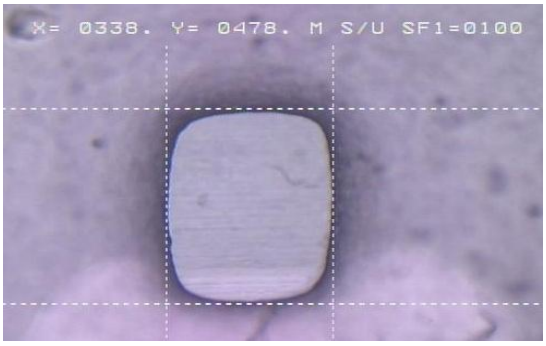

Figure B.1. Control channel on the PDMS

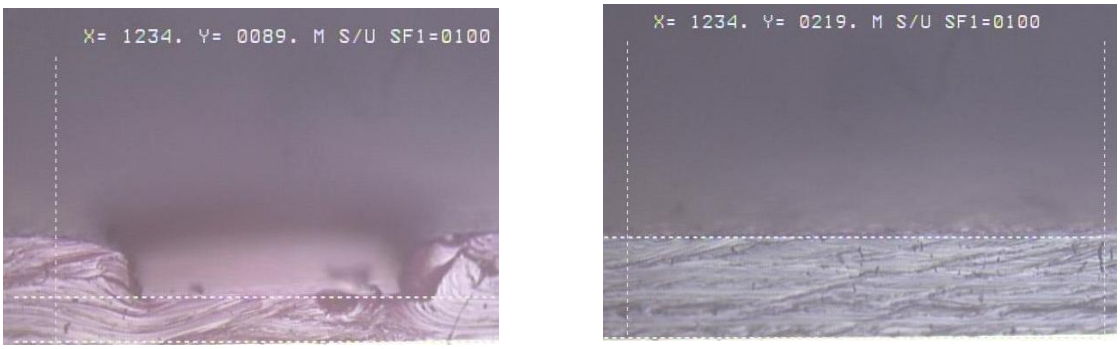

(a) Microvalve thickness **(b) Membrane thickness**

Figure B.2. Control channel dimensions

Surface profiler

The Veeco Metrology Dektak3 surface profiler was used to measure the depth and height of the microchannel, sealing boss, Al mold and electroformed mold. The profiler has a stylus with diamond tip and scans on the surface of the substrate. A graph was then plotted on the computer screen and measurements were taken by

aligning the two grids on the points to measure. The surface profiler was calibrated by a calibration device which consisted of step heights. The step heights were measured several times to check the repeatability and resolution of the system.

Peristaltic pump

Peristaltic pump from Upchurch Scientific was used to pump the water into the device. A peristaltic pump is a type of positive displacement pump used for pumping a variety of fluids. The fluid is contained within a flexible tube fitted inside a circular pump casing. A rotor with a number of rollers is attached to the external circumference compresses the flexible tube [41]. As the rotor turns, the part of tube under compression closes (or 'occludes') thus forcing the fluid to be pumped to move through the tube. The peristaltic pump was calibrated as follows. An empty glass beaker was first weighed on a mass calibration scale. The flow rate on the pump was set to 0.1 ml/min. A stop watch and the pump were turned on simultaneously. After 1 min, the pump was turned off and the beaker was weighed on the mass scale. The final weight of the beaker was subtracted from the initial weight and this resulted in the volume of water collected in the beaker. The volume of water was 0.1 ml and the calibration of the pump was repeated 3 times. Figure B.3 illustrates the pump.

Figure B.3. Peristaltic pump

Pneumatic pressure gauge

The pneumatic pressure is applied on the control channel in the membrane to deflect the membrane into the flow microchannel to actuate the microvalve. Pneumatic pressure was controlled with a pressure regulator (Omega, PRG101-120), precision of 0.25% and measured with pressure gauge (Omega, DPG1000B-100G). The pressure gauge was calibrated with a digital manometer. The pressure gauge and pressure regulator is shown in Figure B.4 [38].

(a) Pressure gauge and (b) Pressure regulator

Figure B.4. Pressure gauge and pressure regulator

A manometer is an instrument to measure pressure of liquid and gasses and is shown in Figure B.5. One end of the PEEK tubing was connected to the manometer and the other end of the PEEK tubing was connected to the pressure regulator and pressure was applied. The reading on the pressure gauge and manometer matched. The pressure gauge was calibrated before running the experiments.

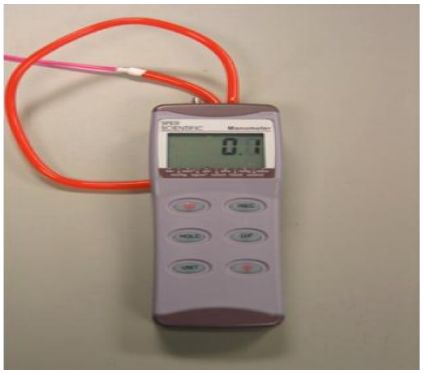

Figure B.5. Manometer

APPENDIX C. CALIBRATION OF FORCE SENSORS

FEA was performed to get a range of clamping pressure that can be applied on the device to prevent fluid leakage and minimize microchannel distortion. As described in Chapter 2 and 3, clamping screws were used to hold the substrates together. It is very important to determine the amount of clamping pressure applied on the substrates. Therefore, flexible force sensors were used to determine the amount of clamping pressure applied on the device.

Flexiforce sensors were purchased from a Tekscan Co. The Flexiforce sensor is an ultra-thin, flexible printed circuit piezoresistive force sensor [26]. The force sensors have two layers of substrate (polyester/polyimide) film. On each layer, a conductive material (silver) is applied, followed by a layer of pressure-sensitive ink. Adhesive is then used to laminate the two layers of substrate together to form the force sensor. The active sensing area is defined by the silver circle on top of the pressure-sensitive ink. Silver extends from the sensing area to the connectors at the other end of the sensor, forming the conductive leads. The sensors are terminated with male square pins, allowing them to be easily incorporated into a circuit. The two outer pins of the connector are active and the center pin is inactive. The Flexiforce single element force sensor acts as a force sensing resistor in an electrical circuit. When the force sensor is unloaded, its resistance is very high. When a force is applied to the sensor, this resistance decreases. The resistance can be read by connecting a multimeter to the outer two pins, then applying a force to the sensing area. The force sensor is shown in Figure C.1 [26].

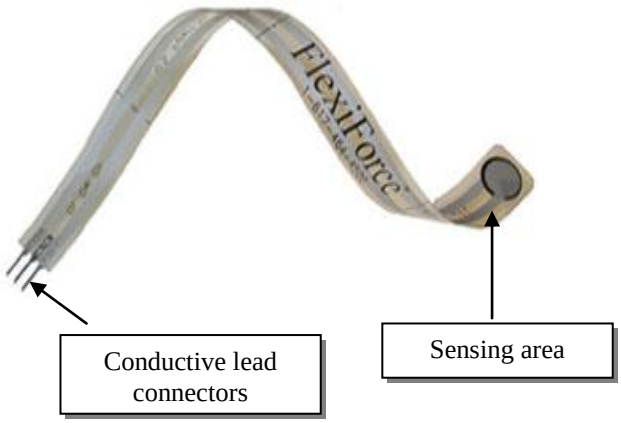

Figure C.1. Flexiforce sensor

The force sensors are calibrated with calibration mass as shown in Figure C.2 and hot press machine as shown in Figure C.3. A multimeter with a range of 20 MΩ resistances is connected to the conductive leads on the sensors to read the resistance. Several calibration weights ranging from 200 gm to ~6 kg are used to calibrate the force sensors. The calibration weight is placed on the sensing area and the resistance is recorded. The weight is gradually increased and the resistance is recorded for each weight. As the weight is increased the resistance is decreased. The sensing area is measured and the force divided by the amount of sensing area gives the pressure applied on the sensor. The force sensors are also calibrated on the vacuum hot press machine. Hot press is a machine where in a known amount of pressure is applied by the hydraulic pump. The machine is shown in Figure C.3 [31]. There are two rams and the graphite plates are placed on the bottom ram. As the machine is turned on, the bottom ram moves in the upward direction to come in contact with the top ram and then a known amount of force is applied.

Figure C.2. Calibration mass

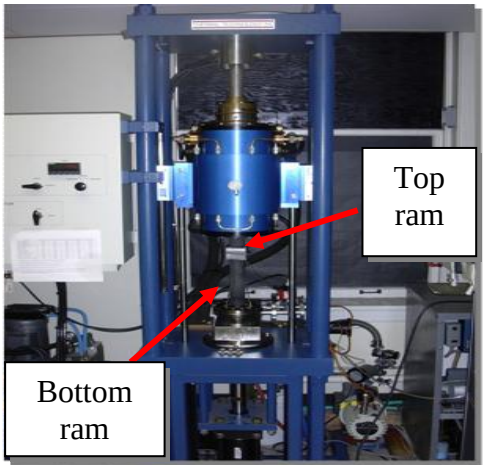

Figure C.3. Vacuum hot press

Graphite plates are used to hold the force sensors together. Since the surfaces of the graphite plates are not flat, two PDMS membranes are placed in between the plates. Force sensors are placed in between two PDMS membranes and PDMS membranes are placed in between two graphite plates. A force calibration gauge is placed on the bottom ram since the force that is displayed on the panel of the hot press is not calibrated. The force sensor assembly is then placed on top of the force

calibration gauge that is on the bottom ram in the hot press. The bottom ram is moved in the upward direction to come in contact with the top ram. As soon as they are in contact with each other, a known amount of force is applied. The multimeter is connected to the conductive leads of the sensors and the resistance is recorded. The forces applied are 252, 300, 352, 390 and 444 lb and accordingly the resistances for all the forces on all the force sensors are recorded. The area of the force sensor that is in between the graphite plates is measured. The force applied on the force sensor divide by the area gives the pressure applied. The graph of resistance versus pressure on the force sensors that was calibrated on hot press and calibration masses is plotted in Figure C.4.

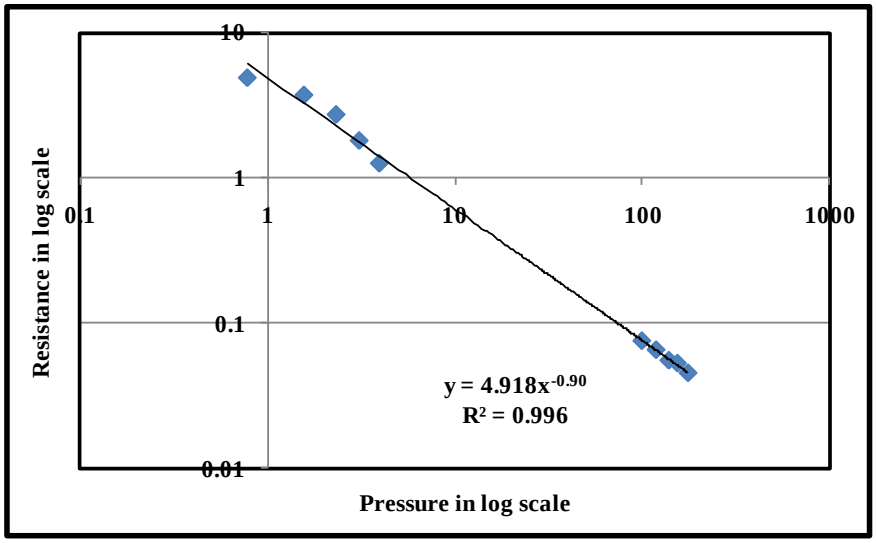

Figure C.4. Force sensor calibration curves using hot press

Force sensors are then placed in between the top and the bottom substrates of the device and clamping pressure is applied as shown in Figure C.5. The top substrate is built without any sealing bosses. 10-32 screws are used to hold the substrates. Torque is applied by the torque screw driver and torque screw driver is shown in Figure C.6 [27].

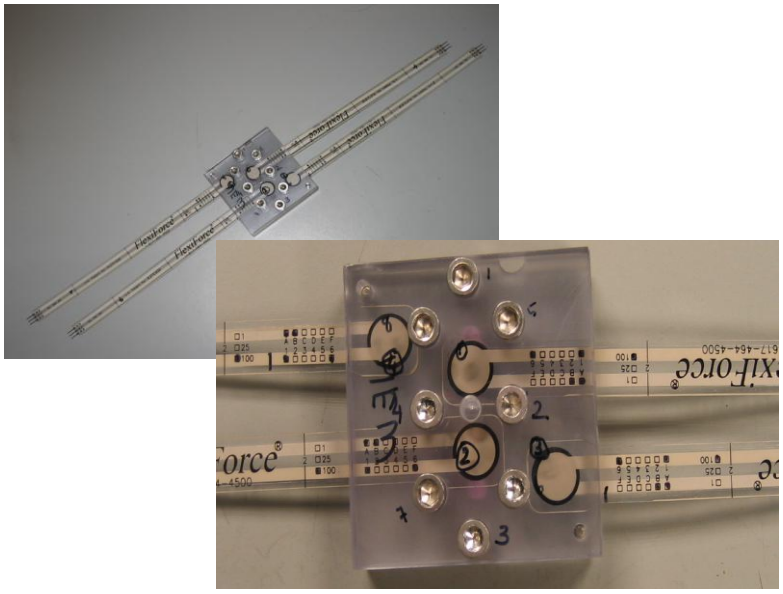

Figure C.5. Force sensors placed in the device

The torque screwdriver is purchased from Itin Scale Co. It features an LCD display for convenient torque readings. The unit is designed for screw tightening torque verification and measures in Peak, Real Time, and Peak Down measuring modes [27]. This torque screwdriver has an accuracy of ± 0.5%. In addition, it features a programmable counter that minimizes assembly errors by identifying mis-tightening and/or defective screws. The units of the torque applied are in lb-in.

Figure C.6. Torque screw driver

The torque is applied on the device by tightening the clamping screws. The multimeter is connected to the conductive leads of the force sensors. As the torque is applied, the resistance is recorded on the multimeter. The torque applied ranged from 0.3 to 6 lb-in and respective resistance is recorded. The graph of resistance versus torque is shown in Figure C.7. The resistance is then compared with the force calibration chart to determine the amount of pressure applied for the respective resistance. From the FEA, the device need a clamping pressure of 40 psi to hold the substrates together without any microchannel distortion and fluid leakage. On the final device, a torque of ~ .8 lb-in was applied on each screw and this resulted 40 psi clamping pressure.

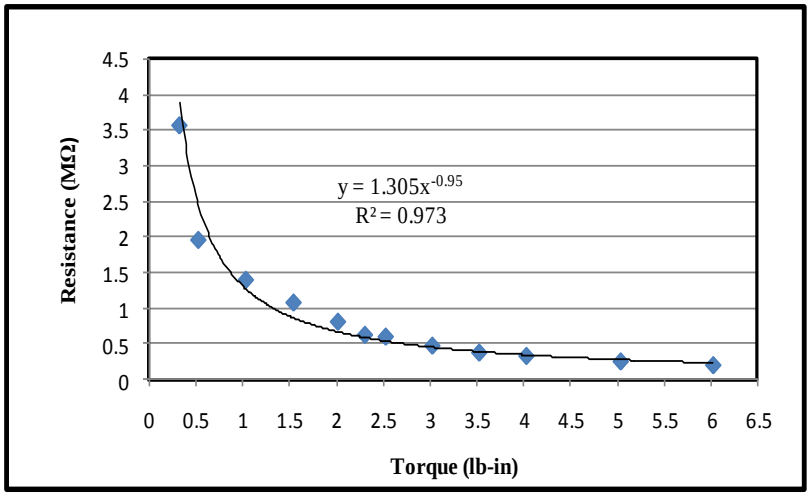

Figure C.7. Calibration curves for torque screw driver

APPENDIX D. LABVIEW INTERFACE

LabVIEW interface is used to control the application of pneumatic pressure to actuate the microvalve. LabVIEW (Laboratory Virtual Instrumentation Engineering Workbench) is a platform for a visual programming language from National Instruments. The graphical language is named "G" [28]. LabVIEW is commonly used for data acquisition, instrument control, and industrial automation. Execution is (the LV-source code) on which the programmer connects different function-nodes by drawing wires. These wires propagate variables and any node can execute as soon as all its input data become available. LabVIEW ties the creation of user interfaces (called front panels) into the development cycle. LabVIEW programs/subroutines are called virtual instruments (VIs). Each VI has three components: a block diagram, a front panel and a connector pane. Controls and indicators on the front panel allow an operator to input data into or extract data from a running virtual instrument. However, the front panel can also serve as a programmatic interface. Thus a virtual instrument can either be run as a program, with the front panel serving as a user interface, or, when dropped as a node onto the block diagram, the front panel defines the inputs and outputs for the given node through the connector panel.

One of the benefits of using LabVIEW interface to actuate the microvalve is the precisely control of application of pneumatic pressure to deflect the membrane into the microchannel to shut off the flow and to precisely control the release of the pneumatic pressure. A block diagram is developed on the block diagram panel. External devices are incorporated to run the LabVIEW program.

Devices

Several external devices are used and are connected to the computer as shown in Figure D.1. A data acquisition card (DAQ card) purchased from National Instruments is used to generate data that can be manipulated by a computer. DAQ hardware usually interfaces between the signal and a PC. It is in the form of card connected to slots (PCI, ISA) in the mother board. DAQ cards often contain multiple components (multiplexer, ADC, DAC, TTL-IO, high speed timers, RAM). These are accessible via a bus by a micro controller, which can run small programs. Driver software that came with the DAQ hardware is installed in a computer and it allows the operating system to recognize the DAQ hardware and programs to access the signals being read by the DAQ hardware.

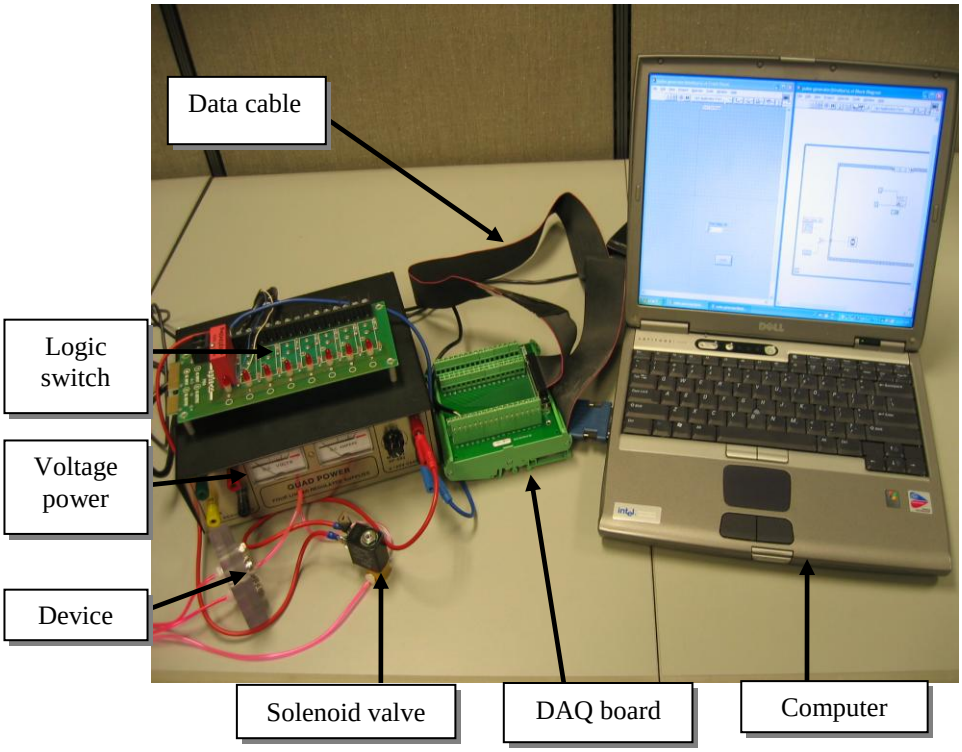

Figure D.1. LabVIEW setup

A DAQ board is used to make the wire connections. It consists of 68 pins, 34 pins for AC supply and 34 pins for DC supply. Two pins are selected and one pin is ground and the other pin is supplying voltage. The DAQ card and DAQ board are connected by a data cable. The outputs from the DAQ board are connected to a logic switch board. The logic switch board is an ON/OFF switch. It turns on when a voltage is applied. There are two wires from the switch board and one of them is connected to the solenoid valve and the other is connected to the voltage power supply. A solenoid valve is an electromechanical valve for use with liquid or gas controlled by running or stopping an electrical current through the solenoid, which is a coil of wire, thus changing the state of the valve [41]. The operation of a solenoid valve is similar to that of a light switch, but typically controls the flow of air or water, whereas a light switch typically controls the flow of electricity. Solenoid valves may have two or more ports: in the case of a two-port valve the flow is switched on or off; in the case of a three-port valve, the outflow is switched between the two outlet ports. The output from the solenoid valve is connected to the voltage power supply. The duration of power flow on the solenoid valve can be specified on the LabVIEW program. When the program is run, power supply gives electricity to turn on the logic switch which ultimately supplies power to the open the solenoid valve. The solenoid valve used is a 3-port valve, where in port A is connected to pneumatic pressure supply on the flow loop, port B is connected to the pneumatic inlet of the microfluidic device and port C is the exhaust port. The main pneumatic system on the flow loop system is turned ON. The LabVIEW program is run and logic switch allows the solenoid valve to open port B and supply pneumatic pressure to the device for the specified amount of time. Then, port C is open and the pneumatic pressure is exhausted and this cycle continues as long as the program is running.

Block Diagram and Front Panel

The front panel is the user interface of the VI. One can build the front panel using controls and indicators, which are the interactive input and output terminals of the VI, respectively [28]. Controls are knobs, push buttons, dials, and other input mechanisms. Indicators are graphs, LEDs, and other output displays. Controls simulate instrument input mechanisms and supply data to the block diagram of the VI. Indicators simulate instrument output mechanisms and display data the block diagrams acquires or generates. The front panel built to generate electric signals to actuate the microvalves consists of a time delay icon and a stop button as shown in Figure D.2. The time delay icon specifies how many seconds to delay running the calling VI. The function of the stop button is to stop the VI in which it executes, just as if one clicks the Abort Execution button on the toolbar. If the input is wired, stop occurs only if the input value is TRUE. The default is to stop as soon as the node that is currently executing finishes.

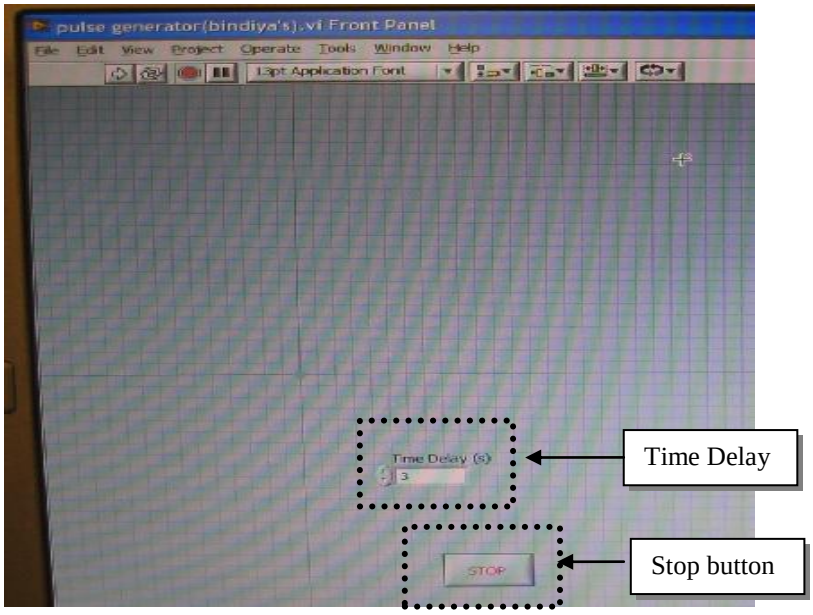

Figure D.2. Front panel

After the front panel is built, code is added using graphical representations of functions to control the front panel objects. The block diagram contains this graphical source code, also known as G code or block diagram code. Front panel objects appear as terminals on the block diagram. The block diagram built to generate electric signals to actuate the microvalves is shown in Figure D.3.

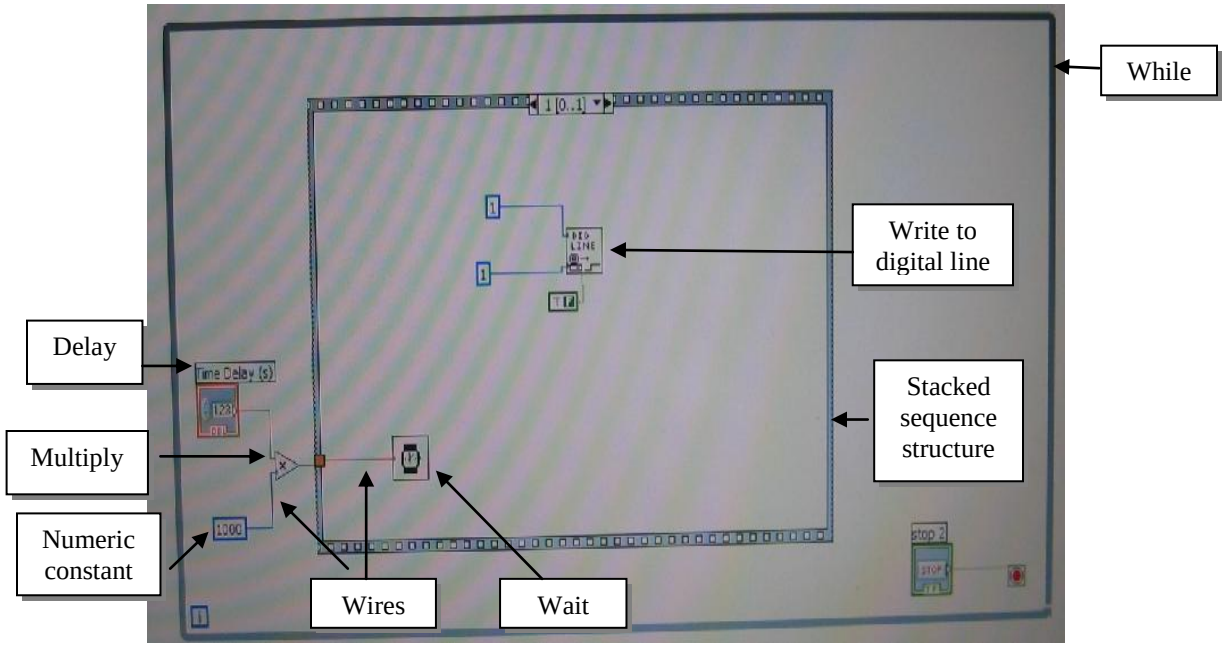

Figure D.3. Block diagram

The block diagram consists of the following:

1. While loop: Repeats the diagram inside it until the conditional terminal, an input terminal, receives a particular Boolean value. The Boolean value depends on the continuation behavior of the While Loop. The While Loop always executes at least once.
2. Time Delay: Specifies how many seconds to wait.
3. Numeric constant: Numeric constant is used to pass a numeric value to the block diagram.
4. Multiply: Since the Time Delay input is given in millisecond, a numeric constant is multiplied to the time delay to convert it from milliseconds to seconds.
5. Wires: Wires are used to transfer data among block diagram.

6. Stacked sequence structure: Consists of one or more subdiagrams, or frames, that execute sequentially. The stacked sequence structure ensures a subdiagram executes before or after another program.
7. Wait (ms): Waits the specified number of milliseconds and returns the value of the millisecond timer.
8. Write to Digital Line: Sets the output logic state of a digital line to high or low on a digital channel that you specify. It consists of following connections:
    a. Port width: It is the total width or the number of lines of the port in bits.
    b. Device: It is the device number assigned to the DAQ device during configuration.
    c. Digital channel: It is the channel name or port number that this VI configures.
    d. Line: It is the individual port bit or line to be used for I/O.
    e. Line state: It is TRUE for high logic, and FALSE for low logic.
    f. Iteration: It can be used to optimize operation when you execute this VI in a loop. When iteration is 0 (default) LabVIEW calls the DIO Port Config VI to configure the port. If the iteration is greater than zero, LabVIEW uses the existing configuration, which improves performance.

APPENDIX E. FEA RESULTS AND STATISTICAL REGRESSION ANALYSIS

Finite element analysis (FEA) is performed to achieve three main requirements as stated in Chapter 2:

1. After applying clamping pressure but before applying flow pressure, determine a feasible set of parameter conditions which does not deflect the PDMS elastomeric membrane into the flow microchannel while conformally sealing the microchannel
2. After applying clamping pressure and introducing flow but before actuating the microvalve, determine a feasible set of parameter conditions which will maintain lamina/membrane conformality adjacent to the microchannel (i.e. flow must stay inside the microchannel); and
3. After applying clamping pressure, flow pressure and pneumatic pressure, determine a feasible set of parameter conditions which will allow the membrane to deflect into the flow microchannel to stop the flow

As explained earlier, Mooney-Rivlin hyperelastic model was used to perform the analysis. The material properties of PDMS material were as follows:

Poission's ratio = 0.499
Mooney constant 1 for 10:1 monomer-to-crosslinker ratio = 34.39 psi
Mooney constant 2 for 10:1 monomer-to-crosslinker ratio = 8.7 psi
Mooney constant 1 for 18:1 monomer-to-crosslinker ratio = 21.16 psi
Mooney constant 2 for 18:1 monomer-to-crosslinker ratio = 5.35 psi

Requirement 1

Fixed parameters:

1. Monomer-to-cross linker ratio (CR) = 18:1
2. Width of flow microchannel (W_f) = 310 μm
3. Depth of flow microchannel (D_f) = 150 μm (with round bottom)
4. Length of control channel (L_c)= 500 μm
5. Width of control channel (W_c) = 310 μm
6. Distance between boss ($Dist_b$) = 320 μm
7. Membrane thickness (T_m) = 150 μm

8. Microvalve thickness (T_v) = 30 μm

Load conditions:

1. Clamping pressure (P_c) = 40 psi
2. Flow pressure (P_f) = 0 psi
3. Pneumatic pressure (P_p) = 0 psi

Experimental parameters:

1. Boss width (W_b) = 150, 200, 250, 300 and 500 μm
2. Boss height (H_b) = 25 and 50 μm

Table E.1. Complete results of requirement 1

$Dist_b$ (μm)	T_m (μm)	T_v (μm)	H_b (μm)	W_b (μm)	L_c (μm)	W_c (μm)	Def_{m_f} (μm)	Def_{m_t} (μm)	D_v (μm)	$Dist_{f\_m}$ (μm)	$Dist_{t\_m}$ (μm)
320	150	30	25	150	500	310	31	1	77	0	0
320	150	30	25	200	500	310	21	3.8	74.87	0	1.5
320	150	30	25	250	500	310	19	9.55	60.58	0	4.51
320	150	30	25	300	500	310	16.8	12.8	41.08	0	7.75
320	150	30	25	500	500	310	11.4	11.8	25.2	0	14.4
320	150	30	50	150	500	310	27	22	84.97	0	17.6
320	150	30	50	200	500	310	20.7	22.5	78	0	23.6
320	150	30	50	250	500	310	19.1	19	60.88	0	29.9
320	150	30	50	300	500	310	16.9	15.6	41.2	0	32.3
320	150	30	50	500	500	310	11.4	11.8	25.2	0	39.4

where, $Dist_b$ is distance between the bosses, T_m is membrane thickness, T_v is microvalve thickness, H_b is height of sealing boss, W_b is width of sealing boss, W_c is width of control channel, L_c is length of control channel, Def_{m_f} is deflection of membrane into flow microchannel, Def_{m_t} is upward deflection of membrane, D_v is microvalve deflection, $Dist_{f\_m}$ is distance between flow lamina and membrane and $Dist_{t\_m}$ is distance between top lamina and membrane.

Requirement 2

Fixed parameters:

1. Monomer-to-crosslinker ratio (CR) = 18:1
2. Width of flow microchannel (W_f) = 310 μm
3. Depth of flow microchannel (D_f) = 150 μm (with round bottom)
4. Length of control channel (L_c)= 500
5. Distance between boss ($Dist_b$) = 320 μm
6. Boss height (H_b) = 25 μm

Load conditions:

1. Clamping pressure (P_c) = 40 psi
2. Flow pressure (P_f) = 20 psi
3. Pneumatic pressure (P_p) = 0 psi

Experimental parameters:

1. Boss width (W_b) = 150, 200, 250, 300 and 500 μm
2. Width of control channel (W_c) = 310 and 350 μm
3. Membrane thickness (T_m) = 150 and 200 μm
4. Microvalve thickness (T_v) = 30 and 50 μm

Table E.2. Results from requirement 2

$Dist_b$ (µm)	T_m (µm)	T_v (µm)	H_b (µm)	W_b (µm)	L_c (µm)	W_c (µm)	Def_{m_f} (µm)	Def_{m_t} (µm)	D_v (µm)	$Dist_{f\_m}$ (µm)	$Dist_{t\_m}$ (µm)
320	150	30	25	150	500	310	17.5	2.02	139.7	0	0
320	150	30	25	200	500	310	11	6	129.4	0.002	3.15
320	150	30	25	250	500	310	9.63	10	135.2	2.34	8.39
320	150	30	25	300	500	310	4.7	13	153.8	10.42	3.01
320	150	30	25	500	500	310	0.72	18.5	138.4	12.98	12.8
320	150	50	25	150	500	310	16.6	2.07	104.1	0	0
320	150	50	25	200	500	310	9.17	6.38	108.5	0	0
320	150	50	25	250	500	310	5.01	11	111.1	0	0
320	150	50	25	300	500	310	3.92	13.8	113.8	3.822	0
320	150	50	25	500	500	310	0.78	18.5	120.6	13.15	2.34
320	200	30	25	150	500	310	30	3.26	166.8	1.23	0
320	200	30	25	200	500	310	26.8	0.49	169.5	9.517	0
320	200	30	25	250	500	310	18.7	3.9	173.9	3.492	0
320	200	30	25	300	500	310	9	8.04	178	7.57	0
320	200	30	25	500	500	310	2.4	15.2	185.1	10.64	0
320	200	50	25	150	500	310	31.3	3.24	146.8	0	0
320	200	50	25	200	500	310	22	0.22	150	0	0
320	200	50	25	250	500	310	18.7	4.1	157.3	0	6.9
320	200	50	25	300	500	310	9.1	8	160.6	1.87	0
320	200	50	25	500	500	310	2.4	15.2	168.2	10.94	0.2
320	150	30	25	150	500	350	15.8	1.76	126.2	3.892	0
320	150	30	25	200	500	350	11.1	5.56	129.8	5.524	0
320	150	30	25	250	500	350	4.44	10.9	135.5	5.13	0
320	150	30	25	300	500	350	4.51	13.4	138.1	10.19	1.05
320	150	30	25	500	500	350	1.56	18.4	143.1	10.09	2
320	150	50	25	150	500	350	16	1.9	105.1	1.537	0
320	150	50	25	200	500	350	11.8	5.67	109.6	1.306	0
320	150	50	25	250	500	350	4.93	10.6	113.6	5.26	0
320	150	50	25	300	500	350	4.24	13.6	117.2	7.89	1.24
320	150	50	25	500	500	350	1.66	18.5	121.6	10.34	2.08

Requirement 3

Fixed parameters:

1. Width of flow microchannel (W_f) = 310 μm
2. Depth of flow microchannel (D_f) = 150 μm (with round bottom)
3. Boss width (W_b) = 150 μm
4. Boss height (H_b) = 25 μm
5. Distance between boss ($Dist_b$) = 320 μm
6. Membrane thickness (T_m) = 150 μm
7. Width of control channel (W_c) = 310 μm

Load conditions:

1. Clamping pressure (P_c) = 40 psi
2. Flow pressure (P_f) = 20 psi
3. Pneumatic pressure (P_p) = 25 psi

Experimental parameters:

1. Monomer-to-crosslinker ratio (CR) = 18:1 and 10:1
2. Length of control channel (L_c)= 500 and 600 μm
3. Microvalve thickness (T_v) = 30 and 50 μm

Table E.3. Results from requirement 3

CR	$Dist_b$ *(μm)*	T_m *(μm)*	T_v *(μm)*	L_c *(μm)*	W_c *(μm)*	Def_{m_f} *(μm)*	Def_{m_t} *(μm)*	D_v *(μm)*	$Dist_{f\_m}$ *(μm)*	$Dist_{t\_m}$ *(μm)*
18:1	320	150	30	500	310	27.88	11.3	166	0	9.3
18:1	320	150	50	500	310	24.22	9.74	141	0	8
10:1	320	150	30	500	310	20.44	9.62	126	0	2.62
10:1	320	150	50	500	310	18.1	8.13	98.7	0	1.03
18:1	320	150	30	600	310	25.29	10.1	162	0	8.56
18:1	320	150	50	600	310	24.42	11	150	0	9.27
10:1	320	150	30	600	310	18.34	10.4	127	0	3.18
10:1	320	150	50	600	310	17.87	8.66	104	0	1.2

Statistical regression analysis

Statistical regression analysis is a technique used to determine the relationship between a dependent variable and independent variables. Regression analyses were performed on the FEA results using Statgraphics Centurion XV software. The regression equation is the key relationship in a regression analysis. The regression equation can be used to determine the unknown values using data. The data was plugged into the software and a multiple factors regression analysis was run. The dependent and independent variables were specified in the multiple factors regression analysis. The software produced an analysis of variance table which had the p-value for the model. P-value is the probability of getting a result at least as extreme as a given data point under the null hypothesis [41]. The smaller the P-value, the more strongly the test rejects the null hypothesis. The regression analysis also produced the values of correlation coefficient, R-squared value, Durbin-Watson statistic etc. If the P-value in the ANOVA table was less than 0.01, then there was a statistically significant relationship between the dependent variable and independent variables at the 99% confidence level. The R-squared value indicates how good one term is at predicting another term. Durbin-Watson (DW) statistic tests the residuals to determine if there is any significant correlation based on the order in which they occur in the data. If the P-value is greater than 0.05, there is no indication of serial autocorrelation in the residuals. The software predicted the independent variables that did not have any significant effect in the regression analysis. Analyses were further made by eliminating the independent variables that did not have a significant effect.

APPENDIX F. PDMS MEMBRANE CASTING

The PDMS membrane is developed by spin casting PDMS over Nickel electroformed mold substrate followed by making the clearance holes for clamping screws. The spin coater with the electroformed mold is shown in Figure F.1 [31]. Below is the procedure:

1. Clean the mold with acetone, methanol and DI water to remove the greasy substances from the substrate.
2. Blow clean air on the mold to dry it.
3. Prepare PDMS Sylgard 184 purchased Dow Corning Co. PDMS is mixed at 10 parts monomer to 1 part crosslinker by mass and 18 parts monomer to 1 part crosslinker by mass. Stir the mixture thoroughly. The mixture is placed in a vacuum chamber at 27 in. Hg for 20 min to evaporate the bubbles formed.
4. Spin onto patterned mold at 810 RPM for 36 sec to achieve ~190 μm thick membrane.
5. Cure it on the hot plate at 100ºC for 6-8 min.
6. Peel the cured PDMS from the mold.
7. Place it on a clean Polycarbonate substrate and make the clearance holes using twisters or needle.

Figure F.1. Spinner with the electroformed mold

APPENDIX G: EXPERIMENTAL PROTOCOL

1. Clean the top and bottom polycarbonate substrates with isopropanol and dry it with air blower.
2. Four PDMS membranes are casted with different control channel dimensions and elastic modulus as explained in Chapter 3. Peel the PDMS membrane carefully from the electroformed mold and place it on the bottom polycarbonate substrate.
3. Align the control channel that is on the membrane to the microchannel on the bottom substrate and pneumatic input on the top substrate under the microscope.
4. Make the clearance holes on the membrane for the clamping screws to pass through the membrane.
5. Clamp all the three substrates with 10-24 clamping screws.
6. Apply toque that result in a clamping pressure of 40 psi.
7. Connect the PEEK tubings to the inlet and outlet of the device and connect it to the peristaltic pump and to the flow loop as described in Chapter 3.
8. Place the PEEK tubing that is connected to the outlet of the device under the optical microscope.
9. Colored water is used to conduct the experiments.
10. Connect the LabVIEW interface and set the delay time to 3 sec on the computer.
11. Set the flow rate to 0.1 ml/min.
12. Set pneumatic pressure to 5 psi and click start on the LabVIEW interface to actuate microvalves.
13. Observe if the water has stopped flowing through the tube. If the water flows even when the microvalve is actuated, then increase the pneumatic pressure till the water flow is blocked.
14. Record the flow rate and pneumatic pressure at which the microvalve is actuated.
15. Repeat these steps for flow rates ranging from 0.1 ml/min to 0.502 ml/min and for remaining three membranes.

APPENDIX H. PRESSURE ACROSS MICROCHANNEL

The pressure drop across the microchannel was measured on the flow loop system shown in Figure H.1. Pressure transducers measure the pressure drop across the microchannel. A T-fitting is connected to the inlet of the microchannel and another T-fitting is connected to the outlet. The T-fitting has three connectors as shown in Figure H.2. One of the ends from the 1st T-fitting is connected with the PEEK tubing that is connected to the peristaltic pump, the 2nd end is connected to the inlet of the device and the 3rd end is connected to the pressure port 1 on the flow loop. One of the ends of the 2nd T-fitting is connected to outlet of the device, the 2nd end is connected to the pressure port 2 on the flow loop and the 3rd end is connected with the PEEK tubing and is immersed in a beaker to collect the water. The outlet of the pressure ports on the flow loop are hooked up to a pressure transducer and the pressure drop across the microchannel is displayed on the display panel. Pressure drop was measured for flow rates varying from 0.1 to 0.502 ml/min. The pressure drop across the microchannel is then compared with the pressure drop calculated using Equation (H.1). The calculated and measured pressure drop is tabulated in Table H.1. The calculated and measured pressure drops match closely with an average error of 14.29%.

$$\Delta P = \frac{128 \mu L Q}{\pi D^4} \qquad (H.1)$$

where ΔP is the pressure drop across the flow microchannel (psi), μ is the viscosity of the liquid (Ns/m^2), L is the length of the flow microchannel (m), Q is the flow rate of the liquid (ml/min) and D is the microchannel hydraulic diameter (m) of flow microchannel.

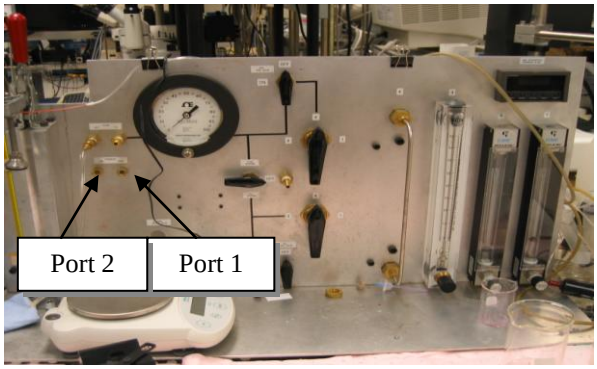

Figure H.1. Flow loop system

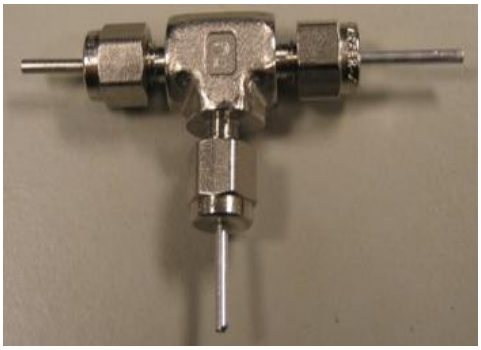

Figure H.2. T-fitting

Table H.1. Comparison of calculated and measured pressure drop across the microchannel

Flow Rate (mL/min)	*Pressure Drop Calculation (psi)*	*Pressure Drop Measured (psi)*	*Difference (psi)*
0.1	0.161432739	0.14	0.0214327
0.201	0.324479806	0.26	0.0644798
0.301	0.485912545	0.44	0.0459125
0.402	0.648959612	0.55	0.0989596
0.502	0.810392351	0.7	0.1103924
		Average Pressure Drop Difference	**0.0682354**

APPENDIX I. EXPERIMENTAL RESULS

Initial experimental results

Initial experiments (i.e. Model 2 from Appendix A) were conducted to study the characteristics of the microvalve when the PDMS membrane is deflected into the microchannel by the application of pneumatic pressure. The deflection of membrane was used to cut-off the flow of water in the microchannel. The fixed parameters in the initial experiments were:

Width of the flow microchannel = 120 μm
Depth of the flow microchannel = ~110 μm
Length of the flow microchannel = 30 mm
Distance between bosses = ~2.6 mm
Width of sealing boss = 477 μm
Height of the sealing bosses = ~73 μm

As described earlier, initial experiments were conducted with two types of membranes, membrane with control channel and membrane without control channel and two types of monomer-to-crosslinker ratios, namely, 18:1 and 10:1. The microvalve thickness and membrane thickness of the PDMS membrane ranged from 40 μm to 220 μm. The flow rate of water in the microchannel was varied from 0.1 ml/min to ~4 ml/min. The cut-off pneumatic pressure and flow rates are tabulated in Tables I.1, I.2, I.3 and I.4.

Table I.1. Effect of flow rate on cut-off pneumatic pressure for 10:1 monomer-to-crosslinker ratio without control channel

Membrane thickness = 45.72 μm		*Membrane thickness = 76.2 μm*		*Membrane thickness = 114.3 μm*	
Flow Rate (ml/min)	***Cut-off Pneumatic Pressure (psi)***	***Flow Rate (ml/min)***	***Cut-off Pneumatic Pressure (psi)***	***Flow Rate (ml/min)***	***Cut-off Pneumatic Pressure (psi)***
0.201	6	0.301	7	0.201	8.5
0.301	7	0.402	12.5	0.251	11
0.351	8	0.452	14	0.301	13
0.402	10	0.502	16	0.351	16
0.452	11.5	0.602	18	0.402	20
0.502	13.5	0.652	19.5		
0.552	16	0.703	22.5		
0.602	18	0.753	24		
0.652	21	0.803	27		
0.703	25	0.853	36		
0.753	27.5				

Table I.2. Effect of flow rate on cut-off pneumatic pressure for 10:1 monomer-to-crosslinker ratio with control channel of W_c = 5.5 mm and L_c = 391 μm

Microvalve thickness = 77.8 μm		*Microvalve thickness = 103.2 μm*		*Microvalve thickness = 159.9 μm*		*Microvalve thickness = 179.4 μm*	
Flow Rate (ml/min)	***Cut-off Pneumatic Pressure (psi)***	***Flow Rate (ml/min)***	***Cut-off Pneumatic Pressure (psi)***	***Flow Rate (ml/min)***	***Cut-off Pneumatic Pressure (psi)***	***Flow Rate (ml/min)***	***Cut-off Pneumatic Pressure (psi)***
0.201	5	0.402	7	0.151	8	0.12	38
0.452	6	0.703	9	0.351	9.5	0.161	39
0.602	7	0.954	10	0.703	11	0.181	40.25
0.803	7.5	1.355	11.5	0.853	12.5	0.211	41
1.054	9	1.556	12.5	1.004	13	0.231	42
1.305	10	1.857	14	1.154	14.5		
1.506	11.5	2.058	16	1.305	16		
1.706	12	2.158	17	1.556	17.5		
1.957	13.5			1.757	19		
2.158	14.5			2.058	20.5		
				2.158	22		

Table I.3. Effect of flow rate on cut-off pneumatic pressure for 18:1 monomer-to-crosslinker ratio without control channel

Membrane thickness = 50.8 μm		*Membrane thickness = 101.6 μm*	
Flow Rate (ml/min)	***Cut-off Pneumatic Pressure (psi)***	***Flow Rate (ml/min)***	***Cut-off Pneumatic Pressure (psi)***
0.251	5	0.251	9
0.351	7	0.402	11
0.452	9	0.552	12
0.552	10	0.602	14
0.602	12.5	0.652	16
0.803	14	0.702	18
1.054	16	0.752	21.5
		0.853	26

Table I.4. Effect of flow rate on cut-off pneumatic pressure for 18:1 monomer-to-crosslinker ratio with control channel of W_c = 5.5 mm and L_c = 391 μm

Microvalve thickness = 47.32 μm		*Microvalve thickness = 52.4 μm*		*Microvalve thickness = 65.1 μm*	
Flow rate (ml/min)	***Cut-off Pneumatic Pressure (psi)***	***Flow rate (ml/min)***	***Cut-off Pneumatic Pressure (psi)***	***Flow rate (ml/min)***	***Cut-off Pneumatic Pressure (psi)***
0.401	5	0.171	7.5	0.261	7.5
0.562	6	0.351	9	0.663	8
0.803	7	0.452	10	1.536	9
0.853	8.5	0.602	12	2.178	10
1.004	10	1.004	13	3.704	11
1.104	11	1.305	14	4.005	12
1.305	13	1.556	15.5		
1.355	13.5	1.757	17.5		
1.556	14.5	1.957	19		
1.757	17	2.158	21.5		
1.907	18				
2.158	20				

Figures I.1 (a), (b), (c) and (d) illustrate the effect of cut-off pneumatic pressure on the 10:1 and 18:1 monomer-to-crosslinker ratio. As expected increase in flow rate of water results in an increase in the cut-off pneumatic pressure required to actuate the microvalves. Because of its lower elasticity, the cut-off pressure for membrane of 18:1 monomer-to-crosslinker ratio is lower than of 10:1 monomer-to-crosslinker ratio. The membranes without control channel require a higher pneumatic pressure to actuate the microvalves, since the membrane is thicker and this result in higher stiffness of the membrane.

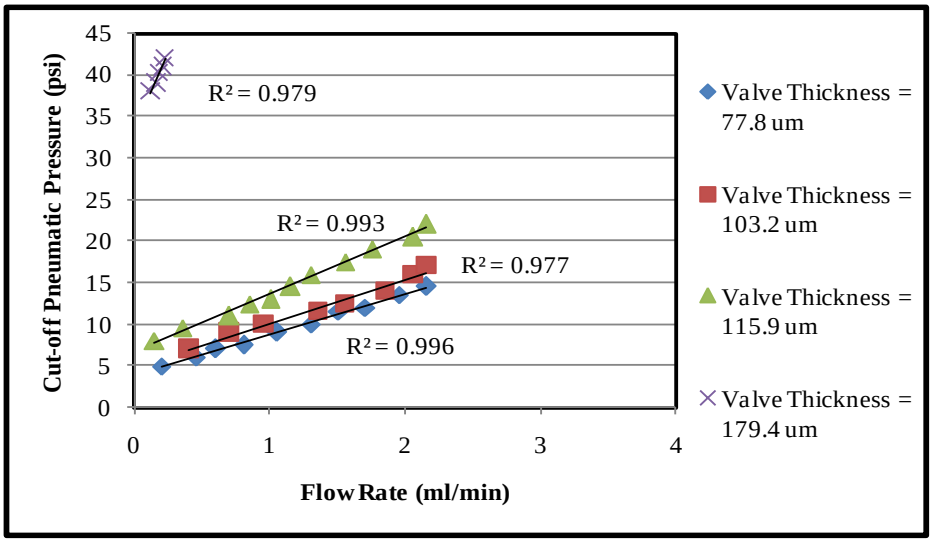

(a) 10:1 monomer-to-crosslinker ratio with control channel

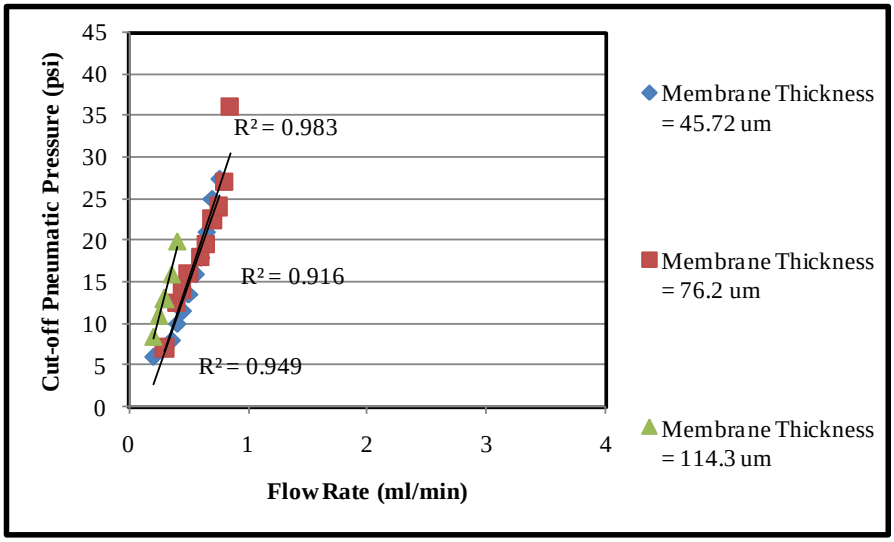

(b) 10:1 monomer-to-crosslinker ratio without control channel

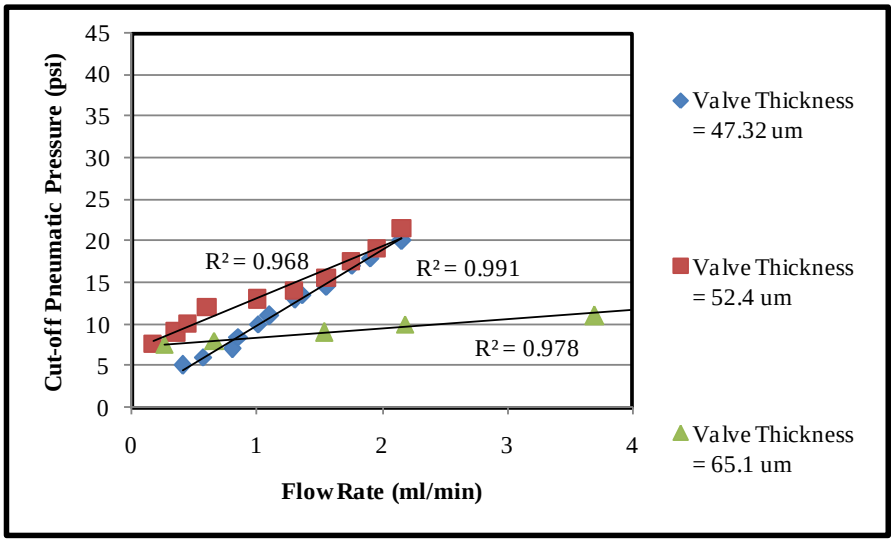

(c) 18:1 monomer-to-crosslinker ratio with control channel

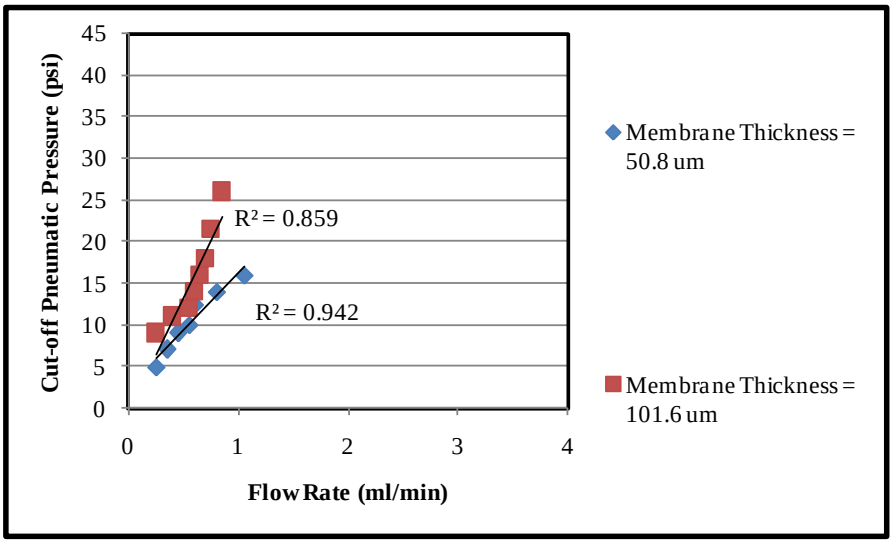

(d) 18:1 monomer-to-crosslinker ratio without control channel

Figure I.1. Effect of flow rate on cut-off pneumatic pressure for 10:1 and 18:1 monomer-to-crosslinker ratio

The R-squared values for all linear regression analyses between flow rate and cut-off pneumatic pressure were close to 1.0, which indicate good repeatability of cut-off pneumatic pressure for a given flow rate. However, there were some discrepancies between the results of different microvalve thicknesses. In general, it was assumed that thinner microvalves will require less cut-off pneumatic pressure. These results were not confirmed in Figure 4.1 (b) and (c). This suggested that there were other important factors associated with actuating the microvalve. Some of those factors were flow pressure, pneumatic pressure, clamping pressure, width, depth and shape of the flow microchannel, and width of the control channel.

Clamping pressure was not tightly controlled in these experiments and was essentially regulated by the amount of torque placed onto the clamping screws. If the clamping pressure applied was too large, then the elastomeric membrane deflected into the microchannel distorting the microchannel dimensions. This required a higher flow pressure for the water to make it through the microchannel which resulted in

higher pneumatic pressure required to actuate the microvalve. If the clamping pressure applied was too small, then fluid leakage was observed. As the flow pressure increased, the PDMS membrane deflected in the upward direction since there was a gap between the top lamina and PDMS membrane. This resulted in the leakage of water outside the microchannel, but remained within the sealing bosses. The leakage occurred because the bosses were located at a distance of ~1 mm from the edge of the microchannel.

Final experimental results

The readings are tabulated in tables shown below. Table I.5 displays the dimensions of control channel along with membrane and microvalve thickness. The PDMS was casted by spinning it at 810 rpm and cured at 100°C for 6-8 min. Tables I.6 and I.7 shows the torque applied on each screw with PDMS of 10:1 monomer-to-crosslinker ratio membrane with control channel dimensions W_c = 618 μm; L_c = 613 μm and W_c = 330 μm; L_c = 469 μm respectively. The cut-off pneumatic pressure and the flow rates are tabulated in Table I.8 for 10:1 monomer-to-crosslinker ratio.

Table I.5. Dimensions of the control channel of 10:1 monomer-to-crosslinker ratio

		Membrane Thickness (μm)					
W_c (μm)	***L_c (μm)***	***1***	***2***	***3***	***4***	***Avg***	***Microvalve Thickness (μm)***
618	613	192	190	188	190	190	52.1
330	469	194	194	196	194	194.5	56.88

Table I.6. Torque applied on each screw with 10:1 monomer-to-crosslinker ratio and W_c = 618 µm and L_c = 613 µm

Torque (lb-in) on each Screw									
1	2	3	4	5	6	7	8	Avg	***Pressure (psi)***
0.8	0.83	0.81	0.82	0.82	0.83	0.81	0.84	0.82	41.21

Table I.7. Torque applied on each screw with 10:1 monomer-to-crosslinker ratio and W_c = 330 µm and L_c = 469 µm

Torque (lb-in) on each Screw									
1	2	3	4	5	6	7	8	Avg	***Pressure (psi)***
0.82	0.83	0.81	0.81	0.8	0.8	0.81	0.82	0.8125	40.83

Table I.8. Cut-off pneumatic pressure for varying flow rates

10:1 Monomer-to-crosslinker ratio			
W_c = 618 µm	***L_c = 613 µm***	***W_c = 330 µm***	***L_c = 469 µm***
Flow Rate (ml/min)	***Pressure (psi)***	***Flow Rate (ml/min)***	***Pressure (psi)***
0.1	12.5	0.1	17.5
0.201	15	0.201	20
0.301	17.5	0.301	23
0.402	19	0.402	25
0.502	21	0.502	27

The readings are tabulated in tables shown below. Table I.9 displays the dimensions of control channel along with membrane and microvalve thickness. The PDMS was casted by spinning it at 810 rpm and cured at 100°C for 6-8 min. Table I.10 and I.11 shows the torque applied on each screw with PDMS of 10:1 monomer-to-crosslinker ratio with control channel dimensions W_c = 618 µm; L_c = 613 µm and

W_c = 330 μm; L_c = 469 μm respectively. The cut-off pneumatic pressure and the flow rates are tabulated in Table I.12 for 10:1 monomer-to-crosslinker ratio.

Table I.9. Dimensions of the control channel of 18:1 monomer-to-crosslinker ratio

		Thickness (μm)					
W_c (μm)	***L_c (μm)***	***1***	***2***	***3***	***4***	***Avg***	***Microvalve Thickness (μm)***
631	616	219	221	219	219	219.5	81.6
338	478	201	201	199	196	199.2	61.63

Table I.10. Torque applied on each screw with 18:1 monomer-to-crosslinker ratio and W_c = 620 μm and L_c = 616 μm

Torque (lb-in) on each Screw									***Pressure (psi)***
1	2	3	4	5	6	7	8	Avg	
0.8	0.83	0.83	0.81	0.8	0.81	0.8	0.8	0.81	40.7081

Table I.11. Torque applied on each screw with 10:1 monomer-to-crosslinker ratio and W_c = 338 μm and L_c = 478 μm

Torque (lb-in) on each Screw									***Pressure (psi)***
1	2	3	4	5	6	7	8	Avg	
0.8	0.81	0.81	0.82	0.81	0.86	0.82	0.8	0.81	41

Table I.12. Cut-off pneumatic pressure for varying flow rates

18:1 Monomer-to-crosslinker ratio			
W_c = 620 µm	*L_c = 616 µm*	*W_c = 338 µm*	*L_c = 478 µm*
Flow Rate (ml/min)	***Pressure (psi)***	***Flow Rate (ml/min)***	***Pressure (psi)***
0.1	11.5	0.1	14
0.201	14	0.201	17
0.301	16.5	0.301	18.5
0.402	18	0.402	20
0.502	20	0.502	22

Comparison with analytical results

The final experimental results were compared with the analytical results. An analytical solution was found in the literature [18] and has been modified to determine the amount of pneumatic pressure required to deflect the membrane and actuate the microvalve. Equations (I.1), (I.2) and (I.3) illustrate the pneumatic pressure required to deflect the microvalve.

$$P_p = \frac{C_1 \sigma_m T_v D_v}{W_c^2} + \frac{C_2 E_v T_v^2 D_v^3}{W_c^4} \qquad (I.1)$$

where,

$$C_1 = \frac{\pi^4 (1 + n^2)}{64} \qquad (I.2)$$

and

$$C_2 = \{\frac{\pi^6}{32}(1 - v_m^2)\}\{\frac{(9 + 2n^2 + 9n^4)}{256} \frac{[4 + n + n^2 + 4n^3 - 3nv_m(1 + n)]^2}{2} \frac{}{[81\pi^2(1 + n^2) + 128n + v_m(128 - 9\pi^2(1 + n^2))]}\} \quad (I.3)$$

where, P_p is pneumatic pressure, σ_m is residual stress in the membrane, T_v is microvalve thickness, D_v is flow microchannel depth or amount of microvalve deflection, E_v is elastic modulus of the microvalve, v_m is Poisson's ratio of membrane, W_c is control channel width, L_c is control channel length and $n = W_c/L_c$

The calculated cut-off pneumatic pressure was then compared with the experimental results. Table I.13 illustrate the pneumatic pressure calculated to deflect the membrane to a depth of 150 μm. The values of residual stress, Poisson's ratio, and elastic modus for 10:1 and 18:1 monomer-to-crosslinker ratio are obtained from the literature [1, 34, 35 and 36]. From Table I.14, it was clear that there were differences between the calculated results and experimental results for flow rate of 0.1 ml/min. The pneumatic pressure calculated was the pressure required to deflect the membrane into the microchannel of 150 μm deep. Extra pneumatic pressure was required to overcome the fluid pressure inside the microchannel. Therefore a correction factor was added to match the experimental and calculated results. The detail calculation of the correction factor is shown in Table I.15. After taking the correction factor into consideration, there was 2.39% error between the experimental cut-off pneumatic pressure and calculated pressure.

Table I.13. Calculated pneumatic pressure

σ_m (psi)	t_v (inch)	d_f (inch)	E_v (psi)	$2*w_v$ (inch)	$2*l_v$	$n = w_v/l_v$	C_1	C_2	P_p (psi)
21.7550	0.0021	0.0059	227.5	0.0243	0.0241	1.0082	3.06	1.47	5.50
21.7550	0.0022	0.0059	227.5	0.0130	0.0185	0.7036	2.27	0.88	15.69
17.5382	0.0033	0.0059	183.8	0.0244	0.0243	1.0065	3.06	1.46	7.02
17.5382	0.0024	0.0059	183.8	0.0133	0.0188	0.7071	2.28	0.88	13.11

Table I.14. Comparison of calculated and cut-off pneumatic pressure for 0.1 ml/min flow rate

CR	W_c (μm)	L_c (μm)	T_m (μm)	Cut-off Pressure Applied (psi)	Numerically Calculated Pressure Calculated (psi)	Difference between Applied Cut-off Pressure and Numerically Calculated Pressure (psi)
10:1	618	613	190	12.5	5.50204195	6.9979581
10:1	330	484	194.5	17.5	15.6998115	1.8001885
18:1	631	616	219.5	11.5	7.02756545	4.4724345
18:1	338	478	199.25	14	13.1187645	0.8812355

The correction factor was then added to each result and is shown in Tables I.16, I.17, I.18 and I.19. As the flow rate increase the correction factor is multiplied by a factor of 0.5 for every increase in flow rate from 0.1 to 0.502 ml/min. There are four tables below and Table I.16 correspond to 10:1 monomer-to-crosslinker ratio and W_c=618 (μm) and L_c=613 (μm), Table I.17 correspond to 10:1 monomer-to-crosslinker ratio and W_c=330 (μm) and L_c=469 (μm), Table I.18 correspond to For 18:1 monomer-to-crosslinker ratio and W_c=620 (μm) and L_c=616 (μm) and Table I.19 correspond to 18:1 monomer-to-crosslinker ratio and W_c=338 (μm) and L_c=478 (μm).

The difference in actual pneumatic pressure and calculated pneumatic pressure is shown in Figures I.1, I.2, I.3 and I.4.

Table I.15. Calculation of correction factor

A	***B***	***C***	***D***	***E***	***F***	***G***	***H = B*C*D*F***	***I = F -GI***	***J = Sum(I)*(H_i/Sum(H))***
CR	***W_c (µm)***	***L_c (µm)***	***T_m (µm)***	***E (psi)***	***Cut-off Pressure Applied (psi)***	***Numerically Calculated Pressure Calculated (psi)***	***Multiplication of above Factors***	***Difference between Cut-off Pressure Applied and Numerically Calculated Pressure (psi)***	***Correction Factor***
10:1	618	613	190	227.5	12.5	5.50204	1.6375E+10	6.9979581	5.1450414
10:1	330	484	194.5	227.5	17.5	15.699	7067410350	1.8001885	2.2205739
18:1	631	616	219.5	183.8	11.5	7.0275	1.5682E+10	4.4724345	4.9271414
18:1	338	478	199.2	183.8	14	13.1187	5916821043	0.8812355	1.8590598
						Sum	**4.5041E+10**	**14.151817**	

Table I.16. Comparison of calculated and applied cut-off pneumatic pressure for 10:1 monomer-to-crosslinker ratio, W_c = 618 µm and L_c = 613 µm

Flow Rate (ml/min)	*Pressure Drop Measured across Microchannel (psi)*	*Numerically Calculated Pneumatic Pressure (psi)*	*Correction factor*	*Numerically calculated pressure + correction factor (psi)*	*Calculated Cut-off Pneumatic Pressure (psi)*	*Applied Cut-off Pressure (psi)*	*Difference (psi)*
0.1	0.14	5.5020	5.313059	10.8151	10.9551	12.5	1.5449
0.201	0.26	5.5020	7.969589	13.4716	13.7316	15	1.2684
0.301	0.44	5.5020	10.62611	16.1282	16.5682	17.5	0.9318
0.402	0.55	5.5020	13.28264	18.7847	19.3347	19	-0.3347
0.502	0.7	5.5020	15.93917	21.4412	22.1412	21	-1.1412
						Average	***0.45383***

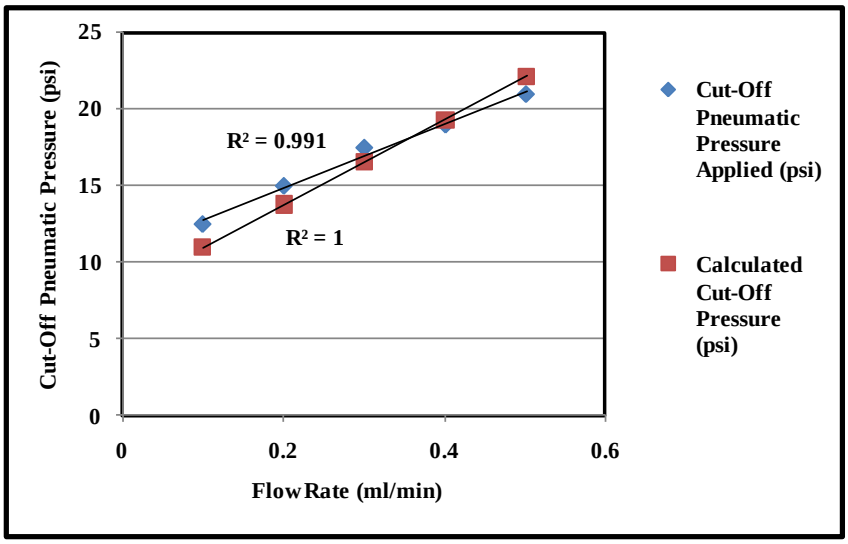

Figure I.2. Comparison of calculated and applied cut-off pressure for 10:1 monomer-to-crosslinker ratio, W_c = 618 µm and L_c = 613 µm

Table I.17. Comparison of calculated and applied cut-off pneumatic pressure for 10:1 monomer-to-crosslinker ratio, W_c = 330 µm and L_c = 469 µm

Flow Rate (ml/min)	*Pressure Drop Measured across Microchannel (psi)*	*Numerically Calculated Pneumatic Pressure (psi)*	*Correction factor*	*Numerically calculated pressure + correction factor (psi)*	*Calculated Cut-off Pneumatic Pressure (psi)*	*Applied Cut-off Pressure (psi)*	*Difference (psi)*
0.1	0.14	15.6998	2.29308	17.9929	18.1329	17.5	-0.6329
0.201	0.26	15.6998	3.43963	19.1394	19.3994	20	0.6006
0.301	0.44	15.6998	4.58617	20.2860	20.7260	23	2.2740
0.402	0.55	15.6998	5.73272	21.4325	21.9825	25	3.0175
0.502	0.7	15.6998	6.87926	22.5791	23.2791	27	3.7209
						Average	***1.7960***

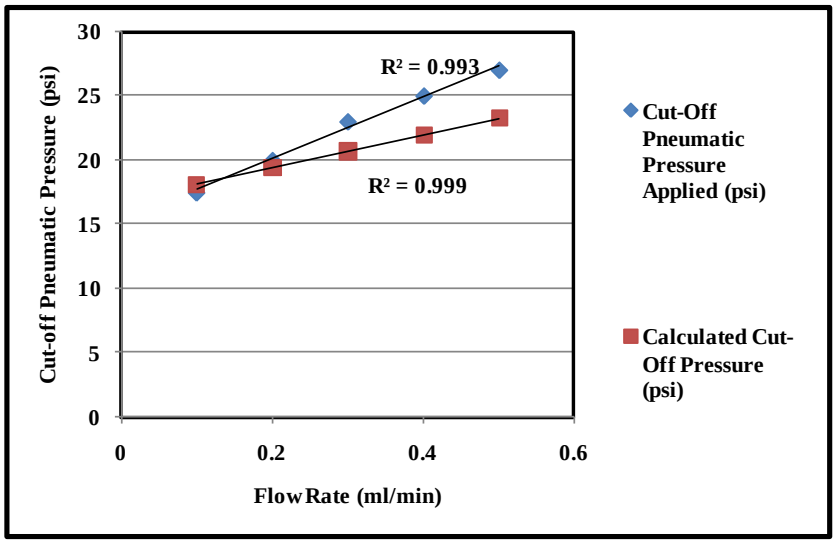

Figure I.3. Comparison of calculated and applied cut-off pressure for 10:1 monomer-to-crosslinker ratio, W_c = 330 µm and L_c = 469 µm

Table I.18. Comparison of pressure drops for 18:1 monomer-to-crosslinker ratio, W*c* = 620 µm and L*c* = 616 µm

Flow Rate (ml/min)	*Pressure Drop Measured across Microchannel (psi)*	*Numerically Calculated Pneumatic Pressure (psi)*	*Correction factor*	*Numerically calculated pressure + correction factor (psi)*	*Calculated Cut-off Pneumatic Pressure (psi)*	*Applied Cut-off Pressure (psi)*	*Difference (psi)*
0.1	0.14	7.0275654	5.088043	12.1156	12.2556	11.5	-0.7556
0.201	0.26	7.0275654	7.632065	14.6596	14.9196	14	-0.9196
0.301	0.44	7.0275654	10.17608	17.2037	17.6437	16.5	-1.1437
0.402	0.55	7.0275654	12.72010	19.7477	20.2977	18	-2.2977
0.502	0.7	7.0275654	15.26413	22.2917	22.9917	20	-2.9917
						Average	-1.621653

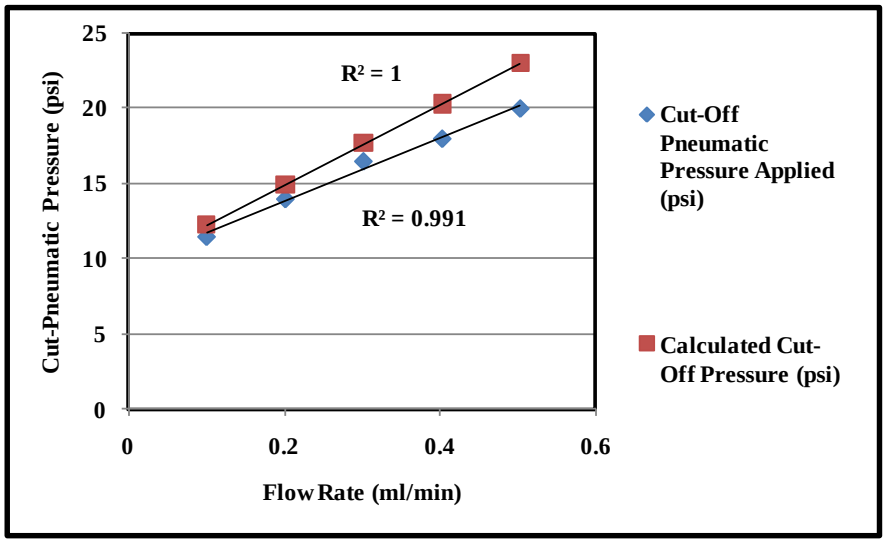

Figure I.4. Comparison of calculated and applied cut-off pressure for 18:1 monomer-to-crosslinker ratio, W_c = 620 µm and L_c = 616 µm

Table I.19. Comparison of pressure drops for 18:1 monomer-to-crosslinker ratio, W_c = 338 µm and L_c = 478 µm

Flow Rate (ml/min)	*Pressure Drop Measured across Microchannel (psi)*	*Numerically Calculated Pneumatic Pressure (psi)*	*Correction factor*	*Numerically calculated pressure + correction factor (psi)*	*Calculated Cut-off Pneumatic Pressure (psi)*	*Applied Cut-off Pressure (psi)*	*Difference (psi)*
0.1	0.14	13.118764	1.919769	15.0385	15.1785	11.5	-3.6785
0.201	0.26	13.118764	2.879654	15.9984	16.2584	14	-2.2584
0.301	0.44	13.118764	3.839539	16.9583	17.3983	16.5	-0.8983
0.402	0.55	13.118764	4.799424	17.9182	18.4682	18	-0.4682
0.502	0.7	13.118764	5.759309	18.8781	19.5781	20	0.4219
						Average	-1.3763

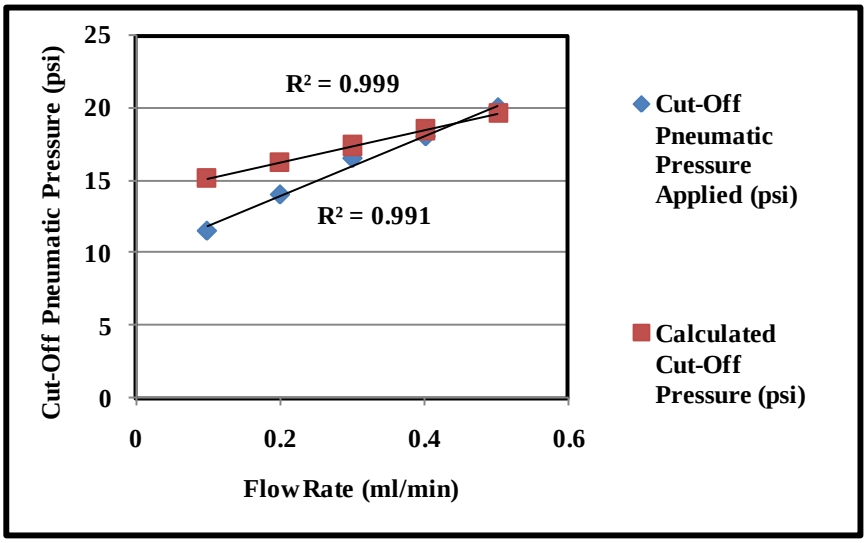

Figure I.5. Comparison of calculated and applied cut-off pressure for 18:1 monomer-to-crosslinker ratio, W_c = 338 µm and L_c = 478 µm

Comparison with finite element analysis

The final experimental results were then compared numerically using COSMOSWorks 2007 to perform FEA. The three requirements of FEA were same as that described in Appendix E:

Requirement 1

In the load condition for first requirement, only clamping pressure of ~40 psi is applied. The load condition is according to the actual loads applied on the device. The dimension of the device is according to actual dimensions of the device. Mooney-Rivlin hyperelastic model is used to run the analysis. The results are tabulated in Table I.20. There was no gap between the top lamina and the membrane.

Table I.20. Results from requirement 1

CR	T_v *(μm)*	T_m *(μm)*	W_c *(μm)*	L_c *(μm)*	Def_{m_f} *(μm)*	D_v *(μm)*
10:1	52.1	190	618	613	23.59	-0.62
10:1	56.8	194.5	330	469	21.57	65.4
18:1	89	219.5	620	616	38.22	-.8
18:1	69	196	338	478	33	82.6

Requirement 2

The load conditions for second requirement are: clamping pressure of 40 psi and fluid pressure are applied and no pneumatic pressure is applied. The second requirement is to see if there is a deflection of membrane in the upward direction. From the results obtained, it is seen that there is no gap between flow lamina and membrane and there is no gap between top layer and membrane. The results are tabulated in Table I.21.

Table I.21. Results from requirement 2

CR	T_v *(μm)*	T_m *(μm)*	W_c *(μm)*	L_c *(μm)*	*Flow Rate (ml/min)*	Def_{m_f} *(μm)*	D_v *(μm)*
10:1	52.1	190	618	613	0.1	24.5	-1.5
10:1	52.1	190	618	613	0.201	24.376	-2.5
10:1	52.1	190	618	613	0.301	24.23	-4.07
10:1	52.1	190	618	613	0.402	24.16	-5
10:1	52.1	190	618	613	0.502	24.027	-6.21
10:1	56.88	194.5	330	469	0.1	22.4	64.83
10:1	56.88	194.5	330	469	0.201	21.95	63.85
10:1	56.88	194.5	330	469	0.301	21.79	63.08
10:1	56.88	194.5	330	469	0.402	21.69	62.6
10:1	56.88	194.5	330	469	0.502	21	61.94
18:1	89	219.5	620	616	0.1	49.765	-0.1725
18:1	89	219.5	620	616	0.201	49.582	-0.61
18:1	89	219.5	620	616	0.301	49.307	-0.88
18:1	89	219.5	620	616	0.402	49.139	-1.69
18:1	89	219.5	620	616	0.502	48.91	-2.799
18:1	69	196	338	478	0.1	34.11	87.31
18:1	69	196	338	478	0.201	33.7	86.92
18:1	69	196	338	478	0.301	33.5	86.31
18:1	69	196	338	478	0.402	33.37	85.93
18:1	69	196	338	478	0.502	33.2	85.41

Requirement 3

The load conditions for third requirement are: clamping pressure of 40 psi, fluid pressure and pneumatic pressure are applied. Figure I.22 shows the microvalve deflection when pneumatic pressure is applied. The detailed results are shown in Table I.22. There is no gap between the flow lamina and membrane and no gap between the top lamina and membrane.

Table I.22. Results from requirement 3

CR	T_v *(µm)*	T_m *(µm)*	W_c *(µm)*	L_c *(µm)*	*Flow Rate (ml/min)*	P_p *(psi)*	$Def_{m\ f}$ *(µm)*	D_v *(µm)*
10:1	52.1	190	618	613	0.1	12.5	26.21	110.9
10:1	52.1	190	618	613	0.201	15	26.9	121.4
10:1	52.1	190	618	613	0.301	17.5	27.24	130.9
10:1	52.1	190	618	613	0.402	19	27.47	136.3
10:1	52.1	190	618	613	0.502	21	27.63	143.3
							Average	***128.56***
10:1	56.9	195	330	469	0.1	17.5	24	128.6
10:1	56.9	195	330	469	0.201	20	24.9	135
10:1	56.9	195	330	469	0.301	23	24.75	142.4
10:1	56.9	195	330	469	0.402	25	25.56	147.2
10:1	56.9	195	330	469	0.502	27	25.57	151.9
							Average	***141.02***
18:1	89	220	620	616	0.1	11.5	49.1	133.5
18:1	89	220	620	616	0.201	14	38.9	152.9
18:1	89	220	620	616	0.301	16.5	51.4	167.6
18:1	89	220	620	616	0.402	18	51.52	176.3
18:1	89	220	620	616	0.502	20	51.6	188
							Average	***163.66***
18:1	69	196	330	478	0.1	14	40.6	150.1
18:1	69	196	330	478	0.201	17	41	159.9
18:1	69	196	330	478	0.301	18.5	41.01	164.5
18:1	69	196	330	478	0.402	20	41.09	169
18:1	69	196	330	478	0.502	22	41.119	174.8
							Average	***163.66***

APPENDIX J. DESIGN RULES AND MACHINING TOLERANCE

Design rules

Based on the results obtained from experiments and FEA, a set of design rules have been formulated. The design rules are based on the amount of different pressure that are applied on the device, the dimensions of the flow and control channel, the dimensions of the sealing bosses and thickness and elastic modulus of PDMS elastomeric membrane. The design rules for each category are listed below:

Pressure

1. Flow pressure inside the microchannel must be less than pneumatic pressure applied to actuate microvalve.
2. Clamping pressure must be greater than pneumatic pressure.
3. If the device consists of stiff polycarbonate substrate of thickness 10 mm with PDMS membrane of 10:1 or 18:1 monomer-to-crosslinker ratio sandwiched between the polycarbonate substrates, then the device can with stand a maximum clamping pressure up to 100 psi.

Distance between the bosses

1. Distance between the bosses can be at a maximum of 15 μm away from the edges of the microchannel.

Boss Width

1. Increase in boss width results in decrease in deflection of PDMS membrane into flow microchannel. Boss width can range from 150-200 μm.

Boss Height

1. Increase in boss height results in decrease in deflection of PDMS membrane into flow microchannel. But increase in boss height result in increase in distance between PDMS membrane and top lamina. This can cause deflection of membrane in the upward direction when a higher fluid flow rate is applied inside the microchannel. Boss height can range from 25-40 μm.

Flow microchannel width

1. Flow microchannel width depends on the application. It is recommended to have flow microchannel width greater than 100 μm. If the microchannel width is too narrow, then higher pneumatic pressure is required to deflect the membrane to block the flow, since the cross-sectional area for the microvalve to deflect becomes small.

Flow microchannel depth

1. Flow microchannel depth depends on the application. As the depth of the microchannel increases, the pneumatic pressure required to actuate the microvalve will also increase.

Thickness of PDMS membrane

1. Thickness of membrane depends upon the elastic modulus of the PDMS membrane. For a lower modulus, the thickness can range up to 300 μm**.** If the thickness is too low, then the membrane can deform into the microchannel and distort the microchannel when a higher clamping pressure is applied.
2. For a higher modulus the thickness can range from 190-250 μm or even higher.

Microvalve Thickness of PDMS membrane

1. Decrease in microvalve thickness can increase in amount of microvalve deflection.
2. For a lower elastic modulus of the PDMS MEMBRANE, the microvalve thickness can be higher than 50 μm but lower than 90 μm.
3. For a higher elastic modulus of PDMS MEMBRANE, the microvalve thickness can range from 30-60 μm.

Width and length of control channel

1. Microvalve deflection increase with increase in width and length of control channel. The width of the control channel depends on the width of the flow microchannel and distance between the bosses. The width of the control channel must be at the least equal to the width of flow microchannel and can vary up to 15 μm greater than the distance between the bosses.

Elastic modulus of PDMS membrane

1. Elastic modulus of PDMS membrane depends on the monomer-to-crosslinker ratio. The above experiments were conducted with 10:1 and 18:1 monomer-to-crosslinker ratios and both worked well.

Manufacturing tolerance

It is very important to fabricate the microfluidic device within the design tolerance. The important factors affecting the microvalve actuation are: width of microchannel, depth of microchannel, control channel width, control channel length, height of sealing bosses, width of sealing bosses, distance between sealing bosses, microvalve thickness and elastic modulus of PDMS membrane. Among them the important factors that must be within the machining tolerances are height of sealing

bosses, width of sealing bosses, distance between bosses, control channel width and control channel length.

The gap between the PDMS membrane and top lamina is directly dependent upon the height of the sealing boss. If there is a gap between the membrane and top lamina, then the increase in fluid pressure may cause an upward deflection of membrane. This results in the fluid leakage outside the microchannel. From the finite element analysis, it is recommended that the height of the sealing bosses be 25 μm with a tolerance of +15 μm. On the other hand, the deflection of PDMS membrane into the flow microchannel decreases with the increase in boss width. Boss width can range from 150-200 μm with a tolerance of -25 μm and +50 μm.

As explained earlier, the distance between the sealing bosses is directly dependent upon the width of the microchannel. Increase in the distance between the sealing bosses results in fluid leakage outside the microchannel when a higher flow pressure is applied. Therefore, it is recommended that the bosses can be located close to the edges of the microchannel with a tolerance of +15 μm.

Increase in the width and length of control channel results in an increase in microvalve deflection. The width of the control channel is also dictated by the width of the flow microchannel and distance between the bosses. The width of the control channel can be either same as width of flow microchannel or the distance between the bosses with a tolerance of +15 μm.